UNIVERSITY OF NOTTINGHAM

CRACK PROPAGATION IN HIGH MODULUS ASPHALT MIXTURES

by

Anthony J Sewell, B Eng (Hons), FCIHT, FIHE, FIAT, MIQ.

Thesis submitted to the University of Nottingham for the Degree of Doctor of Philosophy.

June 2017

DEPARTMENT OF CIVIL ENGINEERING

Abstract

This Thesis was undertaken at the University of Nottingham which has a world class history of research into the fatigue of asphalt materials. The work described in this thesis was part of a research project funded by EPSRC, which attempts to gain a greater understanding of fatigue crack propagation in High Modulus Base (HMB) materials. Following on from Pell, Brown and Read this research has introduced the Compact Tension (CT) Test and Fracture Mechanics principles to examine the behaviour of HMB materials which had relatively little fatigue behavioural understanding on commencement of this research.

This research investigated the fatigue cracking behaviour of twelve High Modulus Base (HMB) binders and mixtures. The research was instigated in response to the introduction of these HMB binders from France, as it was thought that these materials were not particularly well understood. In hindsight, this view was proven to be correct, as numerous problems have been experienced after using such materials.

The Compact Tension test has been proved to be an effective means of testing bituminous mixtures for their crack propagation resistance, allowing the study of temperature effects. Crack propagation is dramatically affected by both binder hardness and temperature. In a pavement, the current approach to design, assuming a single fatigue characteristic, underestimates the life of 35 and 25 pen mixtures. However, it probably overestimates the life of 15 pen mixtures by not accounting for the effects of low temperatures.

My family are my world

Declaration

The research described in this thesis was conducted at the University of Nottingham, Department of Civil Engineering. I declare that the work is my own and has not been submitted for a degree of another university.

Anthony J Sewell

Nottingham

June 2017

TABLE OF CONTENTS

1 Introduction

1.1 History of UK Highways

The Romans introduced the first highway network into the UK. After they left the UK the highway network was left to deteriorate until the 16th century when it was first realised how important this legacy was. As travel between conurbations became more important, a system of funding the construction and maintenance of these highways was required which originated in the form of tolls. Turnpike Trusts replaced the toll system and engineers such as Telford and McAdam implemented their respective designs, which were used until the early 20th Century.

At this point it is alleged that, in Nottingham, a roofing contractor accidentally dropped a barrel of a hot tar onto a granular road surface and realised the possible advantages obtainable if highway aggregates were bound. This method of surfacing quickly spread throughout the UK, especially in the cities to alleviate the dust problems inherent with granular materials. Although at first only used as a sealant, soon the tar and aggregates were mixed to produce a material, which became known as tarmacadam, and later tarmac. The demand for tarmacadam increased dramatically, prompting the construction of local tarmacadam mixing plants. Pavement construction at this time was administered on a localised basis making use of the materials that were readily available in that area.

After World War Two, it was realised that a method of pavement design was required to control the materials used and prevent premature pavement failure. The Ministry of Transport monitored the performance of over 400 trial sections of pavements to form the basis of Road Note 29 [72] first published in 1960. The findings of this work revealed that the service lives of pavements were reducing with differing behaviour from pavements constructed using nominally the same materials but in different areas. Road Note 29 recognised the importance of a good foundation and used the California Bearing Ratio (CBR) method of classification, which was pioneered in California in the 1930s. The first Specification for Highway Works (SHW) [2] was also published allowing pavement engineers to be consistent in their choice of materials. A drainage layer was optional to control the detrimental effects of allowing water to penetrate the pavement. The pavement would then be constructed using a sub-base, a base and surfacing courses. The thickness of the sub-base used was dependent on the CBR value

of the sub-grade. The materials used for the sub-base were specified by Clause 804, which recognised the variability of local UK aggregates. The thickness of the base and of the surfacing courses was dependent on the amount of commercial vehicles predicted to be using the pavement over a 20-year period. Bases could be constructed from combinations of dense tar or bitumen macadam, lean concrete, or wet mix macadam or from a specified thickness of dense tar or Dense Bitumen Macadam (DBM), or Hot Rolled Asphalt (HRA) base. Surfacing materials were made from a rolled asphalt or dense tar or bitumen macadam basecourse, now referred to as binder course, followed by a rolled asphalt wearing course, now surface course. This system of layers has stayed on until the present time. The main changes over the last forty years have been in the design methods and the advancement of material properties.

In all, three editions of Road Note 29 [72] were published in 1960, 1965 and 1970, the latter containing a formula which converted commercial vehicles into 'standard axles', which could be considered to be an early attempt to incorporate analytical methods into design. It was clear that a greater understanding of the fundamental properties of the materials used for construction was required. By this time, two principal types of pavement failure had been recognised, cracking and rutting. Cracking is a fatigue phenomenon due to repeated tensile strains, either induced at the bottom of the (road)base layer, or, according to more recent [59] evidence, occurring at the surface and developing downwards. Rutting can be caused by permanent deformation in all of the layers (structural rutting) or in the upper surfacing layers only (non-structural rutting). The first attempts at a total analytical approach to pavement design were, therefore, aimed at controlling these two failure mechanisms. Research in the late 60s and 70s, therefore, concentrated on the tensile strains generated at the bottom of the bituminous layers and the vertical compressive strains at the top of the sub-grade.

Early work by Pell [56] centred around the fatigue phenomenon and, by the time Road Note 29 arrived, Pell had already published the results of a completed research project on “Fatigue characteristics of bitumen-sand mixes” in 1959. Pell went on to introduce the 'strain criterion' in 1962 [69], which has been greatly used and modified by subsequent researchers. More research into fatigue followed during the 1960s by Gardner [21] and Taylor [68]. Simultaneously, work was undertaken to understand permanent deformation and Thrower [70] publishing his findings in 1975 from research by the Transport and Road Research Laboratory (TRRL). Brown [12] published “A Simplified, Fundamental Design Procedure for

Bituminous Pavements" in 1974, and this was followed by the Shell Pavement Design Manual in 1978 [62], with Shell having originally published a set of analytically based design charts in 1963 [66]. The publication of LR1132 [57] by the TRRL in 1984 signified widespread use of analytical methods in the UK. This method involved the calculation of the two key strains in the pavement induced under a standard wheel load and related them to cracking and rutting failures.

With a greater understanding of how stresses induced in the pavements were related to the subsequent failure of the structure, it became clear that the use of stiffer materials would provide significant benefits to designers. The use of stiffer materials had already been pioneered in France and a working party from the UK published their experiences from a fact-finding visit in 1976 [25]. The French had experienced problems in the 1960s, especially using un-crushed gravel with a binder in the region of 100pen, resulting in severe deformation failures. The French also had different axle weight limitations, but it was felt by the authors that the material grave bitume was largely to blame. The French have since developed a more damage resistant mixture by using a lower binder content (3.5%), minimising the use of un-crushed gravel, increasing the filler and using a stiffer bitumen (40/50 pen). This enhanced material gave significant benefits to designers by allowing the use of thinner layers or by increasing the design life of the pavement. It was realised that, to further the knowledge of pavement engineers, field trials would be necessary so that the benefits of the research innovations could be properly assessed.

The first attempt to transfer this technology to the UK was made by Brown [14] in 1984. A 180m trial section was laid within a new construction on the Hasland Bypass, which is close to Chesterfield in Derbyshire. This trial section was designed analytically and was compared to the traditional empirical design, which formed the rest of the construction. Essentially the difference in the structures was that the analytically designed pavement used a reduced sub-base and a thicker base with a double surface dressing applied to form the surfacing. The traditional construction used a thicker sub-base with a conventional base, binder course and asphalt surface course. The analytical method allowed a reduced thickness by enhancing the mechanical properties of the major structural element, the base. This was achieved by using a stiffer 50 pen binder as opposed to the usual 100 pen binder. Laboratory testing showed the enhanced material performed better in tests for dynamic stiffness, fatigue and permanent

deformation. The trial section proved that materials from outside current specifications could be produced and placed successfully.

In 1982, the TRRL produced a report "A dense coated macadam of improved performance" [35], which compared plant mixed materials of varying compositions. The materials tested included a conventional DBM 100 pen, DBM 50 pen, DBM 50 pen having higher filler content and two tar bound materials. The trial and associated laboratory testing concluded that the enhanced 50 pen materials offered significant benefits including a significantly greater load spreading ability, leading to reduced layer thickness or extended pavement life. Pavement design in the UK was revolutionised by the implementation of LR1132 [57] in 1984. Designers at last had a method of using the strains at the bottom of the bituminous layers and the top of the sub-grade. The method of control of these critical strains was included in the form of design charts. However, LR1132 did not incorporate enhanced materials, only making reference to conventional ones. In 1987 full-scale road trials of 50 pen materials were carried out at five sites in the UK, supervised by the TRL [50]. Again, traditional materials were compared with two similar materials having been made using a stiffer binder and one with a 3% increased filler content. The report concluded that mixing, laying and compaction was marginally more difficult with some of the plant but was certainly achievable. Laboratory testing concluded that the enhanced materials exhibited superior properties to conventional ones being stiffer and more deformation resistant, and their resistance to fatigue was deemed to be at least as good. Financial considerations suggested that a saving of £2 per square metre could be made, which is the same as Brown predicted for the Hasland project almost ten years previously. Later that year HD14/87 [18] was introduced, which allowed the use of 50 pen enhanced materials.

The early 1990s brought about a time of significant change for the highways industry with a growing number of major UK contractors and indeed, later, local authorities being bought out by larger international conglomerates. This coincided with the harmonisation of standards as the European Union progressed. Together, these factors brought innovation and alternative approaches to the industry backed by in house research, which until this time had been left to central government. The main thrust of research still focussed on extending design life by introducing superior materials and so, in 1994, the TRL evaluated a French material Enrobé à Module Élevé (EME) [51].

UK materials were used to produce a material, which fulfilled all the requirements of the French mix design method outlined above. For a number of reasons, it was decided to produce a material, which conformed to UK specifications. The importance of this research is, therefore, made more necessary due to the lack of experience in using HMB materials.

A trial was carried out using UK materials, but graded to suit French specifications. The objective was to test the technology transfer to the UK and to see if this technology could be modified to suit conditions in the UK. A material was also tested at TRL that incorporated the use of the stiff binders into the traditional UK macadam specifications. The macadam was used in the trial to compare the traditional materials produced in the UK to those produced in France. Due to the natural geology and different approach to design, traditional French materials tend to make use of finer gradings. It would be very difficult to produce such materials on a large scale due to the format of the UK quarries, which are planned and built to produce macadams and asphalts. The trial was laid using four materials: two EME; and two Macadam, laid in succession at a width of 4.2m.

The materials were produced using traditional mixing plant and methods and gave no additional problems. Compaction involved comparison of the plant used in France, a 35 tonne Pneumatic tyre roller, with that used traditionally in the UK 8/10 tonne steel-wheel vibratory roller. There were no advantages found by using the pneumatic roller; however, it did give a closer finish and under extreme weather conditions was reported as performing better than traditional machines. It is considered prudent to use a pneumatic roller in France in case of extreme weather conditions and to offset water ingress to the pavement. Laboratory measurements were taken of elastic stiffness: TRL 3-point bend; and Indirect Tensile Stiffness Modulus [10], resistance to rutting [11] and resistance to fatigue cracking (TRL fatigue test). The macadams compared very favourably to the EME materials when tested for elastic stiffness and they performed as well as the EME material during the permanent deformation tests. The EME material outperformed the macadams when tested for resistance to cracking. This, however, was expected as the EME material has a higher binder content. The High Modulus Base (HMB) material, however, produced results similar to those that would be expected from traditional macadams. It can be argued that if the HMB macadams are used in a full depth construction the loads would be more spread out and hence the stresses and strains would be thus reduced, reducing the susceptibility to fatigue cracking. The

costs of producing the material in the UK were forecasted to be around 25% more than those for producing traditional macadams, due to the higher heating costs and increased price of the bitumen. The report recommended the incorporation of HMB materials into trial sections of future UK trunk road contracts.

During 1996, trial sections were laid in the UK on five reconstruction contracts to assess the use of the stiffer bitumens and the resulting structural properties [52]. The sites were selected to make use of different aggregates, mixing plants, methods of laying and, of course, the different weather conditions experienced in the UK. Each trial section was laid adjacent to a control section of traditional material to monitor performance over time. Each section consisted of approximately 1300 tonnes of HMB material. There were no serious problems reported during the manufacture, laying and compaction of the HMB material using traditional UK paving plant. The contractors who all submitted a report found the material no more difficult to handle than the traditional materials. Each trial section was tested for its structural properties by taking cores for evaluation in the laboratory. The cores were tested to check the level of compaction achieved by the Percentage Refusal Density (PRD) method according to the SHW clause 929.2. The results showed almost total compliance with the specification and hence traditional methods of compaction were deemed suitable for future use. The recovered cores were then tested to evaluate the structural properties of the laid materials. The c stiffness modulus was measured in indirect tension (IT-CY) per protocol in BS EN 12697-26, annex C [10] and the TRL 3-point bend test. The results showed that the HMB generally displayed far higher stiffness values, suggesting the material was considerably more efficient at spreading loads. When tested for permanent deformation, the HMB material proved to be difficult to test using accepted methods [11] but, using a modified bridge joint slab tester, the HMB proved to have superior resistance to rutting compared with the traditional macadams. The HMB material was also tested to evaluate its resistance to cracking and produced results similar to the values obtained from the traditional macadams. Nunn [52] stated that the resistance to fatigue would have to be reduced by a factor of four before it negated the benefits of the increased stiffness. Two of the sites were successfully tested for stiffness using the Falling Weight Deflectometer (FWD). The results confirmed that the HMB pavement showed an increased stiffness value compared to the traditional material. Nunn also made recommendations for design thickness stating that using a HMB material can

reduce pavement thickness by 37% compared to a traditional macadam. This would produce a cost saving of 25% even after taking into account the increased mixture production costs. Nunn concluded that HMB material would be suitable for use on heavily trafficked roads or in areas susceptible to rutting [52].

With HMB materials being deemed fit for use on UK highway contracts coinciding with the introduction of DBFO contracts, designers quickly incorporated them into pavement designs. With the advancement of test methods, a method of characterising HMB materials was required, which duly arrived in the form of a TRL report by Nunn [52], produced after trials in 1994 [51], where an end performance specification was used. Fordyce et al [20] proposed a design guide for HMB materials in 1997, which ensured mixtures achieved minimum design stiffness. As advancements in HMB technology moved forward, their use increased on contracts such as the A1-M1 link road in Yorkshire and the A19 reconstruction in Teesside. HMB materials became an even more attractive option when TRL published data suggesting that cracking occurs only in the surfacing as the base layers become stiffer with age [49]. Nunn consolidated this theory by promoting the design of 'long life' pavements [48], which would only require periodic surfacing replacement when surface cracking appeared. This theory was reasonably based on the fact that previous base materials were shown to increase their stiffness modulus over time. However, during routine monitoring of HMB pavements, the FWD surveys and indeed cores showed that the stiffness modulus had not increased and, in some cases, had decreased. Materials using 15 and 25 pen binders were immediately withdrawn from use in 2000 by the Highways Agency pending further investigations.

1.2 Problem Definition

Although the TRL have been investigating the use of HMB materials and recommended their use in contracts for heavily trafficked roads, the use of these materials in the UK has been limited and, therefore, no long-term experience of their performance exists. It is thought that materials which exhibit a high stiffness modulus could be more susceptible to crack propagation, based on the research by Read [58]. The current procedures used to assess fatigue resistance of a bituminous material are thought to be principally affected by life to crack initiation. This point is defined as the point at which micro-cracks coalesce to form a macro-crack. The additional time required for the macro-crack to propagate through the material is accounted for by an empirical shift factor used for all materials. In reality, it is

known that, for thicker types of pavement construction, the time for crack propagation forms the greater part of the total fatigue life of the pavement. The purpose of this research is to quantify this effect in these high stiffness materials.

1.3 The Research Project

The work described in this thesis was part of a research project funded by EPSRC, which attempts to gain a greater understanding of fatigue crack propagation in HMB materials. The objectives of the project were to:

- Carry out a fundamental crack propagation investigation. This is significantly more difficult and time consuming than the more usual fatigue testing, which is thought to be dominated by crack initiation rather than propagation. In reality, crack propagation is not well understood, even in more conventional materials.

- Investigate the temperature, loading rate and stress dependence of fatigue cracking behaviour. This is particularly important in the context of thermal cracking, which is already a serious problem in continental type climates experiencing temperature variations and very cold winters.

- Develop an improved predictive model for pavement cracking.

The overall research philosophy has been to start from a fundamental understanding of HMB materials by performing mechanical testing. This knowledge was then used to develop a Mode I (tensile) test method using the Compact Tension (CT) test configuration seen in Figure 1 to measure the fatigue crack propagation. This method was then used to carry out a large testing programme to categorise the material's fatigue behaviour, including the effects of temperature, loading rate and stress dependence. The methods used to analyse the testing programme make use of the Stress Intensity Factor K (SIF), which will be introduced in full in Chapter 2. The SIF is then used to calculate the Stress Intensity Factor over a range of crack growth lengths within the sample ΔK. The new test method was then modified to account for a mixed Mode I/Mode II test configuration (including shear) and to test site cores from HMB pavements.

This thesis is organised into six chapters. Chapter 2 reviews the literature concerning the crack propagation characteristics of bituminous materials. It also provides a brief description

of the test methods used to characterise HMB materials. Chapter 3 describes the development of a test method, which is used extensively in metals testing, but as yet not for bituminous materials, including finite element analysis depicting stress development in the critical locations within the specimen. A method of monitoring the crack growth from digital images is also described in this chapter. Chapter 4 describes the Mode I experiments carried out on the HMB materials over a range of temperatures, loading rates and stresses. Mixed Mode I/II testing is also described in this Chapter. Chapter 5 describes the modelling of the fracture mechanics parameters found in Chapter 4. Conclusions and recommendations for future research are presented in Chapter 6.

2 Characterisation of Fracture Damage in Asphaltic Materials

There are two major failure mechanisms within asphalt pavements, namely permanent deformation and fatigue cracking. Much research has been undertaken into both of these phenomena but they are still relatively poorly understood especially in modern materials, for which there is little empirical knowledge. This research has attempted to better understand fatigue crack propagation as opposed to crack initiation, which has received wider attention. This chapter begins by an extensive review of the fracture mechanics approach including previous research using this approach for bituminous mixtures. Test methods are then highlighted with particular emphasis on the Compact Tension (CT) test seen in Figure 1, which has been developed for monitoring fatigue crack growth within this project.

2.1 Fracture Mechanics

2.1.1 Introduction

Fracture mechanics is a mechanistic approach is used widely in solid mechanics analysis to characterise and evaluate damage in materials subjected to different types of loading. It is mainly concerned with low stress fracture of high strength materials [24]. During the 20th Century, much work was directed to ascertain a solution to the cause of such fractures. During World War II, 2500 Liberty ships were built of which 145 broke in two and almost 700 experienced serious failures. The results of such investigations revealed that the engineered structures contained a small percentage of flaws. These flaws often resulted in stress concentrations thus allowing a crack to initiate and, if untreated, propagate through the material, causing failure. As the work in fracture mechanics progressed, it became evident that pavement failure occurred in a similar manner, and indeed, the technique began to be applied within the field of pavement engineering [39]. The fracture performance analysis of HMA in much of the previous work is based on the well-known Paris Law [54], which has been used widely albeit in different formats. Equation 2-1 gives Paris Law in its linear elastic mode showing the rate of crack propagation, *da/dN*, as:

$$\frac{da}{dN} = A(\Delta K)^n \qquad (2\text{-}1)$$

where: *da* is the range of crack growth; *dN* is the range of cycles of load application; *K* is the stress intensity factor; and *A, n* are material properties depending on experimental conditions, e.g. waveform, temperature, frequency.

K is a function of stress (σ) and (C) in addition to a specimen geometry factor (Φ), as shown in Equation 2-2.

$$K = \Phi\sigma\sqrt{\pi \mathrm{a}} \tag{2-2}$$

As shown from Equation 2-1, crack propagation (*da/dN*) represents the damage rate in the materials which basically depends on the stress intensity; stress intensity is a function of stress amplitude as shown in Equation 2-2.

In this study, the Paris Law model was used extensively in the analysis of the fracture performance of HMA; therefore, more details about this model are given in the following sections.

2.1.2 Early work on Paris Law

Inglis [28] published his paper "Stresses in plate due to the presence of cracks and sharp corners", in 1913, which provided a mathematical analysis of the stresses in the vicinity of a two-dimensional elliptical opening of arbitrary eccentricity. Figure 2 schematically describes Inglis' analysis. This is recognised as the first significant publication of modern fracture mechanics. Inglis modelled a crack by a slender elliptical perforation and derived the planar stress field precisely. By using the local behaviour at the tip of the ellipse, he inferred the nature of the stresses in perforations and cut-outs of other shapes. He found that the stress concentration at the tip of an ellipse is given by:

$$\frac{\sigma_{max}}{\sigma_a} = 1 + \frac{2a_e}{b_e} \tag{2-3}$$

where: σ_{max} is stress at the end of the major axis of the ellipse; σ_a is the applied stress applied normal to the major axis; a_e and b_e are half the major & minor axes respectively.

In 1920, Griffith published his paper "The phenomena of rupture and flow in solids" [22]. Griffith used Inglis' work to model his results from testing glass specimens. He went on to

state, "The theorem of minimum potential energy may be extended so as to be capable of predicting the breaking loads of elastic solids, if account is taken of the increase of surface energy which occurs during the formation of cracks". This indicates that when a crack is introduced into a solid, a balance must be struck between the decrease in potential energy and the increase in surface energy resulting from the growth of the crack. If equilibrium is not met, then it is feasible that an existing crack would grow. The energy required to extend the crack is, therefore, equal to the surface energy of the material. Griffith showed that the change in potential energy of the plate associated with the introduction of a crack may be found from:

$$U - U_o = -\frac{\pi\sigma^2 a_{0.5}^{2t}}{E} + 4a_{0.5}^{2t} t\gamma_s \qquad (2\text{-}4)$$

where: *U* = potential energy of body with crack, *Uo* = potential energy of body without crack, σ = applied stress, $a_{0.5}$ = one-half crack length, t = thickness, E = modulus of elasticity and γ_s = specific surface energy.

Griffith went on to discuss various aspects of fracture and deformation of solids. However, his principal contribution remained his theory of 'minimum potential energy' for elastic materials. Griffith was aware that his theory would not be directly applicable to metals and went on to publish subsequent papers to verify this statement [23].

From the period between 1920 and 1950 all of the work carried out in the field of fracture mechanics focussed on applying the Griffith criterion to the brittle fracture of metals. Irwin [29] and later Orowan [53] modified the Griffith criterion by including the work done due to plastic deformation. Irwin [30] while attempting to clarify the dynamics of rapid fracture in ductile metals considered that the major features in the development of fast fracture were the following:

- An initial stage of crack advance by creeping (plastic flow)
- A sharpening of the crack head contour
- The release of stored energy as part of the instability was reached

The major observation here was that the work required to extend a crack in metals "must include the work done due to plastic deformation. For this interpretation, the work done

against surface tension is generally not significant." Irwin used the energy source term (the elastic energy per unit crack length increment), to show that:

$$\sigma = \sqrt{\frac{EC}{\pi a}} \tag{2-5}$$

where C is a constant reflecting the surface energy release of the crack propagating in an elastic plate; other parameters as before.

Orowan [53] stated that "the crack propagates if the plastic strain at its tip reaches a critical magnitude." He extended Griffith's work to accommodate the energy of plastic deformation in the fracture process so that:

$$\sigma = \sqrt{\frac{2E(\gamma_S+\gamma_P)}{\pi a}} = \sqrt{\frac{2E\gamma_S}{\pi a}\left(1+\frac{\gamma_P}{\gamma_S}\right)} \tag{2-6}$$

where: γ_S = specific surface energy, γ_P = plastic deformation energy and $\gamma_p > \gamma_s$.

From the work of Griffith and Orowan it can be noted that there is a point of instability. The elastic energy release rate (also referred to as the crack driving force) reaches a critical value, whereupon fracture occurs. This value measures the intensity of the crack tip stress field as long as the influence of plastic deformations accompanying fracture extension is limited to an area close to the crack.

This concept is still used today in linear elastic fracture toughness characterisation of materials. Irwin [29] used Westergaard's semi-inverse method to relate the strain energy release rate associated with crack extension to the stress field at the tip of a crack. He also showed that the intensity of the crack tip stress field could be represented by the stress intensity factor, K. From Irwin's paper a value of stress intensity, K, can be found to be equal to:

$$K = f(\sigma, a) \tag{2-7}$$

where the functionality depends on the configuration of the cracked component and the manner in which the loads are applied. Irwin introduced three different modes of loading which all involve different crack displacements:

- Mode I. Opening or tensile mode, where the crack surfaces move directly apart.
- Mode II. Sliding or in plane shear mode, where the crack surfaces slide over one another in a direction perpendicular to the leading edge of the crack.
- Mode III. Tearing or antiplane shear mode, where the crack surfaces move relative to one another and parallel to the leading edge of the crack.

Various investigations took place following the publishing of Irwin's paper, which were all aimed at characterising the stress intensity factor and the distribution of the stresses and displacements in the vicinity of the crack tip for different specimen geometries. The American Society for Testing and Materials (ASTM) formed a special technical committee in 1959 to study the brittle fracture of high strength materials that were being used in various missile and rocket motor cases.

The committee's brief was the rapid development of test methods for characterising the resistance of high strength metallic materials to brittle fracture. The committee produced five reports between 1960 and 1964 and all developed the use of the KIC (fracture toughness value) approach. The use of the stress intensity factor parameter resulted in a better understanding of the effects of thickness, yield strength, and constraint on fracture toughness evaluations. The work focused the attention on the stress field distribution and on the stress field intensity at the tip of the crack. The findings enabled the K_C approach to be applied to subcritical crack growth under cyclic load fluctuations, as seen in Figure 3.

Paris et al [55] linked the stress intensity factor to the analysis of fatigue crack growth. They showed that the rate of crack growth per cycle is governed by the stress intensity factor, over the stable range of crack growth. The concept of describing the stress distribution near the crack tip was introduced using the co-ordinate system seen in Figure 4.

Paris stated that K was a measure of the effect of loading and the geometry of the specimen and these will change during any period of crack growth. However, if β is the ratio of the maximum to minimum load on a cracked body during a cycle of loading, and if K is directly proportional to the magnitude of loading, then:

$$\beta = \frac{P_{max}}{P_{min}} = \frac{K_{max}}{K_{min}} \quad (2\text{-}8)$$

where P = load

So, the amount of crack extension per cycle of loading could be derived from:

$$\frac{\Delta a}{\Delta N} = f(K_{max}, \beta) \quad (2\text{-}9)$$

assuming that the stresses near the root of the crack are described by K_{max} and β for a given material. So, for any load cycle N, given the geometry and loading:

$$\beta = \beta(N) \quad (2\text{-}10)$$

And K can be computed for any crack length and the maximum load at any given cycle from:

$$K_{max} = K_{max}(Na) \quad (2\text{-}11)$$

Therefore, substituting equations 2-9 and 2-2 into 2-7 Paris found the rate of crack extension to be:

$$\frac{da}{dN} = f(N, a) \quad (2\text{-}12)$$

Paris also introduced the link between K and the normal stresses in the vicinity of the crack tip:

$$\sigma_{xx} = \frac{K_1}{\sqrt{2\pi r}} \cos\frac{\theta}{2}\left(1 - sin\frac{\theta}{2} sin\frac{3\theta}{2}\right) \quad (2\text{-}13)$$

$$\sigma_{yy} = \frac{K_1}{\sqrt{2\pi r}} \cos\frac{\theta}{2}\left(1 + sin\frac{\theta}{2} sin\frac{3\theta}{2}\right) \quad (2\text{-}14)$$

$$\tau_{xy} = \frac{K_1}{\sqrt{2\pi r}} \sin\frac{\theta}{2} \cos\frac{\theta}{2} \cos\frac{3\theta}{2} \quad (2\text{-}15)$$

Equation 2-10 was modified by Paris and Erdogan [54] in 1963 using regression analysis for repetitive loading conditions resulting in the well-known Paris Law, which has already been given in Equation 2-1.

The law introduced by Paris was found to be suitable for use in bituminous material testing [28] and has been used for the derivation of *K* values during this project.

2.1.3 Crack Growth

In many cases, serious failure occurs when the hair cracks grow creating cracks in a critical length during loading by mechanism such as fatigue. Linear Elastic Fracture Mechanics (LEFM) analysis has been used to characterise crack growth rate by means of Paris' Law [54]. It is worth noting that Paris' Law was developed based on the analysis of propagation of a single crack in homogeneous materials, which were metallic specimens. In this law, the rate of crack propagation is a function of the stress intensity factor as detailed in Equation 2-1.

Hertzberg [24] showed that for an abundance of data, for a given material, the da/dN versus ΔK curve assumes a sigmoidal shape as seen in Figure 3. This curve shows that for the regions of high and low ΔK values the ΔK dependence of crack growth rate increases notably. The curve shows three distinct regions of fatigue crack growth response;

- Region I, crack growth rate decreases rapidly with decreasing ΔK and approaches lower limit at K_{th}.
- Region II mid-range of crack growth rates where power law dependence prevails
- Region III acceleration of crack growth resulting from local fracture as K_{max} approaches K_c.

As stated in Chapter 1, this project has primarily involved an investigation into crack propagation. Region I and III will only be mentioned in passing for the remainder of this thesis. Region II however is the area to be investigated where crack propagation occurs and the region that is suitable for Paris' Law to be applied. The next section is a review of the research undertaken, which has attempted to apply fracture mechanics principles to bituminous materials.

2.1.4 Application of Fracture Mechanics to Bituminous Materials

Moavanzadeh [42] is credited with the first attempt at the application of FM principles to assessing bituminous materials. He investigated the fracture behaviour of bitumen and noted that this element was the primary controlling factor in the cracking of bituminous mixtures.

Moavanzadeh also noted that brittle fracture was the primary mode of failure, especially at low temperatures, because the large deformation involved in ductile rupture would not be expected for bituminous mixtures in service conditions. Three-point bend tests were used to study the critical strain energy release rate, *Gc*, rather than the fracture surface energy, *γ*, and for plane strain conditions, the value of *Gc*, was given by:

$$G_c = \frac{1-v^2}{E}\sigma^2 d f\left(\frac{a}{d}\right) \quad (2\text{-}16)$$

where; E = Elastic modulus given by the slope of the load-deflection curve, v = Poisson's ratio (assumed to be 0.5), σ = Bending stress at fracture, d = Depth of the unnotched portion of the beam and $f\left(\frac{a}{d}\right)$= Function of the notch to depth ratio.

In conclusion it was stated that the Griffith theory of brittle fracture could be applied to the fracture behaviour of bitumen at sufficiently low temperatures, and the critical strain energy release rate was confirmed to be a true material property. The suitability of FM's application to bituminous mixtures, was further investigated by Bahgat and Herrin [5], who tested a variety of sand sheet asphalt mixtures. Four-point bend samples with various notch lengths were tested at different loading rates at a constant temperature of -10˚C. Bueckner's equation [15] was used to calculate the fracture toughness, *Kc*, for a beam of homogeneous material with a single notch subjected to pure bending as follows:

$$K_c = \frac{6M_c}{B(d-a)^{\frac{3}{2}}} f\left(\frac{a}{h}\right) \quad (2\text{-}17)$$

where; *Mc* = Applied moment at the edge of the beam, d = Beam depth, a = Crack depth, B = Beam width and $f\left(\frac{a}{h}\right)$ = Function of the notch to depth ratio. However, due to the heterogeneous nature of bituminous materials, the K_c value was considered the "pseudo-fracture toughness" value.

The stress intensity factor, K, defines the stress field at the crack tip, and the maximum stress intensity factor that causes failure is the critical value of, K_C, this value is known as the fracture toughness of the material which is a material property and represents its resistance to fracture when a crack is present. Therefore, K_C can be defined as a measure of a material's resistance to crack extension when the stress state near the crack tip is predominantly plane

strain [3]. The critical intensity factor, K_c, was used as a failure criterion for bituminous materials [1]. In this work, an approach, to characterize the resistance of asphalt concrete mixtures to fatigue-crack propagation, was developed based on the crack-layer theory, i.e. the system consisting of a main crack and its surrounding damage area. The philosophy behind this approach is that the resistance of asphalt concrete mixtures to crack propagation depends on the energy expended on irreversible processes (damage) in the vicinity of the crack tip. A relationships based on the thermodynamics of irreversible processes was developed to extract parameters characteristic of the pavement's resistance to fracture. This can provide a guide to the paving mixtures superior resistance to fracture and aid the lifetime assessment of load-bearing structures manufactured from these mixtures. Kim and El Hussein (1997) [32] evaluated the fracture performance of HMA using the K_c at low temperatures, between - 5°C and -30°C. The results showed that fracture toughness (K_c) increased by decreasing the temperature until - 15°C and then decreased thereafter. The reduction of fracture toughness below -15°C is explained as the effect of internal damage due to differential thermal contraction that is a consequence of the large difference in coefficients of thermal contraction between aggregate and bitumen.

It is known that hot mix asphalt (HMA) is a composite material comprising coarse and fine aggregates, filler and bitumen. This composite nature, environmental factors and test conditions play an important role in the performance behaviour of HMA, e.g. fatigue, rutting and cracking, to make performance prediction complex and difficult [76, 77]. This complex behaviour is due to the response of these components under loading – the stiffness of the aggregates is several times higher than that of binder, and deformation occurs in the binder leading to non-linear behaviour in the HMA. In addition, rotation, slippage and interaction between aggregates all contribute to this non-linear and complex behaviour [41]. This represents a major issue when studying crack growth in non-homogeneous, heterogeneous and viscoelastic materials, such as HMA where numerous cracks are created in the specimens under repeated loading conditions [44, 45]. A modification based on Schapery's work (1984) [59] was made to Paris' Law by replacing the K parameter with *J*-integral, as shown in Equation 2-39; this essential change in Paris' Law made it more suitable to characterise conditions at the crack tip [33, 34].

$$\frac{d\alpha}{dN} = AJ^n \qquad (2\text{–}18)$$

This important change in the Paris' Law paid more attention to improving the performance of this model and allowed a different perspective to understanding the mechanisms of crack propagation for developing more models. However, all these attempts were set off from Schapery's work (1984) on Paris' Law. In this regards, and for example, Si et al (2002) [63] developed a model based on the modified Paris Law using the *J*-integral [63], given in Equation 2-40. This model is based on the assumption that the micro-crack is circular in shape, and is used to calculate the fatigue life in terms of number of loadings necessary to create a crack at a specific radius.

$$N_i = \frac{\frac{n+1}{2n+1} {C_R}^{2n+\frac{1}{n+1}}}{A^{1/n}\left(\frac{b}{4\pi}\right)^{\frac{n}{n+1}}} \tag{2-19}$$

where N_i is the i^{th} number of cycles, C_R is the crack radius in mm, A and b are constants and n is a parameter that depends on the relaxation coefficient.

Masad *et al*. [41] used the same modified Paris' Law and crack radius concept to derive a model to evaluate the fracture performance of cylindrical small samples prepared from fine aggregate matrix (FAM) and tested for fatigue in stress and strain test modes using a Dynamic Shear Rheometer (DSR). This model considered more variables in predicting fracture performance, where adhesive bond energy, dissipated energy and relaxation modulus test coefficients were included as shown in Equation 2-20.

$$C_R = \left[\left(\frac{2n+1}{nb+1}\right)^{n+1}\left(\frac{G_R bc}{4\pi G_1 \Delta G_f}\right)^{n} N^{nb+1}\right]^{\frac{1}{2n+1}} \tag{2-20}$$

where: C_R is the crack radius; b and c are regression coefficients for dissipated pseudo-strain energy vs N (number of cycles); G_R is the reference modulus; G_1 is the relaxation coefficient; ΔG_f is the adhesive bond energy; and n is a material constant related to relaxation test based on Schapery's work for crack growth in viscoelastic materials [59, 60, 61].

Noteworthy, C_R was used as a crack growth index in evaluating the fatigue performance for different FAM mixes, and the results gave the same ranking order to other approaches, e.g. number of cycles at failure and cumulative dissipated energy [41]. Also, the results of the

crack growth index were found to be consistent with field observations and independent of fatigue test mode [6].

Despite being somewhat controversial, e.g. crack radius, still in all the concepts that were adopted by researchers in developing these aforementioned models, Paris' Law is still the basis for developing advanced work. It is still used extensively by researchers in studying crack propagation of asphalt concrete.

Research undertaken to date has mainly focussed on the application of fracture mechanics principles, mainly in the form of the Paris Law, to bituminous materials. The focus of many research projects over last few decades on this analysis method indicates that there is much disagreement and a different, but more consistent approach would be useful. Most researchers have applied the Paris Law criteria to traditional test methods used for bituminous materials testing. Metals testing use a test configuration, known as the Compact Tension (CT) test. The following section reviews the development of the CT test with a view to developing its use for the crack propagation analysis of bituminous materials.

2.2 The Compact Tension (CT) Specimen

In literature, several types of crack propagation tests are available for the determination of material crack properties. These properties are usually evaluated using the overall response of a sample when subjected to a specific loading mode. The response of the material depends on the specimen's geometry, test conditions and material factors. The most common types of crack propagation tests are: Indirect Tension Test (ITT) [40], Direct Tension Test (DTT) [7] 3PB-test [3] and the Semi Circular Bending (SCB) test [3, 43]. All these tests have been used in evaluating the fracture characteristics of HMA.

The CT specimen was introduced into the fracture mechanics arena in 1965 by Manjoine [40]. He developed the specimen configuration shown in Figure 5 to simulate crack growth in a closed cylindrical vessel under internal pressure. The specimen was attached to the loading frame by a threaded grip and a pin was transversely passed through a reamed hole. The load was applied at a constant head rate and measurements of the deflection were taken using a clip gauge. The plane strain fracture toughness value (K_{IC}), which is a material parameter, was calculated. In conclusion the test was deemed suitable for measuring the fracture toughness

values of metals. It was also concluded that the specimen orientation made the test particularly attractive, as it was relatively simple to manufacture.

Wessel [75] further developed the CT specimen, under the name of the Wedge Opening Loading (WOL) specimen, to allow the fracture toughness (K_{IC}) of intermediate materials to be determined, allowing their use for thin walled pressure vessels if suitable. Development had been hindered as a large test configuration was needed to test non-high strength metals. Wessel recognised the fact that specimen size requirements restricted the implementation of *KIC* evaluation programs. Efforts were concentrated on developing a relatively small, compact and efficient specimen. The configuration, proposed by Manjoine [40], was refined after a precise stress analysis was carried out and the plastic deformation found using Manjoine's configuration eliminated. Wessel [75] reported that the specimen could be used for fatigue cracking and determining crack growth rates as a function of the stress intensity factor, *K*. Various configurations were tested and the results compared to known K_{IC} values for calibration. The testing was carried out in a number of machines and attention was drawn to the alignment of the specimen especially at the pin, where a universal joint was added to aid self-alignment. Notch opening was measured using both extensometers and clip gauges. Results from a series of tests on four different metals were then reviewed. Wessel [75] then went on to propose a configuration using a two pin loading arrangement and a draft standard for K_{IC} testing.

Chan et al [16] took the results obtained by Wessel, and applied a FEA to them as seen in Figure 6, using the same test configuration. He hoped to be able to compute the stress intensity factors and hence use them in design and so eliminate testing saving time. The results he reported were deemed satisfactory, although he had difficulty in accounting for crack tip stress singularity, but it was stressed this could be improved by using more advanced computers.

Newman [46] applied the boundary collocation method to a two-dimensional compact tension specimen to gain stress intensity values. Different specimen configurations with and without pinholes were considered, to examine the effect that the pinholes exhibited. Newman reported:

- That the pin holes reduced stress intensity factors when the a/W ratio was less than 0.4.

- The pin holes also increased crack opening displacements at the load line and outer edge of the specimen.
- That the effects of Poisson's ratio and the plane strain or plane stress assumptions on stress intensity were found to be less than 0.5% for all a/W ratios considered.

He concluded by presenting an improved model to calculate stress intensity;

$$f\left(\frac{a}{W}\right) = 4.55 - 40.32\left(\frac{a}{W}\right) + 414.7\left(\frac{a}{W}\right)^2 - 1698\left(\frac{a}{W}\right)^3$$

$$+3781\left(\frac{a}{W}\right)^4 - 4287\left(\frac{a}{W}\right)^5 + 2017\left(\frac{a}{W}\right)^6 \quad (2\text{-}21)$$

For $0.2 \leq a / W \leq 0.8$

Slepetz and Carlson [64] used the CT configuration to test composites of uni-directional and cross ply S-glass/epoxy and graphite/epoxy. Fracture toughness values were determined by the compliance calibration technique and by measuring the area under the load displacement curve. The uni-directional specimens gave results which were consistent with other methods of testing, however the cross ply were inconsistent. This paper was mentioned to highlight the possibilities of using such a test on non-metallic materials.

Srawley [65] proposed a polynomial expression for the CT specimen in 1976;

$$\frac{(KB\sqrt{W})}{P} = \frac{(2+\alpha)(0.886+4.64\alpha-13.32\alpha^2+14.72\alpha^3-5.6\alpha^4)}{(1-\alpha)^{\frac{3}{2}}} \quad (2\text{-}22)$$

for $0.2 \leq \alpha \leq 1$

where: K = Stress Intensity Factor, P = Applied force, B = Thickness, W = Width (depth), α = Average crack length,

This expression is suitable for use for α /W values from 0.2-1 as opposed to 0.45-0.55, to which traditional fracture toughness testing had been restricted. The reported accuracy was 0.5% and was suitable to be applied to the study of fatigue crack growth.

As part of an experimental program to determine stress intensity threshold values Backlund and Mackerle [4] presented detailed FEA of CT specimens. Attention was paid in particular to the behaviour of the pin holes. For the CT configuration, two different types of meshes were used and the results compared seen in Figures 7 and 8. Two types of load were applied, a concentrated and a distributed, to a variety of crack lengths which were formed by applying boundary conditions to the line of symmetry. The expression;

$$K = \frac{P(2W+a)}{B(W-a)^{\frac{3}{2}}}\left[1.562 - 0.328\frac{a}{W} + 0.067\left(\frac{a}{W}\right)^2\right] \quad (2\text{-}23)$$

was presented, but with reported accuracies of +/- 2%, so it will not be considered to replace the Srawley proposal. Parameters are the same as in the previous equation.

Little et al [37] undertook a FEA of stationary cracks, in a compact tension specimen configuration, during their study using viscoplastic analysis. The study modelled exactly the same configuration that Newman had used earlier. The specimen was modelled in one half and vertical displacements were placed along the line of symmetry, ahead of the crack. In the vicinity of the crack tip region, a refined mesh was constructed. In total, the mesh consisted of 158 noded, isoparametric elements as seen in Figure 9. The results of the analysis complemented and supported earlier work concerned with small scale yielding.

Dowling and Wilson [19] presented work that they had carried out into the analysis of blunt notch CT specimens. They were interested in the crack initiation phase at areas around drill holes, etc., as seen in Figure 10.

The stress concentration factor was derived in the conventional manner using FEA:

$$K_t = \sigma/S \quad (2\text{-}24)$$

where; σ= maximum principal stress at the notch and

$$S = \frac{2P(2w+a)}{b(w-a)^2} \quad (2\text{-}25)$$

From fracture mechanics:

$$\sigma = \frac{2K}{\sqrt{\pi r}} \quad (2\text{-}26)$$

where

K = Stress intensity calculated hypothetically where the notch is collapsed to form a crack on the major dimension, where *r* = notch radius.

If equations 2-23 and 2-24 are combined to estimate a value for *K*

$$K_{fm} = \frac{2K}{S\sqrt{\pi r}} \tag{2-27}$$

where subscript *fm* distinguishes this estimate from the actual value of *K*.

For CT specimens, K can be expressed as:

$$\frac{Kb\sqrt{w}}{P} = f(a/w) \tag{2-28}$$

where; *f(a/w)* = dimensionless function of the relative notch (hypothetical crack) depth; and combining equations 2-24 2-25 and 2-27 gives:

$$K_{fm} = f(a/w)\frac{(1-a/w)^2}{2+a/w}\sqrt{\frac{w}{\pi r}} \tag{2-29}$$

In conclusion, the authors reported that the behaviour of K is similar to that when any other type of notch is analysed.

Tobler and Carpenter [71] used Newman's results to perform a 2-D and 3-D finite element analysis of the CT specimen. The FEA was based on the configuration used in the previous references but added the use of quarter points to exactly model the elastic strain singularly. In conclusion compared to the existing boundary collocation solutions, they stated:

- The present 2-D FE solutions agree to within 2% or less.
- Assuming plane stress with ν between 0 and 0.3, the 2-D numerical solutions are in near agreement with the 3-D FE results and with experiment: the differences do not exceed 4% at a/W = 0.35 and at higher a/W the differences are negligible.
- The effect of a plastic zone at the crack tip on the unloading compliances was found to be less than 5%.

- Various assumptions about pin loading, a slight shift of the pin hole spacing, and moderate notch modifications to create knife edges at the load line in j-integral test specimens have negligible effects on the calibrations.

The CT specimen has been used for Mode I fatigue crack propagation work in metallurgy successfully since it was first introduced in 1965. It has, however, not been used for testing bituminous materials, as these have, due to their viscous nature, the ability to creep, which would make the pin loading difficult. It was decided to continue to follow the CT approach as this is the preferred test method for metals testing and as such would be useful to compare results with previous fracture mechanics approaches, which generally use beams.

2.3 Summary

Fatigue cracking failures in major UK pavements are rare. This fact can be attributed to the research, which has taken place to better understand the fatigue phenomenon. Superior materials have now been introduced which have evolved from focused research that has taken place. However, for these materials, although based on sound theoretical designs, there exists no long-term knowledge of their behaviour. Indeed, recent investigations into certain test areas have resulted in the withdrawal of some of these stiffer materials due to the somewhat unusual results, which were found. Although, as stated, fatigue failures have been substantially reduced within the UK, these problems have indicated that the ultimate bituminous material for load spreading ability may not be given purely by high stiffness. Indeed, there is reason to suggest that there may well be a limiting stiffness value, which is the optimum design value for penetration grade bitumen. It appears that the decision to investigate these stiffer materials has been vindicated.

The important advances in fracture and fatigue cracking work for bituminous materials have been reviewed within this chapter. The important variables within the cracking process have been highlighted, together with the solutions that have been provided by the subsequent research.

Design aspects have been mentioned due to the relevance that they have to the way that the test methods have evolved. From complicated arrangements, the ITFT has evolved as a simple to operate, cheap method of ranking the fatigue behaviour of bituminous materials.

However, this method of testing is primarily associated with the initiation part of the fatigue process. To better understand the propagation part of the fatigue process the theory of fracture mechanics has been chosen.

The evolution of fracture mechanics has been reviewed up to the implementation of the Paris Law, which has been used by many researchers to analyse crack propagation for bituminous materials. The Paris Law approach, which was the first repeated load application of fracture mechanics has been used to analyse bituminous materials. This approach has been reviewed and suggested as a proper approach for use within the boundaries of this research. Other researchers have found difficulties when using this approach, due to the nature of the materials, and this has produced a wide range of results and no standard test method; therefore, essential modification was introduced to Paris' Law represented by using J-integral instead of K intensity factor. However, this modification does not stop using the Paris Law in crack propagation analysis. The Compact Tension test, which is used for metals testing, has been highlighted as a potential standard test. The compact tension test has been introduced and a review made of the major developments that have taken place up to the implementation of the British Standard.

2.4 Proposed Test Method for this Research

Fatigue crack propagation in asphalt materials has, largely, been neglected within the UK due to the empirical nature of the research undertaken. To understand fatigue crack propagation more thoroughly it is clear from the research reviewed that a suitable test method is necessary. One such test, the CT test, has been identified as having the potential to meet the need. Previous methods used to determine fatigue and the reasons they were not selected for this programme are:

- Beams – problems with dimensions, creep.
- Cores (ITFT) - crack initiation limitations and permanent deformation (creep).
- Trapezoidal test - heating of the sample, difficulties in fabricating the specimens and the complexity in the behaviour.

As yet, the major test used to determine fatigue within the metals industry, the CT test, has not been used to test asphalt. This may be for various reasons such as softer binders and lack of control equipment. A key purpose of this research is to attempt to develop this test, for use with bituminous materials. The test method has been chosen due to:

- Its compact nature which may allow it to be used in the field.
- Its widespread use in metals testing showing it to have a proven track record.
- Control equipment being available.
- The increased use of stiffer binders allowing for the configuration to be manufactured.

The results obtained in this study have been analysed using the Paris Law approach and compared with results from previous attempts using this method.

3 Development of the Compact Tension Test

2.1 Introduction

Fatigue crack propagation work, especially within the UK, has traditionally been carried out using beam testing. Typical data, when analysed using the fracture mechanics approach, tend to give variable results. Indeed, it appears from reviewing the work of previous researchers that they have generally published results from various test configurations and, as yet, have been unable to standardise either the test method, or the results. There, therefore, appears to be a need to develop a standard test and method of monitoring crack growth. One such test, which is the industry standard for metals testing, has shown good potential. The Compact Tension (CT) test has been reviewed in Chapter 2 and shows great potential for development for use with bituminous materials. Development within the metals testing industry has prompted British Standard 7448 [9] to be published, which set out guidelines for standard specimen geometry.

This chapter describes the development of the CT test for monitoring crack propagation within bituminous materials. The design and manufacture of the CT specimen is described in detail. The CT specimen has also been analysed using the ANSYS finite element package to check on the stress distribution, especially around the loading pins. The design of the test apparatus is outlined, including the upgrade of the load frame to a digital control system. The preliminary fatigue tests, which were carried out to check the functionality of the test method, are presented. Finally, the system of recording the digital images through the duration of a crack propagation test is described.

3.2 Design of the Compact Tension Specimen

The CT specimen has been refined over the years after its introduction by Manjoine [55] in the early sixties. British Standard 7448 [9] was introduced in 1991 following work carried out in America. This standard gives a method for determining the plane strain fracture toughness, critical crack tip opening displacement and critical *J* values of fracture toughness, which characterises the toughness of the material near the outset of the crack extension. The standard sets out specimen design criteria for the standard test specimens, rectangular cross section three-point bend, square cross section three-point bend, straight notch compact and stepped

notch compact. The standard dimensions for a valid result are obtained by referring to Table 1.

The specimen required was, therefore, similar to the one used in this study, which is shown in Figure 11.

The dimensions were selected so that the specimen could be manufactured using a standard 150mm concrete cube mould. It should be noted that the only measurement that does not comply with the standard is the half height, which is specified as being 72mm (max 72.5mm) when 75mm is used due to the mould dimensions and the difficulties encountered when trying to trim such a small width. To ensure that the specimen could withstand the loading induced during a test, especially around the loading pin area, a Finite Element Analysis was carried out using the proposed specimen dimensions.

3.3 Finite Element Analysis of Compact Tension Specimens

To gain a greater understanding of the stresses induced within the asphalt CT specimen a Finite Element Analysis (FEA) was carried out using the ANSYS computer program. In a FEA the (elastic) continuum (with its infinite degrees of freedom) is replaced by a finite number of structural elements of finite size, interconnected by a series of nodal points (nodes). The displacements found at the nodes when a load is applied, are the unknowns in the problem. The resulting simultaneous equations, obtained by substituting the nodal displacements and the nodal co-ordinates, can be solved yielding a pair of constants. This allows expression of all displacements inside the element in terms of the nodal point displacements. There is continuity between adjacent elements as the linear displacements at the interface between two elements would be the same in both elements, as the displacements of the two mutual nodal points at the ends of the interface are prescribed to be equal for both elements. The strains are constant within each element if the displacements vary linearly. The interconnecting forces between the elements can also be expressed by the nodal displacements. The equilibrium equations of the nodes are established using the two components of the nodal forces (X and Y direction) and balancing each component against the sum of the component forces of the other elements meeting the node. Forces acting at the boundary of the nodal points are then equated to the external loads or stresses. All of the resulting system of equations is then solved within the ANSYS program giving a stress

distribution for a variety of crack lengths within the CT sample. The results of the FEA can be found in Figure 12.

The FEA was undertaken using a model based on those presented by researchers [37] who developed the specimens, which were reviewed in Chapter 2. The outcome of the analysis showed that the largest stresses are found at the tip of the notch. The model is scaled to the same dimensions as the proposed design and makes use of lines of symmetry. It was found from Figure 12 that the largest stresses were found at the end of the starter notch and not at the loading pins. This result showed the sample shape to be feasible and prompted the manufacture of trial specimens.

3.4 Manufacture and Properties of Compact Tension Specimens

3.4.1 Binders and Aggregates

The range of penetration grades of binders adopted for this project is from 15 pen to 50 pen and full details of their penetration and softening point values can be seen in Appendix 1. For this project, the most common two crushed rock aggregates in the UK have been considered, namely limestone and granite. Limestone has been considered the primary aggregate, as this accounts for over 50% of all UK crushed rock consumption [26]. Figure 13 shows the particle size distribution of the HMB mixtures adopted in this project. The aggregate grading was arrived at in accordance with the specifications in BS4987 (2005) for a 20mm dense binder course recipe mixture (Table 15 in BS4987), with a stipulated binder content of 4.7% by total weight of mix. Appendix 2 provides full details of individual and combined aggregate density measurements and results. Mixtures were then compacted into cubical 150mm steel moulds, as seen Figure 14, using a vibratory compaction tool for two minutes on each face with a 149mm square compaction foot. Compaction was followed by density and voids measurements.

A calibration of the compaction time was carried out to ensure that the amount of air voids present was the same as the target figure. This was undertaken by compacting three specimens for different durations. The specimens were then checked for density and air voids. Each specimen was then sliced into three parts and each slice checked for density and air voids to ensure uniform compaction. The results of this calibration are displayed in Table 2. From these results, it is shown that a compaction time of two minutes per side gave a uniform

and suitable rate of air voids throughout the sample and was therefore used as the standard for this project.

3.4.2 Stiffness and Fatigue Properties of HMB Mixtures

The stiffness modulus of each specimen was measured in indirect tension (IT-CY) at 20°C according to the protocol in European standard 12697-26, annex C [20].

Traditional dense bitumen macadams utilise the aggregate interlock effect to produce their strength and stiffness, but the binder plays a key role in bonding the particles together after compaction. The introduction of stiffer binders has now become commonplace with the stiffness of the material being influenced by the penetration grade of the bitumen used. Figure 15 shows the effect that the penetration grade of the bitumen has on the stiffness value of the mixture.

HMB grade bitumens are produced by further air blowing the bitumen feedstock, which has already been blown from the short residue, a product of distillation. The Shell Bitumen Handbook [27], stated that "the blowing process dehydrogenates the short residue, resulting in oxidation and polycondensation, increasing the overall molecular size of the asphaltenes already present in the feed and forming additional asphaltenes from the maltene phase". The asphaltene content of the bitumen has a great influence on the rheological characteristics of the bitumen. Increasing the asphaltene content produces bitumens that exhibit lower penetration values. So, with reference to Figure 15, the 15 pen bitumen would have higher asphaltene contents than the 50 pen and hence lower volumes of resins, aromatics and saturates, which together make up the remaining constituents of bitumen.

The Indirect Tensile Fatigue Test (ITFT) makes use of the same load frame and actuator as the stiffness test. A larger actuator, reservoir and load cell were required to allow the ITFT to be carried out on HMB materials at 20ºC. The HMB mixtures behaved as expected with the 15 pen grades showing a longer fatigue life compared to the higher pen grades, except for source B.

Figure 16 shows the 50 pen material tested at 20ºC compared to a 35, 25 and 15 pen mixtures all from the crude source B, all at 20ºC. From this figure it can be noted that the 35 pen material performs better than the 50 pen and the 25 pen performs better than the 35 pen. However the 15 pen material performs worse than the 50 pen material. It was observed during

testing that the stiffer the material becomes, the less permanent deformation occurred before brittle fracture. The material does not perform nearly as well as would be deduced from the 40ºC test results or the other sources.

3.4.3 Pre-test Preparation of the Compact Tension Specimen

The design of the CT specimen requires two holes and a notch, which have been previously shown for the design in Figure 11. The holes are to allow the load to be applied via two pins, which are inserted into the holes. The load holes need to be positioned accurately and at 90° to the surface of the specimen. The best method of forming these holes is to take a core from each position which removes the material and leaves a smooth surface. To comply with the design tolerances of the specimen, a 30mm core barrel was used to form the holes. From preliminary attempts it became clear that a method of supporting the core barrel was required to prevent any lateral wander and, hence, distortion of the load holes. To achieve the required support, a jig was made which ensured the core barrel entered the sample at 90°, as seen in Figure 17.

The jig is fixed to the specimen by two screw clamps, which ensure the holes are formed at identical places on each sample. The sample with the jig fixed onto it is then placed on a table, which is secured to the coring rig as seen Figure 18. The table is levelled using the four corner adjustment screws to ensure that the sample is seated in a completely horizontal position. Two 30mm cores are then taken from the sample, which form the loading holes in the sample.

The starter notch in the CT specimen for this design was specified to be 6mm wide. To achieve this, a 5mm stone saw blade was used, which gave a notch width of approximately 6mm. The notch has to be in the middle of the specimen and a marker line was applied using spray paint and the jig as shown in Figure 19. The specimen was then clamped to the saw frame, at 90° to the saw blade, using a G clamp. To ensure the notch was cut in the centre, the blade was lowered directly behind and the specimen moved so that the guide line lined up directly with the blade. The specimen was then passed under the blade and the notch was cut into it, as seen in Figure 19. When the blade was approaching the end of the guide line, the notch was measured, at each end and in the centre. The blade was then passed through the notch making fine adjustments to ensure the length cut was within acceptable tolerances.

3.5 Development of the Test Rig

3.5.1 The Control System

The apparatus was designed to fit into the Instron 1332 100kN load frame seen in Figure 20. The load frame is a rigid structure consisting of a support base, cylindrical steel columns, a solid steel platen and a moveable crosshead. The base consists of two rectangular cross section leg weldments, which contain the support columns on which the platen and crosshead are mounted. The crosshead can be moved up and down the columns providing a working area of varying dimensions. The lower crosshead houses the load cell and servo hydraulic actuator. A 'Rubicon' digital materials testing control system, supplied by Denison and Mayes, controls the load frame. The system was designed to accommodate the specific requirements of static, fatigue and fracture test applications. A purpose built environmental chamber was fitted to the load frame to allow testing of samples at constant temperature, also shown in Figure 20.

3.5.2 The Test Rig

The test rig was based on that used within the metals testing industry. The object was to allow a load to be transferred from the load frame to the sample, without causing any point, or impact loads, to the loading points. To minimise the chance of point or impact loading within the sample a set of "bushes" was made. These bushes were machined to fit into the core holes within the sample. The bushes were glued into place prior to testing so that the load would be transferred to the sample over the whole length of the core hole.

Two pins were made up to fit through the bushes and into a cradle, which was fixed to the load frame platens. To allow the sample to be placed onto the cradle, a universal joint had to be inserted into the system.

3.5.3 Preliminary Testing

Preliminary testing was carried out to determine whether the test was going to be functional. Thirteen samples were prepared, using the same bitumen, to the method mentioned earlier in the chapter. The specimens were loaded in tension using a standard sinusoidal waveform between 0.1kN and 2.5kN at a frequency of 5Hz and a temperature of 20°C. Each of the specimens was tested to failure, with the load and number of cycles being recorded. The

sample details are shown in Table 3. A plot of load against number of cycles is presented in Figure 21. The results showed a good correlation and proved the test was potentially suitable to be used for fatigue crack propagation analysis.

3.6 Development of the Test Method

It was necessary to develop a standard test method so that each specimen was tested under the same conditions and results could be compared. For standard Mode I testing, it was decided to monitor the displacement at the end of the notch.

3.6.1 Measurement of Crack Opening Displacement (COD)

To measure the COD it was necessary to attach a LVDT across the notch opening. It was found that a 10mm LVDT was sufficient to measure the amount of displacement during a test. The LVDT was attached to the sample by a clamp set up, as shown in Figure 22.

The LVDT was attached to the specimen by gluing the fixing clamp to the surface with superglue. To ensure each measurement was taken from an identical position a template was used to position the fixing clamp. The LVDT was connected directly to the control system and was available to control the test if required. The data acquisition system was capable of storing test information generated by the LVDT throughout the duration of a test.

3.6.2 Monitoring Crack Growth

During testing, fatigue cracks initiated at the end of the notch and propagated through the specimen until failure occurred. To quantify crack growth, a method of monitoring the crack throughout the duration of the test is required. One major problem is the environmental chamber which makes the space available for equipment very limited. Previous approaches to monitoring crack growth had been made by Read [58] who used images taken throughout the duration of the test to record the crack length. This method was particularly attractive due to the space restrictions and the unknown duration for the test. Since the work by Read, undertaken in 1996, the development of technology for cameras has been focused on digital format. There are many advantages to using digital methods over the traditional and with falling costs, it was decided to pursue this method to see if it was feasible.

3.6.2.1 Digital Camera

The main objective when monitoring crack growth was to take measurements of the crack length throughout the duration of the test. With the space confinements of the environmental chamber the method chosen was required to fulfil a number of criteria;

- Cost of equipment.
- Ability to be controlled by a computer.
- Sufficient storage space (20+ images).
- Work over a range of temperatures.
- Focus crack from distance of 150mm.
- Produce images suitable for measuring crack length.
- User friendly file transfer.

After many possibilities had been identified, the camera chosen was the Ricoh-4200 digital camera. The identified benefits included;

- Cost one tenth of using conventional methods such as Single Lens Reflex (SLR), with no need for film processing.
- Has a remote control option via an infrared connection.
- Uses smart media storage cards (16MB for up to 30 images).
- Can be used at temperatures below 0°C.
- Has a built-in macro lens with a x3 zoom.
- Produces images of 1.32 million pixel quality.
- Smart media cards can be removed to transfer images quickly.

The file transfer system was complimented by adding a smart media transfer system. Two 16MB smart media cards were also used to allow the system to be used continuously. This system allowed up to 30 images to be removed from the camera and transferred to a PC via

the transfer system in less than one minute. A macro lens was also required to allow the images to be taken from the 150mm fixing point. It was found that extra lighting was required on the sample due to the enclosed nature of the environmental cabinet. To ensure that the lighting had no effect on the temperature of the sample a sealed dichroic bulb, which is normally found in perishable food fridges, was used. The test set-up is shown in Figure 23.

3.6.2.2 Remote Operation of Digital Camera

It was essential to operate the camera remotely to take images at regular intervals during a test. The camera could be operated by a remote control from a PC using an infrared trigger. The software which operated the remote control was analysed to find the code for taking a picture. From the work by Read [58], who monitored crack opening using a strain gauge across the notch, it was decided to operate the camera by using the LVDT data. The LVDT output data were channelled into a separate PC so that they could be analysed for use in triggering the camera. A program was then written using the LABVIEW code to analyse the LVDT data and trigger the camera. The amplitude (peak to peak) of the LVDT signal over the 1^{st} few cycles of the CT test, i.e. when the movement is smallest and before the crack has time to grow, was recorded. Obviously, the displacement would increase as the test proceeds and the crack grows. When the ratio of the two amplitudes dropped below the next trigger value, then the computer sent a signal to the remote control to take a photo which in turn triggered the camera. The system was calibrated using a number of test specimens until images were consistently taken at regular intervals. The program saved the results of the data collection as a general text file which noted the image number and the number of cycles at which it was triggered.

3.7 Mode II Orientation

3.7.1 Introduction

The mode I type orientation is applicable to classical fatigue crack propagation from the bottom of the pavement structure. Over recent years, however, it has been noted that this type of ‘bottom up cracking’ is rarely observed on modern well-constructed pavements. Nishizawa et al [47] have reported that theoretical fatigue does not agree with field experience for modern pavements and has proposed a figure of 200 micro-strain with the fatigue criterion not being valid below this. All modern analytical design methods restrict the tensile strains

generated at the underside of the structure to below 200 micro-strain, and hence are controlling fatigue.

Top down cracking is less well understood but was highlighted by Nunn et al [52] who investigated a number of sites in the UK. Cores taken from these sites were examined and showed signs of top down cracking only. This mode of failure is poorly understood and has, to date, received little attention from researchers. It is known, however, that asphaltic materials due to their composition are susceptible to ageing. Indeed the life of a well designed and constructed pavement structure is now governed by premature failure within the surfacing which if left untreated, will propagate to the lower structural layers resulting in structural failure. Of course the surface of the pavement structure is also directly subjected to trafficking and this will also contribute to this top down cracking. Other surface cracking which generally occurs in the longitudinal fashion is thought to be induced, by thermal stresses.

In reality it is likely that a combination of all of the above mentioned factors contribute to the deterioration within the upper surfacing. The investigations by Nunn showed most of the cracks were confined to the surface course layer of the pavement structure. These findings were consolidated by further rheological investigations which showed that ageing was generally confined to a few millimetres at the surface. Some cracks had propagated down through the upper layers into the base. The propagation of such cracks must therefore have furthered by either trafficking stresses or by thermal stresses. It is known that the traffic loading at the surface is very complex, with a blend of mode I (tensile), and mode II (shear) present; see Figure 24. The CT test was investigated to try to simulate crack propagation due to mixed mode stresses.

3.7.2 Development of the Compact Tension Test for Mixed Mode Configuration

The CT test was modified by inserting an extra pin-hole in the specimen on the opposite side to the usual ones, as shown in Figure 25. The hole was inserted using the jig previously described so that it was at the same orientation as the usual ones. The sample was then tested using the procedure described in this chapter but using diagonal loading points. The notch was obviously not in the centre of the loading points and hence was influenced by a proportion of shear stress as well as tensile stress. This mixed mode configuration was

analysed using the ANSYS FE program and Figure 26 shows the model in a deformed position which also confirmed an element of shear stress to be present.

The preliminary testing proved to be very difficult with failures often occurring at the loading point. As a high proportion of the cycling is devoted to crack initiation at the end of the notch it was decided to pre-crack the specimen under mode I conditions. This proved to be successful and allowed the testing to be completed. After a number of preliminary tests had been undertaken a pre-crack length of 5mm was used as standard. The test configuration is shown in Figure 27.

3.7.3 Mode II Test Results

It was quickly established that the crack propagation tended to move quickly to a mode I situation with all failures occurring almost perpendicular to the loading points. Figure 28 highlights this clearly, showing the crack moving away from the end of the pre-crack, until a mode I situation occurs, where it propagates in mode I. The crack leaves the line of mode I only when fast fracture takes place. This was experienced in all mode II tests and, therefore, mode I testing was concentrated on.

3.8 Discussion

Many researchers have undertaken research programmes of asphaltic materials using fracture mechanics as a method of analysing the results. This is probably due to the nature of asphalt and the difficulty in measuring fatigue parameters. With the increasing usage of stiffer materials and the development of standard testing methods for metals testing, in particular the CT test, it was decided try to implement such a test for asphalt.

This chapter has outlined the development of the CT test for use with asphaltic materials. The design of the test was taken as closely as possible from the guidelines stated in BS 7448 [9]. The design of the CT test was subjected to an FE analysis which indicated that using HMB materials in such a test would be suitable for fatigue testing. A digital control system was acquired to undertake the testing programme. After studying the test procedure for metals testing, a rig was developed which allowed the samples to be tested using the digital control system and existing load frame.

A method of manufacturing CT test specimens was developed in the laboratory. To allow further usage of the test, standard laboratory moulds were used for the production of samples. The samples were made to the requirements of the relevant BS using typical materials that would be used within the industry. A compaction method of the specimens was developed, using a vibratory compaction tool commonly used in laboratories with asphaltic materials. The samples were checked for density and air voids using standard laboratory methods. A method of preparing the specimens for the test rig was developed and a jig produced to ensure standardization. A temperature control cabinet was designed and manufactured to house the test and allow different temperatures to be used. Preliminary testing was undertaken on a number of samples, which indicated that the test method was suitable for determining the material's behaviour when subjected to cyclic loading.

A method of monitoring crack propagation during testing was developed using the advancing technology of the digital camera. A suitable camera was obtained which was mounted on a dedicated frame. A control program was used to trigger the camera linked to the LVDT mounted across the notch, allowing a range of frames to be taken during the test. A method of measuring the crack length was developed which made use of image analysis software and is described in a subsequent chapter.

The test configuration was modified to allow a proportion of Mode II stress to influence the propagation of the crack. A pre-crack was initiated under mode I conditions when the loading orientation was changed to allow mixed mode propagation to occur.

3.9 Summary of Work Done

- The Compact Tension Test has been developed for use with asphaltic materials for the first time.
- A method of specimen manufacture and control has been developed using standard UK guidelines.
- Preliminary testing has been undertaken, which produced encouraging results.
- An environmental chamber was designed and fitted to allow testing to be accurately undertaken over a variety of temperatures.

- A method of capturing fatigue crack propagation by digital image capture has been developed.
- Mixed mode testing has been undertaken using a modified version of the CT test.
- The results from mixed mode testing showed clearly that the crack propagates towards mode I from where it propagates in Mode I orientation only.

4 Results of Compact Tension Testing

4.1 Introduction

The Compact Tension test, described in Chapter 3, has been used to monitor Mode I fatigue crack propagation within bituminous samples. From each test, a series of images monitoring the crack are taken and a method of obtaining the actual lengths from these is described here. From Chapter 2, it was proposed that the Paris Law would be used as a fracture mechanics based analysis of the testing. This chapter describes the main test programme for quantifying fatigue crack propagation within bituminous materials. A method of analysing the data obtained from the tests is described. The results of the testing programme are then presented. Finally, the results are compared with some of those which have been reported by the researchers highlighted in Chapter 2.

4.2 Measuring Mode I Crack Growth in Compact Tension Samples

From each CT test, a number of images are saved, which have to be analysed to find the actual crack length. Previous work by Read [58] measured the actual distance the crack has travelled, as opposed to the straight line distance. Read [58] used white paint to better identify the crack length and this method has been used for this work. Due to the method of computing the stress intensity factor, which requires the straight line distance, it was decided to concentrate on this parameter. Each image was stored in a JPEG format and analysed using the following software.

4.2.1 Image Analysis Software

UTHSCSA ImageTool is an image processing and analysis program designed for research work. The software can acquire, display, edit, analyze, process, compress, save and print 8 and 16 gray scale and up to 24 bit color images. It can read and write over 22 common file formats including BMP, PCX, TIF, and JPEG, and also provides a generic import function that makes it possible to view image data from many unsupported file formats. Image analysis functions include dimensional (distance, angle, perimeter, area) and gray scale measurements (point, line and area histogram with statistics). Useful features of the software include standard image processing functions such as contrast manipulation, sharpening, smoothing, edge detection, median filtering and spatial convolutions with user-defined convolution masks. Spatial calibration is available to provide real world dimensional measurements such

as millimetres, microns, feet, miles, etc., for linear measures and area. Image Tool was written using Borland's C++ version 5.02.

4.2.2 Method of Measuring Crack Length

From the set of images, the onset of crack growth was defined, for the purpose of this work, as the point at which the first visible crack was noticed at the end of the notch. It was then necessary to measure each image until failure occurred. The crack length found on each image was then measured relative to the end of the notch. Before measurements could be taken the image analysis software needed to be calibrated.

4.2.3 Calibration of Image Tool

To allow calibration of the image analysis software a reference needed to be scribed onto each sample. On each sample, marks were made in pencil at 0, 10 and 100mm. As stated previously, the software allowed a spatial calibration using numerous units of measure. To calibrate the software, a line is connected between the two reference points and the actual distance entered. The calibration is then checked against other known values over different distances. If the software is giving accurate readings the crack lengths can be measured.

4.2.4 Measurement of Crack Length

After each test, every image was examined to establish the point of crack initiation. The crack length of each subsequent image was then measured as seen in Figure 29 to obtain a range for the test. From the image analysis software results (whose details can be found in appendix 3), the results can then be plotted as crack growth v number of cycles. Figure 30 shows a typical plot of crack length versus the number of loading cycles for an HMB mixture containing 50 pen binder. It can be seen from this figure that the crack growth curve is not smooth. This is because:

- The material is not homogeneous
- The crack can travel behind aggregates and be invisible
- The material contains air voids
- The white paint can sometimes affect the visibility of the crack
- Mixture variations
- Localised compaction problem
- Images taken from one side only

Due to financial constraints, measurements could only be taken from one side of the test. This fact coupled with the materials not being homogeneous can, in some cases, produce results like these shown in Figure 30. To analyse the test results using the Paris Law Equation 2-1 method, it is necessary to differentiate the crack length with respect to the number of cycles. It is reasonable to assume that the variation in measured crack length would be localised due to the position of the larger aggregate particles. It is also reasonable to assume that the average rate of crack growth over the width of the specimen would be smooth. It is, therefore, considered appropriate to apply a suitable smoothing technique to the raw crack growth data. The information stored during the test includes the maximum and minimum readings from the LVDT. The crack opening displacement or COD can be found by deducting the minimum LVDT value from the maximum (W). A plot of COD against number of cycles is shown in Figure 31 for the same material.

The COD is a measure of how much the crack opens under the application of each load cycle. It is directly related to the actual crack length, increasing as the length of the crack increases. It can be assumed that COD measurements are relative to the whole width of the crack and will be largely unaffected by small aggregate fragments or other localised anomalies, which have previously been listed. A relationship between crack length and COD exists and a typical example of this is shown in Figure 32. This relationship can be used to impose the influence of crack length over the whole width of the sample. This more representative crack length can then be re-plotted as shown in Figure 33.

4.3 Stress Intensity Factor

The stress analysis of cracks has been introduced in Chapter 2. The major loading influence when using the traditional approach to fatigue cracking within a pavement structure is mode I, or tensile mode. Mode I cracking occurs when the crack surfaces move directly apart as shown in Figure 34.

Mode I loading is encountered in the majority of engineering situations involving cracked components. Using the equation developed by Irwin (Equation 2-5), the stress and displacement fields can be determined. Mode I loading can be analysed as a 2-dimensional plane extensional problem of the theory of elasticity. K_I is known as the crack tip stress intensity factor for mode I loading. K_I values are determined by the boundaries of the body and the loads imposed, consequently formulas for their evaluation come from a complete

stress analysis of a given configuration and loading. Although there are many different types of testing configuration, expressions have been developed for most of the common ones.

K_I can physically be regarded as the intensity of load transmittal through the crack tip region as caused by introducing the crack into a state of unrest. Formulas for K_I may be regarded as formulas reflecting the redistribution of load paths for transmitting force past a crack. It is, therefore, plausible to observe that small amounts of plasticity or other non-linearities at the crack tip do not seriously further disturb the load redistribution. $K_{I,}$ therefore, represents the intensity of the linear elastic stress distribution surrounding a crack tip, where small amounts of non-linearity at the crack tip are embedded well within the field and do not significantly disturb it. Thus, each set of calculated K_I values, from CT testing, represents a unique crack tip stress field environment for small scale yielding. The stress intensity factor has units of force x length$^{-3/2}$.

As the K_I value is a linear factor, in linear-elastic stress equations, it must be proportional to the applied load and, therefore, must contain other characteristic lengths, such as crack size etc. This implies that the flaw size effects can be fully analysed only if stress analysis effects are included. From Tada [108] the geometry of the CT specimen used to calculate K_I is shown in Figure 35.

Using Figure 35 the stress intensity value K_I can be calculated from:

$$K_I = \sigma_n \sqrt{b-a} F_2\left(\frac{a}{b}\right) \qquad \textbf{Equation 4-1}$$

Where σ_n = applied stress, n = number of stress applications; a & b are the dimensions given in Figure 35.

$$\sigma_n = \frac{2P(2b+a)}{(b-a)^2} \qquad \textbf{Equation 4-2}$$

$$F_2\left(\frac{a}{b}\right) = 0.443 + 2.32\left(\frac{a}{b}\right) - 6.66\left(\frac{a}{b}\right)^2 + 7.36\left(\frac{a}{b}\right)^3 - 2.8\left(\frac{a}{b}\right)^4 \qquad \textbf{Equation 4-3}$$

4.4 Mode I Test Results

4.4.1 Main Testing Programme

The method of manufacturing the CT specimen has been outlined in the previous chapters. The overall aims of the project were to quantify mode I crack propagation in high modulus base materials (HMB's). For the duration of this work, HMB materials were defined as those containing bitumen with a penetration value of 50 or lower. In total twelve HMB bitumens from three different sources were used in the testing programme. The sources of the bitumen are confidential and will be known as source A, source B and source C. To cover the range of temperatures experienced within the UK, three standard ones were selected: 10, 20 and 30°C. A standard sinusoidal waveform was used for the main test programme. From work previously undertaken by Nunn [59], a frequency of 5Hz was used on three-point bend testing and hence was considered as standard for this work. The main variables for the main testing programme are now listed:

- Mixture - Limestone 20mm Dense Bituminous Macadam (DBM)
- Temperature - 10°C, 20°C and 30°C (0°C was used in a limited number of tests)
- Waveform – sinusoidal
- Frequency 5Hz
- Bitumen - 3 sources (12 total)
- Stress - three stress levels for each variable

For each of the 12 bitumens, a set of 9 specimens was tested, three at each temperature, at different stress levels resulting in a total of 108 separate tests. To obtain the Paris Law parameters, A and n, each of the individual test results was analysed using the process outlined in this chapter. A typical CT specimen result is shown in Figure 36. The results of the CT testing programme are presented in Appendix 4.

4.5 Summary of CT Test Results

For each combination of bitumen source, nominal penetration and temperature, three tests were carried out and the fitted values of A and n were averaged. Some appreciable scatter was experienced, which is thought to be an unavoidable consequence of specimen size and the type of test being undertaken. The average values and Coefficients of Variation (COVs) for the Paris Law parameters, A and n, are given in Table 4. The COV has been defined as the

standard deviation divided by the mean (multiplied by 100%). For the constant *A*, the COVs have been calculated using logarithms (to the base 10) of *A*, i.e. the variability has been quantified on a logarithmic scale. It can be seen from the data in Table 4 that the general trend is for the value of *n* to decrease and *A* to increase with increasing temperature for each of the materials. This indicates that the harder the bitumen the greater the sensitivity is to applied stress, and hence overloading. It can also be seen that there is a wide range of variability in fitted values of *A* and *n*, with COV ranging from less than 2% to approximately 50%.

Figure 37 shows a plot of *A* against *n* on semi-logarithmic scales. It can be seen from this figure that there is a very good linear correlation between these two parameters of the form:

$$\log_{10}(A) = D_1 n + D_2 \qquad \textbf{Equation 4-4}$$

Fitted values for the constants were found to be $D_1 = -6.15$, $D_2 = -3.35$ with an R^2 value of 0.998. It should be noted that, although the R^2 value is very high, *A* is plotted on a logarithmic scale, which significantly reduces the scatter. A relationship of this form between *A* and *n* for bituminous materials has also been found by other researchers [17]. Previous research has indicated that the stiffness modulus of a bituminous material plays a key role in resistance to crack growth [17]. The average stiffness moduli and variability (quantified by the COV) for these materials are shown in Figures 38 and 39 at 10, 20 and 30^{o}C (12 tests were conducted at each condition). The stiffness moduli were measured using the Indirect Tensile Stiffness Modulus (ITSM) [10]. It can be seen from these figures that, as expected, the stiffness moduli decrease with increasing binder penetration.

Figure 40 shows a plot of *n* versus the measured stiffness modulus of the asphalt mixture. It can be seen from this figure that, for all the materials, there is a general trend for the value of *n* to increase with increasing stiffness modulus indicating that the stiffer mixtures display a higher sensitivity to stress (and hence overloading). Also shown in Figure 40 are straight lines that have been fitted to the data (using a least squares technique) at each nominal penetration grade (the colours for the fitted lines match the colours for the symbols) using an equation of the form (each straight line has been forced to go through the origin):

$$n = D_3 \, S_{mix} \qquad \textbf{Equation 4-5}$$

where D_3 is a constant, and S_{mix} is the stiffness of the bituminous mixture.

Values for the gradients of the straight lines (D_3) for mixtures containing each nominal grade of binder are given in Table 5. It can be seen from the data in this table that, except for mixtures containing the nominal 35 pen grade binder, the fit is good, resulting in reasonable R^2 values. It can also be seen from Figure 44 that mixtures containing the nominal 15 pen binders displayed the lowest gradient indicating that the value of the exponent *n* in the Paris Law (Equation 2-1) is least sensitive to variations in stiffness of the mixture. The best fit line for the mixtures containing the nominal 35 pen binder displays the highest gradient indicating that the value of the exponent *n* in the Paris Law is most sensitive to variations in stiffness of the mixture. The best fit line for the mixtures containing the nominal 25 Penetration grade binders lies between the best fit line for the mixtures containing the nominal 15 pen binders and the best fit lines for the mixtures containing the nominal 35 pen binder.

It can be seen from Figure 41 to Figure 48 that the sensitivity to applied stress decreases with decreasing binder penetration and decreasing temperatures, i.e. increasing binder stiffness modulus. At low stress level, mixtures with softer bitumen give rise to the highest crack propagation rates but this reverses at high stress level. Figure 41 to 43 show the predicted crack growth rate versus the SIF curves for each of the binders at 10, 20 and 30^{o}C. It can be seen from these figures that, as expected, the general trend is for the predicted crack growth rate to increase as the SIF increases. It can also be seen from these figures that there is a range of gradients for the different binders and the general trend is for this to reduce as the temperature increases. There is no particular pattern to the order of the binders and the combined values of the gradient and constant *a* mean that some of the curves cross.

Figures 44 to 48 show the predicted crack growth rate versus SIF curves for each of the binders individually at the three temperatures. For all the binders, the slope of these curves is greatest at 10^{o}C and lowest at 30^{o}C. This indicates that the asphalt is more sensitive to changes in stress levels at lower temperatures. It can also be seen from these figures that the curves tend to cross indicating that at low stress levels the highest predicted crack growth rate is at 30^{o}C whereas at high stress levels the highest predicted crack growth rate is at 10^{o}C.

These findings are in line with observations made by Read in 1996 [58]. This is further illustrated in Figure 49 where the variation in the Paris Law constant *n* with temperature is shown for the mixtures containing 15 and 50 pen grade binders. It can be seen from this figure that, although there is a relatively large amount of scatter, the general trend for mixtures

containing both binder grades is for *n* to decrease as the temperature increases. At 10^{o}C, *n* is typically between 4 and 7 and the type of fracture is brittle in nature. At higher temperatures, failure becomes more ductile, i.e. creep deformation, and the value of *n* reduces to between 1 and 2 at 30^{o}C. This indicates that the sensitivity to applied load is reduced as the temperature increases. As higher temperatures transform material's behaviour towards elasto-plastic from elastic, it is questionable if LEFM can still be applied to analysing HMA samples.

Though not apparent from the averages shown in Figure 41 to Figure 48, there were large differences between the performances of different mixtures. At 20 and 30 °C, Binder B showed the poorest performance over most of the stress range shown, supporting the findings from the ITFT tests at 20°C (not shown for brevity). Differences in crack propagation rate of a factor of 10 or more were common, with nominally similar grade binders.

4.5.1 Discussion of Compact Tension Test Results

The development of the CT test, described in the previous chapter, has been used to quantify fatigue crack propagation. A major test programme has been undertaken at various temperatures using 12 HMB binders with a standard asphaltic mixture.

The method of obtaining fatigue crack lengths, using the image capture equipment has been outlined, which has proved to be a success. A process of calibrating the image software has been used to obtain accurate readings of crack length. Typical data obtained during the image capture have been presented which have been related to the number of cycles which had been applied using the control program.

A typical plot of crack length against cycles has been used to highlight the scatter, which is obtained due to the non-homogeneous nature of the materials tested. A method of smoothing these results has been highlighted using the data obtained from the LVDT, which is mounted across the specimen's notch.

The evaluation of the stress intensity factor, which is required for the analysis using the Paris Law method, is described. The stress intensity factor can be regarded as the intensity of load transmittal through the crack tip region as caused by introducing the crack into a state of unrest. Clearly as the crack grows, the intensity will increase due to changes within the

geometry of the sample and methods of determining these values for each measurement of crack length have been presented.

The test programme was undertaken on sets of nine samples of each of the twelve HMB bitumens using the standard material. The set of nine samples were split into three sets of three, which were tested at three temperatures, namely 10, 20 and 30°C. Each individual sample was tested at different stress levels at each of the three temperatures.

From the tests, it was shown that the sensitivity to applied stress increases with decreasing binder penetration and decreasing temperatures, i.e. increasing binder stiffness modulus. At low stress level, mixtures with softer bitumen give rise to the highest crack propagation rates but this reverses at high stress level.

4.6 Conclusions

- The Compact Tension (CT) test has been successfully adapted for assessment of crack growth in bituminous materials under tensile (Mode I) repeated loading.
- Linear Elastic Fracture Mechanics (LEFM) techniques have been used to determine the Mode I stress intensity factor.
- The Paris Law has been used to successfully model the rate of crack propagation.
- Results show that the general trend is for the value of n to decrease and A to increase with increasing temperature for each of the materials indicating that, the harder the bitumen is, the greater the sensitivity to overloading.
- A good correlation was found between the values of A and n in the Paris Law.
- A good correlation was found between the values of A (or n) in the Paris Law and the mixture's stiffness modulus.
- Results showed that mixtures containing the nominal 15 pen binders were least sensitive to variations in stiffness of the mixture and mixtures containing the nominal 35 pen binder were most sensitive to variations in stiffness of the mixture.

5 Modelling of Crack Propagation in Pavement Structures

5.1 Introduction

There can be no underestimation of the importance of the highways network within the UK. However, due to the nature of politics within the UK and, in particular, the short-term stay of leadership before election, a long-term strategy has been unable to be maintained. For many years maintenance budgets have been cut in favour of spending towards areas such as health and education for which public concern, in the past, has been higher. The rate of vehicle ownership has however increased over the years, as has the annual amount of mileage travelled by the owners. This combination, coupled with resentment to paying large percentages of fuel tax, which is not always used to improve travel infrastructure, has contributed to a greater need to improve highways.

The move towards long life pavements is a positive step; however, the new materials have little historical performance data. The previous chapters have attempted to better understand these new materials and focussed on some of the problems which could be envisaged. A new test method and indeed analysis approach have been applied to the materials. These approaches are, however, only successful if they can be readily applied to some form of pavement simulation, which should indicate what level of performance could be expected from their use. In this chapter an attempt is made to apply such a pavement modelling technique to the CT results and hence predict what level of performance can be expected in terms of fatigue. The approach is a new method, in the UK, of determining pavement life predictions, which incorporates fracture mechanics parameters determined from the CT test.

5.2 Conventional Pavement Design Models

Most conventional approaches for determining the fatigue life of a flexible pavement structure relate the horizontal tensile strain at the base of the asphalt layer to fatigue life using an empirical relationship determined from laboratory testing. Typically, the laboratory test geometry is chosen to simulate the stresses and strains generated in the asphalt layer of a pavement structure and un-notched specimens are often used. This means that the fatigue life measured comprises both the number of cycles to initiate the crack and the number of cycles to propagate the crack through the specimen. The relative proportion of these two phases depends on the mode of loading in the test, i.e. controlled load or controlled displacement.

The approach proposed here differs in that the detailed stress distribution in the vicinity of a crack is considered rather than just the tensile strain at the bottom of an un-cracked asphalt layer. This stress distribution is used to determine the SIF which is related to the rate of crack growth via the laboratory testing.

There are many analytical pavement design models available for the pavement designer to use. Most previous designers have used methods which tend to rely on empirical relationships between distress and stresses and strains. This is mainly due to there not being a suitable test method for predicting the fracture mechanics parameters successfully. Current pavement design in the UK is largely based on the method described in LR1132 [57]. This method uses a linear, multi-layer elastic model of the road to calculate permissible levels of the horizontal tensile strain at the underside of the binder course and vertical strain at the top of the subgrade induced by a standard wheel load. These strains are used to predict the fatigue life and the deformation life of the road in terms of the cumulative number of 80kN standard axles. The model was calibrated using performance data from 34 sections of experimental road at an equivalent reference temperature of 20^{o}C. The method is used to design roads that are predicted to carry up to 200 million standard axles. This method uses the BISAR (Bitumen Stress Analysis in Roads) system to calculate the stress at the underside of the pavement and then, considering the pavement to be a beam, calculates the Stress Intensity Factor (SIF) at the end of an assumed crack tip. Using the CT test data, the model can then be used to calculate the life expectancy of a typical pavement in terms of fatigue for the materials and temperatures tested. An advantage of this method is that it allows new materials to be used.

5.3 Pavement Distress

Pavement distress takes the form of many types, some of which, for flexible pavements, are summarised in Table 6. The form of distress, which manifests itself as fatigue, is prevalent due to one of two origins:

5.3.1 Bottom Up Cracking

It has long since been thought that cracks initiate in the base of the bound layers and, due to the repetitive loading of the traffic, grow upwards to the top. This is a reasonable assumption to make when considering engineering principles of pavement structures. It has been shown more recently [66], however, that cracks can originate at the surface and grow downward.

These top down cracks will be covered in the next section. The majority of mechanistic designers have used the bottom up method when considering failure mechanisms within flexible pavements. The design process calculates the fatigue life of the pavements by considering the tensile stress or strain at the bottom of the bound layers. The life is based upon the number of cycles that the crack will take to propagate up through the asphalt under the influence of the stress field produced by the contact between the tyre and the pavement. If a normal contact pressure is assumed then the maximum horizontal tensile stress occurs at the bottom of the bound layers, schematically shown in Figure 50, as does the maximum horizontal compressive stress at the surface.

5.3.2 Top Down Cracking

There is as yet no universally accepted theory to explain the cause of top down cracking. The whole phenomenon cannot readily be explained using only the tensile stress at the bottom of the bound layers. Most researchers have found the horizontal stresses and strains generated in the upper half of the bound layers due to normal loads to be compressive. Recent research [65] has indicated that there is a relationship between the highly non-uniform three-dimensional contact traction and pressure distribution measured between the tyre and the pavement, which induces large horizontal tensile stresses in the top section of the pavement structure. Shear tractions have also been found in both transverse and longitudinal directions. The surface of the pavement is also subjected to the elements, which has implications of ultra violet effects, oxidation and daily thermal cycles.

5.3.3 Evaluation of Pavement Distress

The amount of damage generated due to vehicle loading depends on several factors associated with the vehicle and the pavement structural characteristics. Much work was undertaken in the 1960s in America to determine the damaging effect of vehicles on pavement structures. The resulting report by AASHTO [1] brought about the concept of the equivalent single axle load. The number of equivalent standard axles can be found from:

$$N = \left(\frac{P}{P_0} \right)^n \qquad \textbf{Equation 5-1}$$

where;

P = axle load kN

P_0 = Standard axle load

n = exponent (usually 4 for flexible pavements)

It is argued [55] that the exponent of 4 is generally unsuited to the modern vehicles, which have changed axle loads, axle group configuration, tyre sizes and tyre pressures as well as changes to pavement construction and traffic volumes. The concept, however, suggests that the load applied by a car will cause negligible damage but that applied by a Heavy Goods Vehicle (HGV) will cause a more noticeable amount which will contribute to the failure of the pavement. It is fair to say that the damage caused to pavements is applied during the passage of HGVs, occurring in the contact area between the tyre and the surface of the pavement.

To limit the damage caused to pavements, the increase in traffic loading on the pavement should be minimised. This can be achieved by:

- Designing pavements to reduce the damage effect, this can be achieved by incorporating enhanced materials and better surface finishes (reduced ‘bouncing’).
- Increasing the number of axles in the axle configuration.
- Using better suspensions such as air suspensions.
- Not using super single tyres.

The maximum horizontal tensile strain at the bottom of the asphalt layer is considered to be an indicator for the potential damage due to repetitive loading of the structure. To adequately model the lifespan of a pavement, using classical methods, these stresses need to be calculated for the pavement configurations which are to be modelled.

5.4 First Response Pavement Model

To estimate crack growth in realistic flexible pavement structures using results from the CT test, a simplified modelling approach has been adopted. The analysis described in the following sections simulates the number of load applications to failure for a 'major road', representative of a UK motorway or trunk road and a 'minor road', representative of UK County road. Both pavement structures were modelled as three layer systems comprising:

i. an asphaltic layer (surfacing + binder course + base),

ii. a 200mm granular sub-base layer,

iii. a semi-infinite subgrade or soil layer.

The thickness of the asphalt layer was taken to be 350mm for the major road and 150mm for the minor road, all other structural parameters being the same for both. For each pavement structure, calculations were undertaken for the nine 20mm (maximum aggregate size) dense binder course mixtures used in the CT testing at the three test temperatures of 10, 20 and 30^{o}C. The methodology used to calculate the Stress Intensity Factor (SIF) is described in the following paragraph.

To determine the SIF in a cracked three-dimensional pavement structure subjected to traffic loading typically requires the use of advanced numerical techniques such as FEA. However, this can be complex and time consuming and often an approximate approach will suffice [17]. It is well known that, assuming the stiffness modulus of the asphalt layer is at least an order of magnitude greater than the stiffness modulus of the granular sub-base, an asphalt layer can be approximated as a beam (or plate) in bending when subjected to traffic loading [73].

To calculate the maximum horizontal stresses within typical pavement configurations, the Shell Pavement Design software package, BISAR 3.0, was used. The BISAR program was developed for the analytical examination of pavement structures. For a range of inputs the stresses, strains and displacements at any position within a multi-layered system can be calculated. The program is divided into three input sections and two output sections. The three input sections are for Loading, Layers and Positions.

- Loads – data is required from the load on the wheel and the radius of the contact area.
- Layers – data is required regarding the number of, the thickness, the elastic modulus and the Poisson's ratio of the layer.
- Positions – The x, y and z co-ordinate position within each layer where the stresses and strains are calculated can be specified. Figure 51 shows the horizontal strains calculated from the BISAR software, using details discussed in the next section, due to the increase in stiffness of the asphalt layer.

5.5 Application of Fracture Mechanics to cracking in Flexible Pavements

The fracture behaviour of an asphalt pavement will depend on the stress level, the presence of a flaw, material properties and the mechanism by which the fracture proceeds to completion. The majority of mechanistic pavement design methods assume that the crack will originate from the bottom of the asphalt layer and propagate normal to the direction of maximum tensile stress, i.e. mode I crack growth [55]. Fracture mechanics assumes that every structure contains flaws, which induce stress concentrations with the potential to form cracks. In an asphalt pavement, these starter flaws would be air voids, moisture, uncoated aggregate or too much dust. As the binder is visco-elastic, the temperature can affect the behaviour of cracks within the structure. When temperatures are low, the pavement behaves in a brittle manner and cracks can propagate by fast fracture. When the temperature is higher, cracks are more likely to propagate by progressive micro plastic straining at the crack tip. An assumption that the materials behave in a homogenous linear elastic manner was necessary [55].

Consequently, provided the bending moment, or the maximum horizontal tensile stress at the base of the asphalt layer, can be determined in a realistic way, crack growth from the base of the asphalt layer can be approximated as a plate in plane strain with a crack propagating from one edge towards the other. It has been shown that, under these conditions, the SIF is given by [24]:

$$K_I = \sigma\sqrt{\pi a}\ F(a/b) \qquad \textbf{Equation 5-2}$$

Where a is the crack length,

σ is the maximum tensile stress due to the constant bending moment,

b is the thickness of the asphalt layer, and

$$F(a/b) = \sqrt{\frac{2b}{\pi a}\tan\left(\frac{\pi a}{2b}\right)}\left\{\frac{0.923 + 0.199\left(1-\sin\left(\pi a/2b\right)\right)^4}{\cos\left(\pi a/2b\right)}\right\}$$ **Equation 5-3**

The maximum tensile stresses at the base of the asphalt layer for each combination of asphaltic material, pavement construction and temperature have been calculated using a standard semi-infinite 3-dimensional layered elastic simulation of a pavement structure [13]. A 40kN standard wheel load applied over a circular contact area of diameter 315mm (simulating a super-single tyre) was applied to the pavement surface. The response was calculated at the base of the asphalt layer directly under the centre of the loaded area. The stiffness moduli and Poisson's ratios for the subgrade and granular sub-base were taken to be 60MPa and 0.4 and 100MPa and 0.4 respectively and Poisson's ratio for the asphaltic material was taken to be 0.35. The stiffness modulus of the asphaltic material was obtained from Figure 38. It should be noted that, in reality, the stiffness modulus of the asphaltic material would be greater than the values given in Figure 38 because typical traffic loading is faster than the loading in the ITSM test. This effect has not been included in the analysis. It should also be noted that no correction has been made for the differences in the traffic loading part component of the CT test loading frequency.

The predicted horizontal tensile stresses at the base of the asphalt layer are shown in Tables 7 and 8 for the minor and major pavements respectively.

It can be seen from these tables that, as expected, the horizontal tensile stresses at the base of the asphalt layer decrease as the layer thickness is increased. It can also be seen from these tables that the horizontal tensile stress at the base of the asphalt layer increases as the stiffness modulus of the asphalt increases, i.e. as temperature decreases. This is because the horizontal tensile stress at the base of the asphalt layer increases as the ratio of the stiffness modulus of the asphalt layer and the stiffness modulus of the granular layer is increased.

The number of load applications to failure, N_f, was calculated by re-arranging and numerically integrating Equation (5-4):

$$N_f = \frac{1}{A}\int_{a_0}^{h}\frac{da}{\Delta K_I^n}$$ **Equation 5-4**

Where h is the thickness of the asphalt layer, and

a_0 is the initial crack length (taken as 1mm).

In the numerical integration, the increment in crack length was taken to be 1μm.

5.6 Discussion of Modelling Results

The results are also shown in Table 7 and Table 8 in terms of millions of standard axle loads (msa) required, causing the crack to propagate through the asphalt layer. It can be seen from this data that, as expected, the general trend is for the major pavement to withstand more load applications than the minor pavement. It can be seen from Table 7, for the minor pavement, that for the mixtures containing bitumens A and C the greatest number of load applications is predicted for the mixtures containing the 15 Penetration binder at 10^{o}C whereas for mixtures containing bitumen B, the greatest number of load applications is predicted for the mixture containing the 35 Penetration binder at 10^{o}C. The situation for the major pavement structure (Table 8) is similar for mixtures containing binders A and B. For mixtures containing binder C, the greatest number of load applications is predicted for the 25 Penetration binder at 10^{o}C.

Figures 52 and 53 show the predicted number of load applications to failure plotted as a function of the stiffness modulus of the asphalt layer for the minor and major pavements respectively. It can be seen from both of these figures that the general trend is for the predicted number of load applications to failure to increase as the stiffness modulus of the asphalt layer increases. It can also be seen from these figures that there is considerably more scatter in the predicted data for mixtures containing bitumen B compared to mixtures containing bitumens A and C. The reason for this is unknown. Figure 54 shows normalised pavement lives from Source A and Source B.

The measured values from the Compact Tension testing have been used to model pavement life. Each of the individual CT test result has been used in the model and the summarised results have been presented. The pavement thickness values have been taken from Volume 7 the design manual for road and bridges, which gives recommended values. The stress distribution was calculated using the BISAR software developed by Shell. To calculate the Stress Intensity Factor, it was assumed that the structure behaves similar to a pure bending beam. As expected, the stiffer materials exhibited the greater pavement life expectancy.

In principle, the approach detailed above should apply to any pavement structure incorporating asphaltic materials provided the stress distribution within the asphaltic layer can be determined. It is generally accepted that the thin asphalt pavements operate under controlled strain conditions whereas thick asphalt pavements operate under controlled stress conditions. The approach outlined should be equally applicable to both provided the stress conditions can be calculated.

5.7 Conclusions

- Fracture mechanics analysis was successfully used to predict pavement performance in terms design life, based on assuming a pre-cracked bitumen bound layer.
- Results show that there is a good correlation between the stiffness modulus of the asphalt mixture and the predicted number of load applications to failure.
- The predicted number of load applications to failure increases as the stiffness modulus of the asphalt increases.

6 Overview, Summary, Conclusions and Recommendations.

6.1 Overview

Pavement design procedures in France allow the use of a High Modulus Base (HMB) material known as Enrobé à Module Élevé (EME). EME is a bituminous material that uses a harder grade of bitumen compared to traditional materials. The use of these material results in typical thickness reductions of 25% to 45% in French road designs compared to more traditional bituminous base materials. Typical cost savings are up to 14% depending on the amount of bitumen used in the material. Alternatively, the material can be laid in conventional thicknesses resulting in a longer life pavement, requiring only resurfacing at suitable intervals. The aim is then for the base to last indefinitely, reducing maintenance to replacement of the thin wearing course periodically. Research carried out in the UK by the Transport Research Laboratory (TRL) resulted in the development of a material with similar properties based on a UK Heavy Duty Macadam modified with harder grades of bitumen [62]. This research led to the Highways Agency (HA) introducing three grades of HMB to the UK: HMB15 (15 Pen binder); HMB25 (25 Pen binder); and HMB35 (35 Pen binder).

However, the use of these materials in the UK was new and, therefore, no long-term experience of their performance existed. There was also some evidence that materials that exhibit a high stiffness modulus could be more susceptible to crack propagation [58]. The current procedures used to assess fatigue resistance of a bituminous material tend principally to reflect life to crack initiation. This is defined as the point at which micro-cracks coalesce to form a macro-crack. The additional time required for the macro-crack to propagate through the material is accounted for by an empirical shift factor used for all materials. In reality, it is known that, for thicker types of pavement construction, the time for crack propagation forms the greater part of the total fatigue life of the pavement. The main aim of this research was to carry out a fundamental investigation into crack propagation in HMB materials.

As the project progressed, some of the early UK contracts that had utilised HMB materials with 15 pen binder started displaying unexpected problems, detected by an unexplained drop in stiffness modulus, and in 2000 the Highways Agency (HA) suspended the use of HMB15 and HMB25. Consequently, this project has proved to be extremely timely and was enabled through an HA award to further investigate the problems associated with HMB materials.

Results from this and other similar projects provided the basis for the re-introduction of these materials with an improved specification.

6.2 Summary

This research investigated the fatigue cracking behaviour of twelve High Modulus Base (HMB) binders and mixtures. The research was instigated in response to the introduction of these HMB binders from France, which has been explained in the preceding overview, as it was thought that these materials were not particularly well understood. In hindsight, this view was proven to be correct, as numerous problems have been experienced after using such materials.

6.2.1 Material Description

Early in the project it was recognised that the constituent materials could have a significant effect on the performance of HMBs, particularly with respect to crack propagation. To restrict the number of variables to a sensible level, a standard 20mm dense binder course mixture was used with one main limestone aggregate type, with a small number of tests performed using a granite aggregate for comparison. It was recognised that the grade and source of binder would have a significant influence on the performance of the material so four nominal binder grades were chosen, namely 15, 25, 35 and 50 pen, each from three different sources referred to as A, B and C. A limited number of tests were also performed using a polymer modified binder, based on a 25/35 penetration grade.

In summary, it was evident that there were large differences between the behaviour of the different binders, even at nominally similar penetration grades. This would be expected to lead to significant differences in mixture stiffness. However, there was nothing to suggest that any one binder should perform better than the others in inhibiting fatigue cracking of mixtures.

6.2.2 Crack Propagation Testing

Early in the project it was decided to develop a crack propagation test method that could induce both pure Mode I, i.e. tension, and mixed Mode I/Mode II, i.e. tension + shear, stress states. After reviewing the literature, the Compact Tension (CT) test was identified as being potentially suitable for this purpose [4]. Consequently, a relatively large amount of time was

devoted to developing the CT to be suitable for testing bituminous materials. Specimens were compacted in a standard concrete cube mould using a vibratory hammer with a preheated square foot. A purpose-built jig was designed and manufactured to allow the pin holes to be cut using a 30mm core drill and the starter notch to be cut using a 5mm stone saw. The load was applied to the specimen perpendicular to the notch through circular pins that are located in aluminium bushes to limit creep deformation taking place during the test. Tests were performed under controlled load. Testing was carried out over a range of temperatures (10 – 30°C), load levels (0.2 – 3.3kN) and loading frequencies of 2.5 and 5Hz. A Linear Variable Differential Transducer (LVDT) was used to measure the Crack Opening Displacement (COD). Crack growth was measured using an automatic digital camera and an image analysis technique that was developed specifically for this test.

6.2.2.1 Mode I Results

Analysis of Mode I tests was carried out using a Fracture Mechanics approach. It was shown that the resulting crack growth curve is not smooth. This is likely to be due to the way that the crack grows around individual large aggregate particles. Unfortunately, this curve had to be numerically differentiated for use in the Paris crack propagation law [64], which resulted in a large amount of scatter. Consequently, a method of smoothing the crack growth curve was required. A number of different approaches were investigated. It was found that the measured COD versus number of cycles plot was significantly smoother as this is an overall measure of the compliance of the specimen. Consequently, a relationship was developed between the COD and the measured crack length using linear regression and the Crack Tip Opening Displacement was used to produce a smoothed crack growth curve. This smoothed curve was then numerically differentiated and plotted against the Mode I stress intensity factor range, calculated using standard linear elastic Fracture Mechanics techniques, on double logarithmic scales to determine the Paris Law constants, A and n. The constant n defines the slope of the line and the constant A defines the rate of crack growth (da/dN) at a Mode I stress intensity factor range of $1 N/m^{3/2}$. The constant n characterises the sensitivity of the crack growth process to applied stress. For example, a high value of n indicates that a relatively small change in stress would result in a relatively large change in the rate of crack growth.

For each combination of bitumen source, penetration and temperature, three tests were carried out and the results averaged. Some appreciable scatter was experienced which is thought to be an unavoidable consequence of specimen size. The results showed two key facts:

- The harder (colder) the bitumen is, the greater the stress sensitivity. At low stress level, mixtures with softer bitumen gave rise to the highest crack propagation rates but this reverses at high stress level. Thus, colder or harder grade mixtures were sensitive to overloading. These findings are in line with observations made by Read [58].

- Though not apparent from the averages, there were large differences between the performances of different mixtures. At 20 and 30°C, Binder B showed the poorest performance over most of the stress range considered, supporting the findings from ITFT tests at 20°C. Differences in crack propagation rate of a factor of 10 or more were common, with nominally similar grade binders.

6.2.2.2 Mixed Mode Results

A limited number of mixed Mode I/Mode II tests were undertaken using a modified form of the standard CT geometry. An additional pin hole was drilled in the sample so that the load could be applied at an angle to the plane of the notch. The procedure was first to induce a starter crack under Mode I loading and then to apply the angled load, thus inducing both tensile (Mode I) and shear (Mode II) stresses at the crack tip. The crack changed direction and grew in a direction approximately perpendicular to the line of the loading. A Finite Element analysis of this test configuration confirmed that the direction of crack growth was approximately such that there were no shear stresses at the crack tip – the crack effectively orientated itself so that it continued to experience Mode I stress. All the specimens tested displayed this behaviour. This has important implications for the modelling of surface-originating cracks in an asphalt pavement, where complex stresses result in a non-vertical direction of maximum tension.

6.2.3 Fracture Mechanics Modelling and Predictions

Results from CT testing naturally lend themselves to a Fracture Mechanics based modelling approach. However, to apply this approach to a realistic pavement structure requires the Mode I Stress Intensity Factor (SIF) to be calculated for various pavement structures and

crack lengths. It is well known that, assuming the stiffness modulus of the asphalt layer is at least an order of magnitude greater than the stiffness modulus of the granular sub-base, an asphalt layer can be approximated to a beam (or plate) in bending when subjected to traffic loading [73]. This can be achieved using Finite Element Analysis but can be very time consuming and extreme care has to be taken when generating the mesh around the crack tip. To simplify this, the program BISAR has been used to generate the stresses and strains within the modelled pavement structure.

An inherent difficulty in Fracture Mechanics is the need to assume a starter crack and, unfortunately, the predicted life to failure is highly influenced by the assumed starter crack length. However, at crack lengths of between 10% and 50% of the total bituminous layer thickness, an approximately linear relationship was noted [31] between the logarithm of inverse crack propagation rate and crack length. Extension of this relationship back to zero crack length allowed pavement life predictions to be made independent of any starter crack. The predictions averaged only 3×10^6 standard axles at 20°C but it is recognised that a large factor is commonly required to adjust laboratory derived fatigue performance to that in the pavement. This is because, in the pavement, cracks have time to 'heal' during rest periods between load pulses. At 10°C, the average life prediction is over 100 times as long, but at 10°C much less healing would occur. At 30°C, the prediction is 100 times less but, in reality, the effect of healing would be much greater at 30°C. The relative contributions to fatigue failure of different temperatures is an ongoing research area. However, if all the predictions are normalised to those for mixtures with a 50 pen binder, then effectively assuming predictions for this material are correct, leading to averaging over the three bitumen sources and including the strain-based predictions. If the Fracture Mechanics derived points for 15 and 25 penetration at 20°C are treated as anomalous, there is a clear trend for predicted lives to be greater for 35 and 25 pen mixtures than for those of 50 pen, but a clear danger that 15 pen mixtures are less good. This is most apparent at 10°C, giving rise to the suspicion that the danger would increase further at even lower temperatures. Interestingly, in this study, the stiffness and fatigue data for the selected polymer modified mixture combined to give pavement life predictions similar to those for the unmodified 15 pen grades.

These deductions have only been made possible by acknowledging that fatigue behaviour is radically different at different temperatures, a fact which is not currently taken into account in

most pavement design procedures. It appears that a test at 10°C or lower is needed to characterise bituminous mixtures reliably for UK design.

6.3 Conclusions

The following are the key findings of this project:

- The Compact Tension test has been proved to be an effective means of testing bituminous mixtures for their crack propagation resistance, allowing the study of temperature effects.
- Crack propagation is dramatically affected by both binder hardness and temperature.
- In a pavement, the current approach to design, assuming a single fatigue characteristic, underestimates the life of 35 and 25 pen mixtures. However, it probably overestimates the life of 15 pen mixtures by not accounting for the effects of low temperatures.

6.4 Recommendation for Further Work

6.4.1 Performance of HMB Materials

This research has highlighted the problems of implementing a material into service without making a comprehensive assessment of its long-term behaviour. It is clear that this research has been both warranted and worthwhile. The industry has suffered from being spoon fed over the last half century with recipe specifications inhibiting adequate pavement research. This factor together with the introduction of equipment that measures stiffness properties of bituminous materials has resulted in the quest for stiffer materials without paying attention to their limitations. In hindsight it is clear that proper attention should have been afforded to mixture design. In France, a well-documented procedure has been developed as evaluated by Nunn and Smith [36], which assesses variables such as ageing, deformation, fatigue and water resistance. It is recommended that this system be investigated to see if it is feasible to use within the UK.

6.4.2 Top Down Cracking

Results from mixed mode testing show that the crack propagates towards mode I propagation. This could contribute to the phenomenon of top down cracking, which from field observations has been show to grow only part of the way through the pavement structure. These cracks are starting to form at the surface of a pavement as mixed mode cracks then at a depth could slow

down as they try to move to mode I conditions. A finite element program should be used to model the propagation of surface cracks to verify if they slow down as they move towards mode I conditions.

6.4.3 Binder Embrittlement

Results from ageing tests carried out on HMB mixtures have shown that the 15 pen materials suffer from short-term ageing. This could be as a result of the bitumen having a higher proportion of heavy fractions, for stiffness and, less lighter fractions, which aid adhesion. As grades as low as 25 pen have performed adequately, research should be undertaken to check if HMB 35 and 25 pen grades would fail sooner than expected. This could occur if 50 pen was an optimum grade for mixtures used in the UK. If 50 pen grades, which fail now after completing a service life well above that which was designed for, have failed due to ageing, and losing lighter fractions in an ageing process, then it is feasible that other HMB materials could become embrittled sooner than expected. A study on the ageing process is, therefore, required to better understand the failure processes within asphaltic materials.

6.4.4 Fatigue of Asphaltic Materials

Fatigue behaviour is radically different at different temperatures, a fact which is not currently taken into account in most pavement design procedures. It appears that a test at 10°C or lower is needed to characterise bituminous mixtures reliably for UK design.

7 Figures

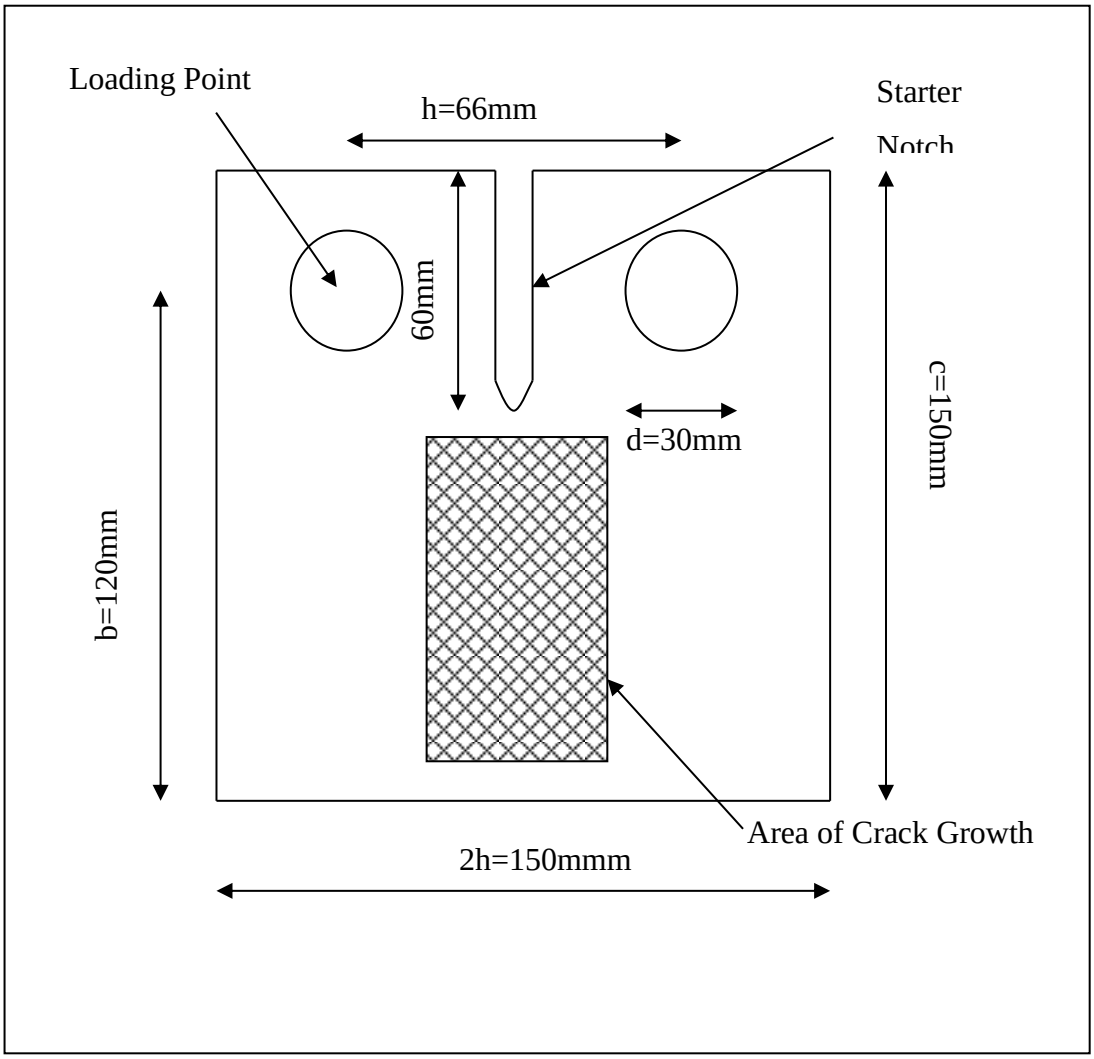

Figure 1: Compact Tension Test Configuration.

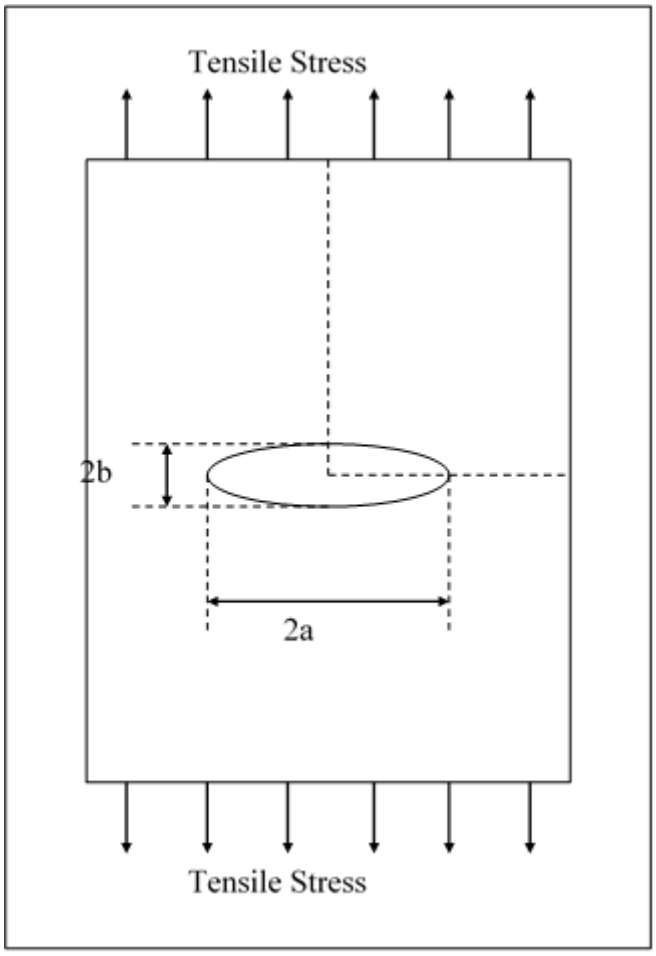

Figure 2: Inglis' experimental work on 'stress concentration at the tip of an ellipse' [43].

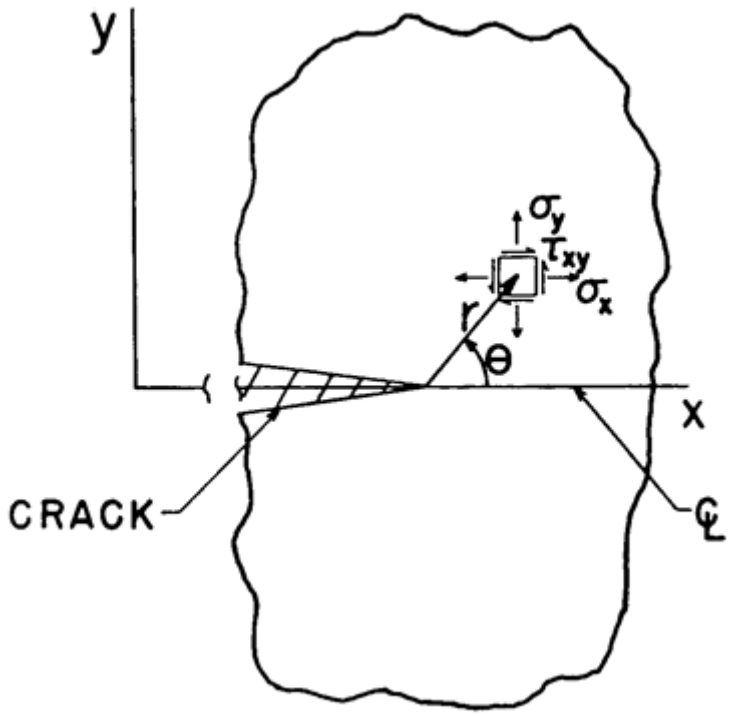

Figure 3: Coordinate system used to describe stresses near a crack tip

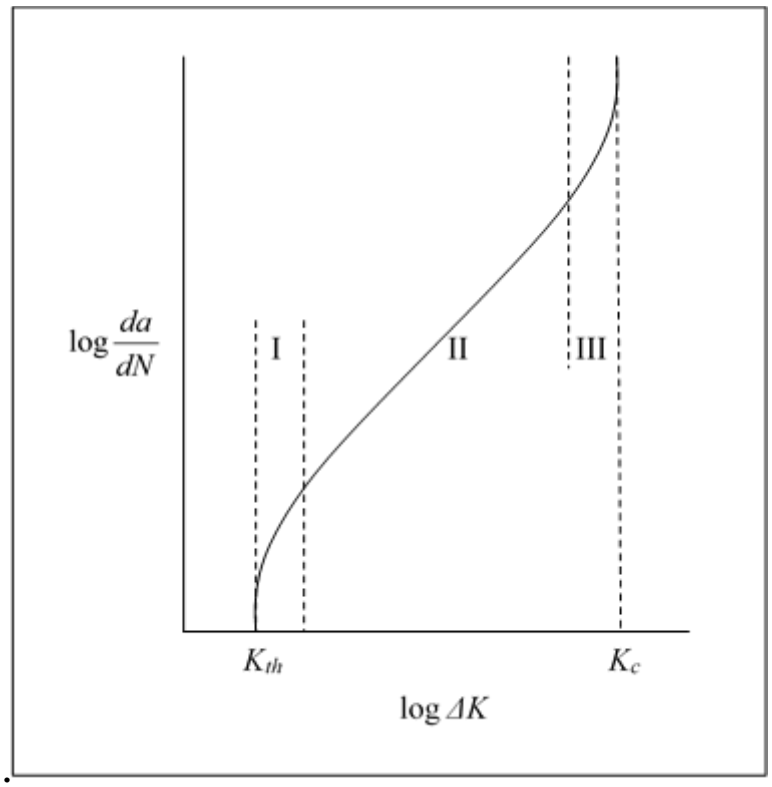

Figure 4: Regions of *ΔK* values during crack propagation.

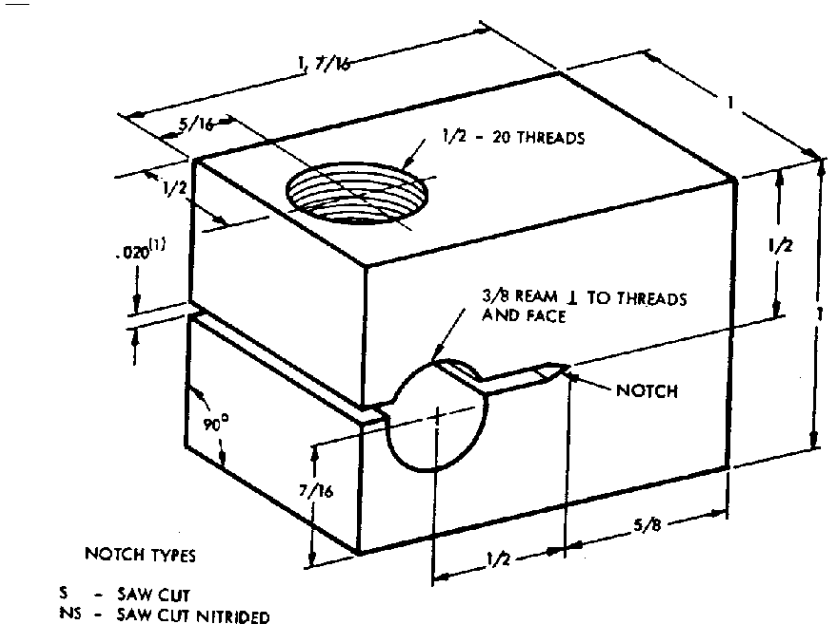

Figure 5: The CT specimen introduced by Manjoine [57].

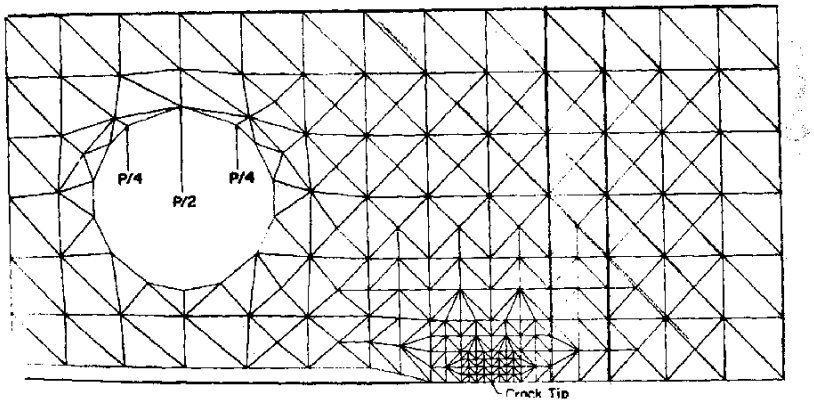

Figure 6: Finite Element analysis of CT specimen by Chan et al [28].

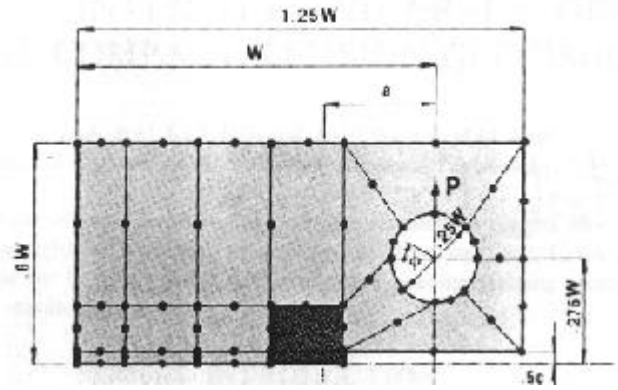

Figure 7: Coarse mesh used by Backlund and Mackerle [6].

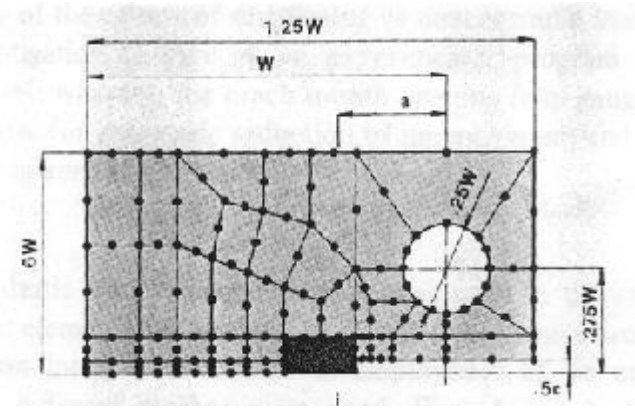

Figure 8: Fine mesh used by Backlund and Mackerle [6].

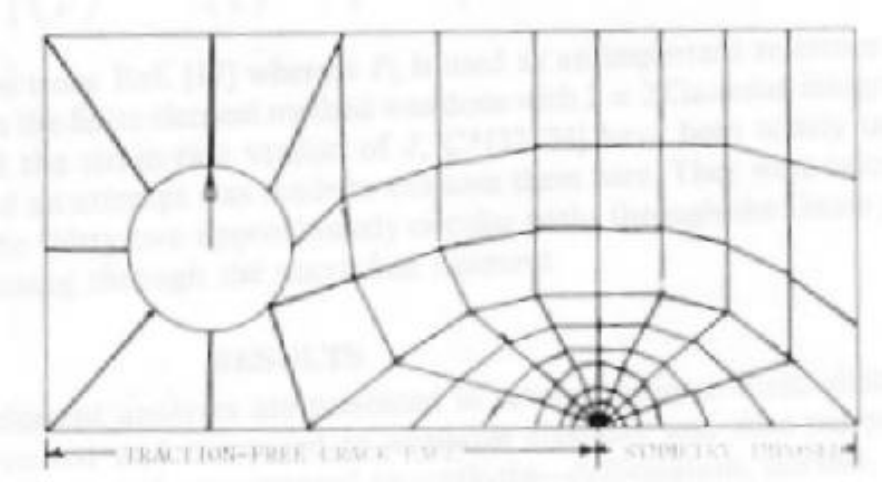

Figure 9: Finite element analysis, of stationary cracks, in a compact tension specimen configuration by Little et al [50].

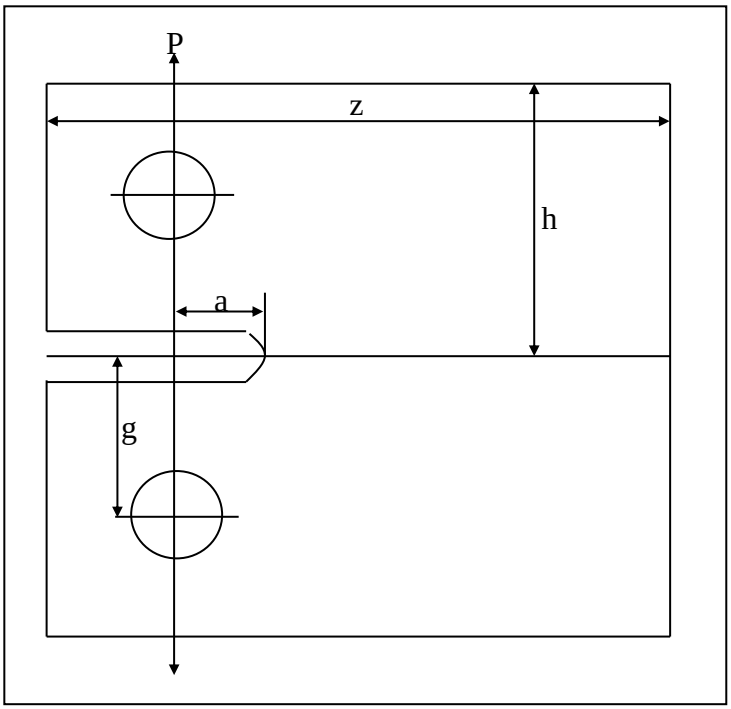

Figure 10: Blunt notched specimen by Dowling and Wilson [33].

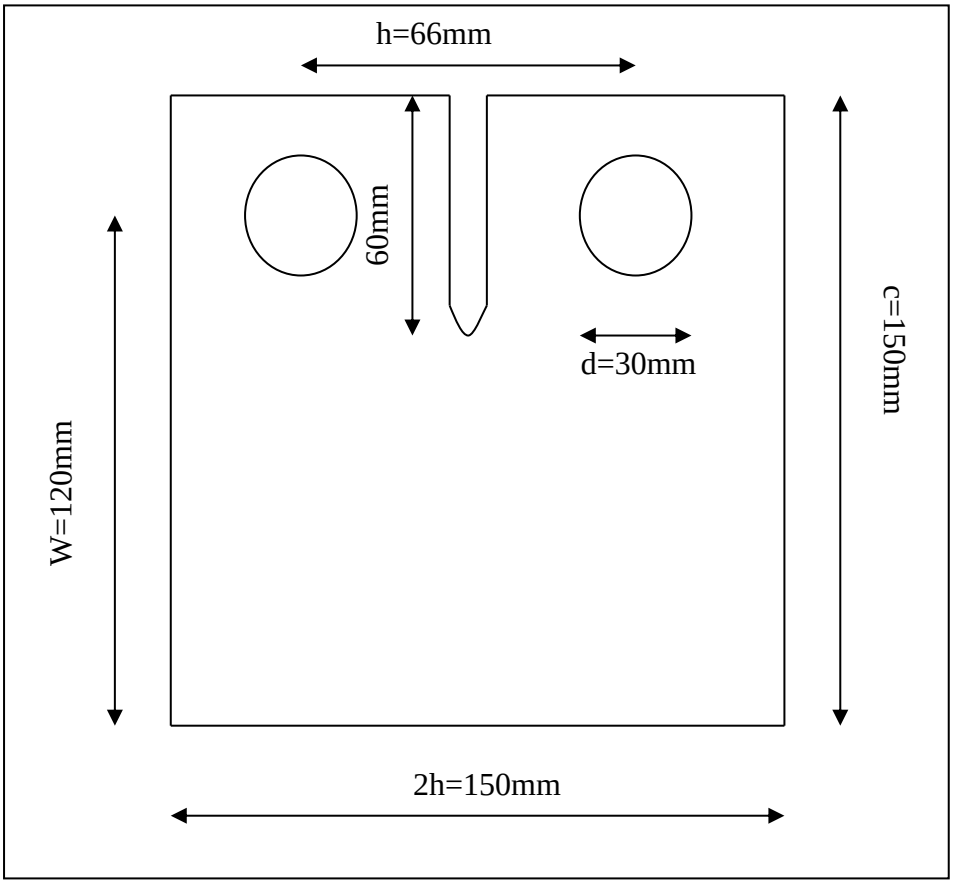

Figure 11: Design of Compact Tension Specimen.

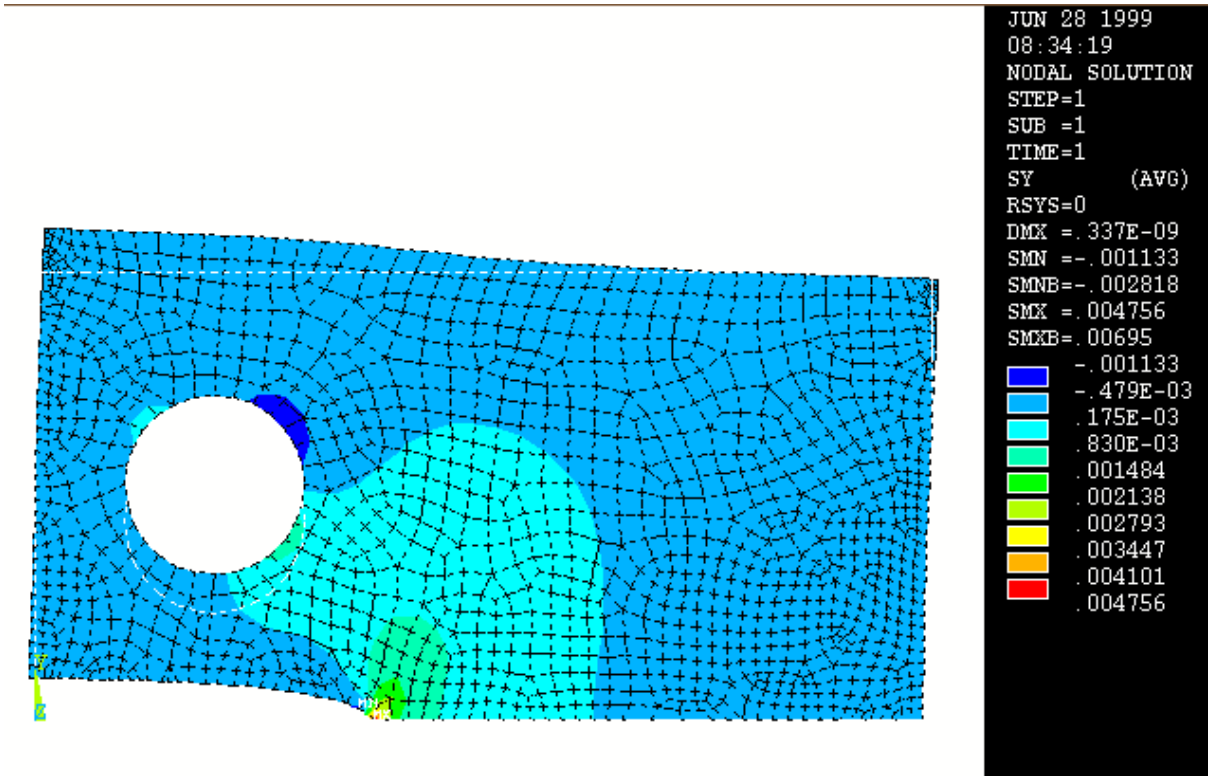

Figure 12: Finite Element Analysis of Compact Tension Specimen.

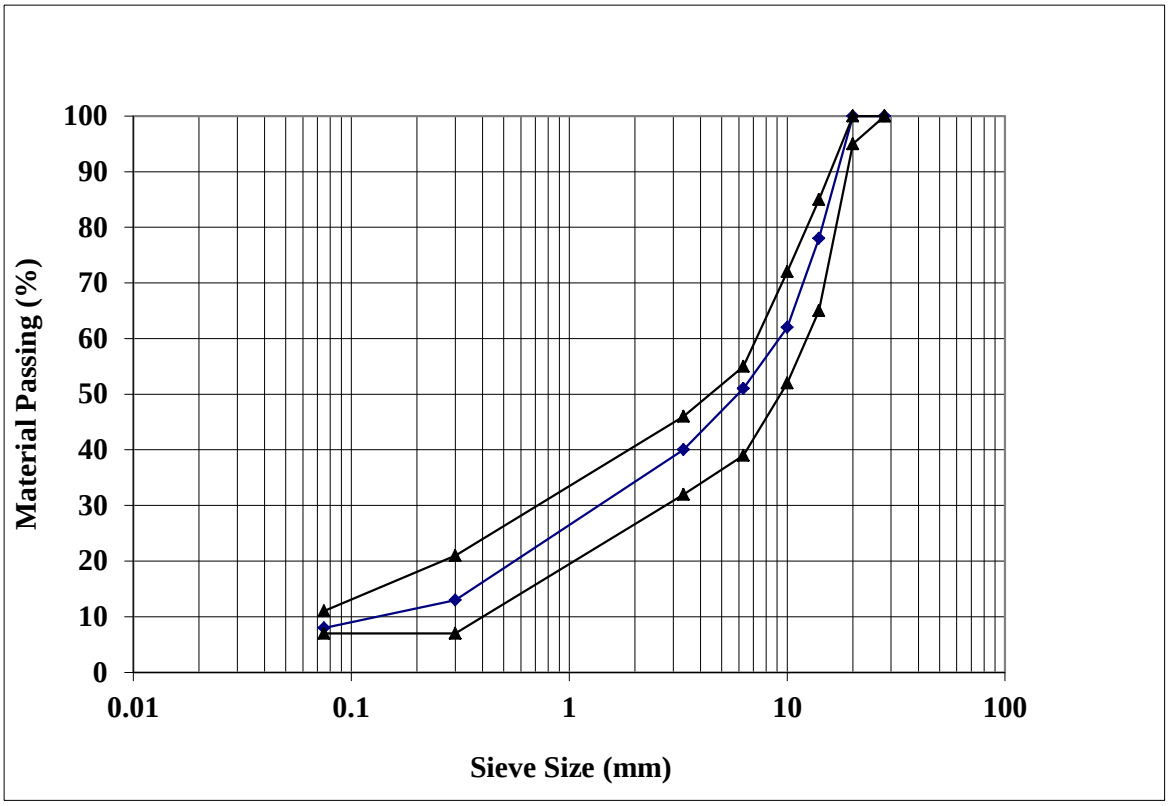

Figure 13: PSD of Limestone Aggregate used for HMB samples.

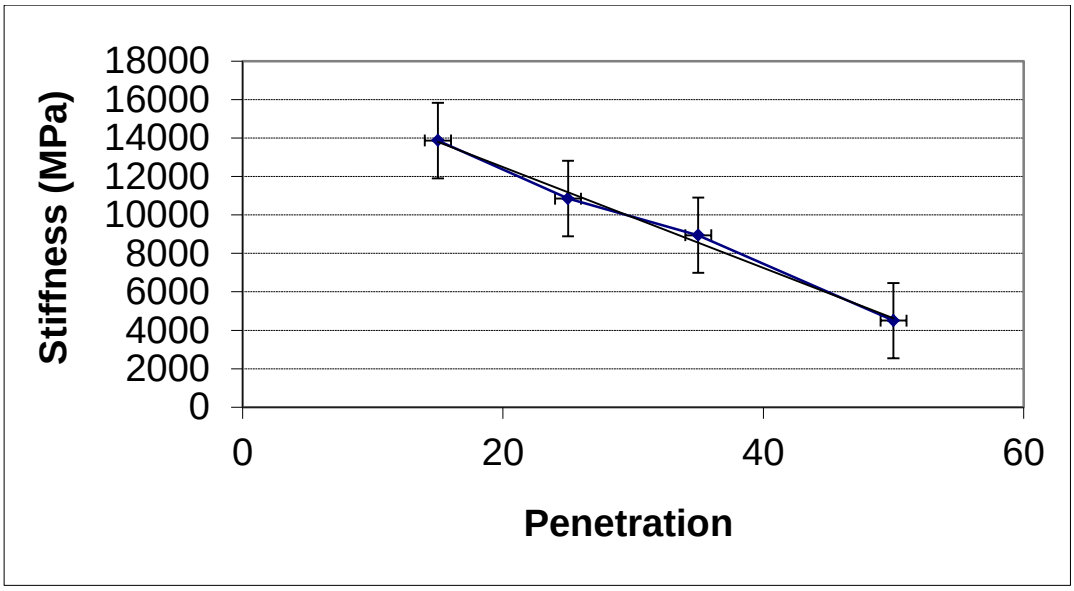

Figure 14: Effect of bitumen penetration on the stiffness of HMB materials at 20ºC (average of 12 ITSM results per point).

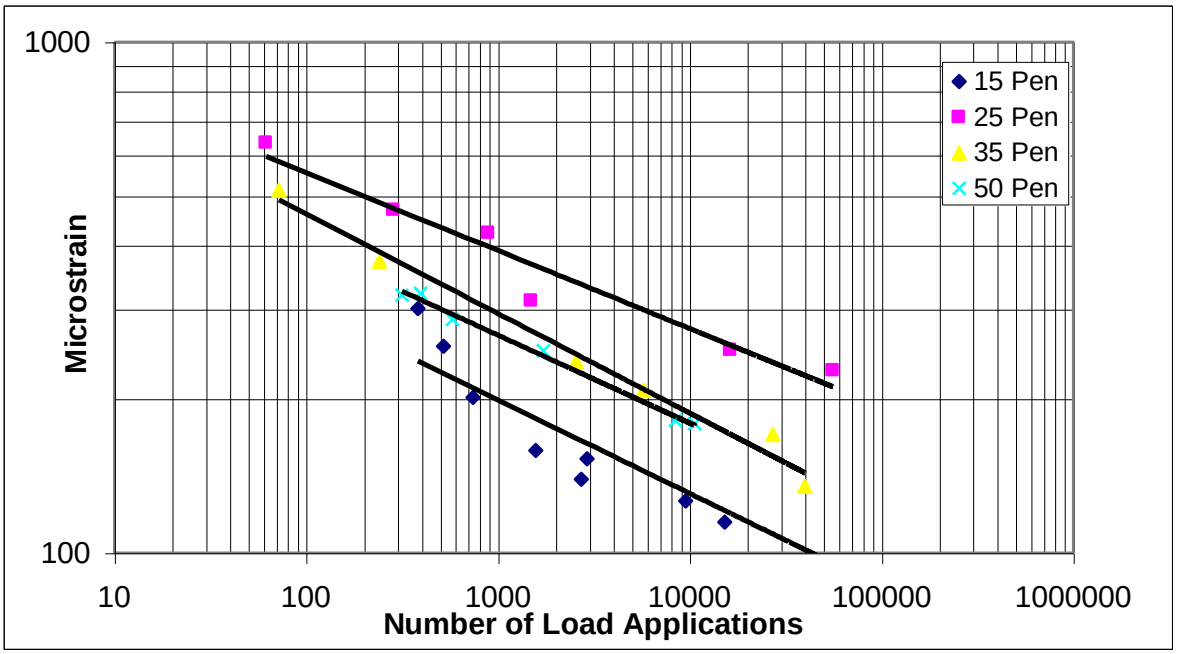

Figure 15: Wohler fatigue lines for 15, 25, 35 and 50 pen HMB's from the same crude source tested at 20ºC.

Figure 16: Vibratory (Kango) Hammer and Cube Mould used in compaction.

Figure 17: The Compact Tension Jig

Figure 18: Forming the Load Holes into the Compact Tension Specimen.

Figure 19: Making the Notch Saw Cut.

Figure 20: The Instron 1332 100kN Load Frame.

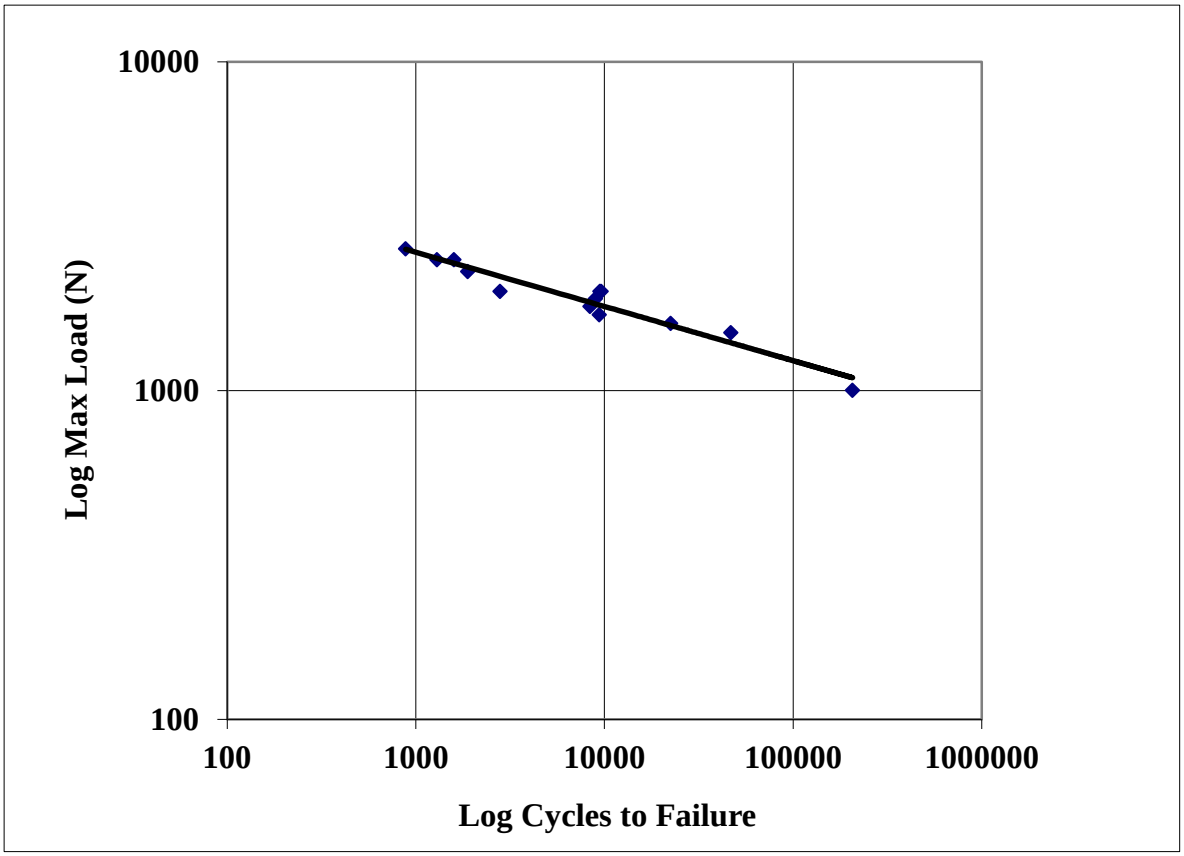

Figure 21: Preliminary Testing of Compact Tension Specimen.

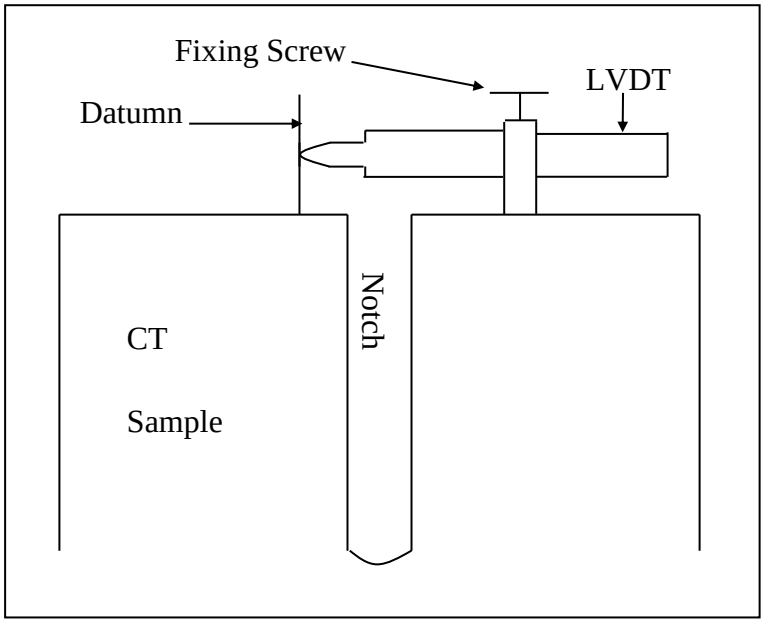

Figure 22: LVDT Set-up to Monitor COD.

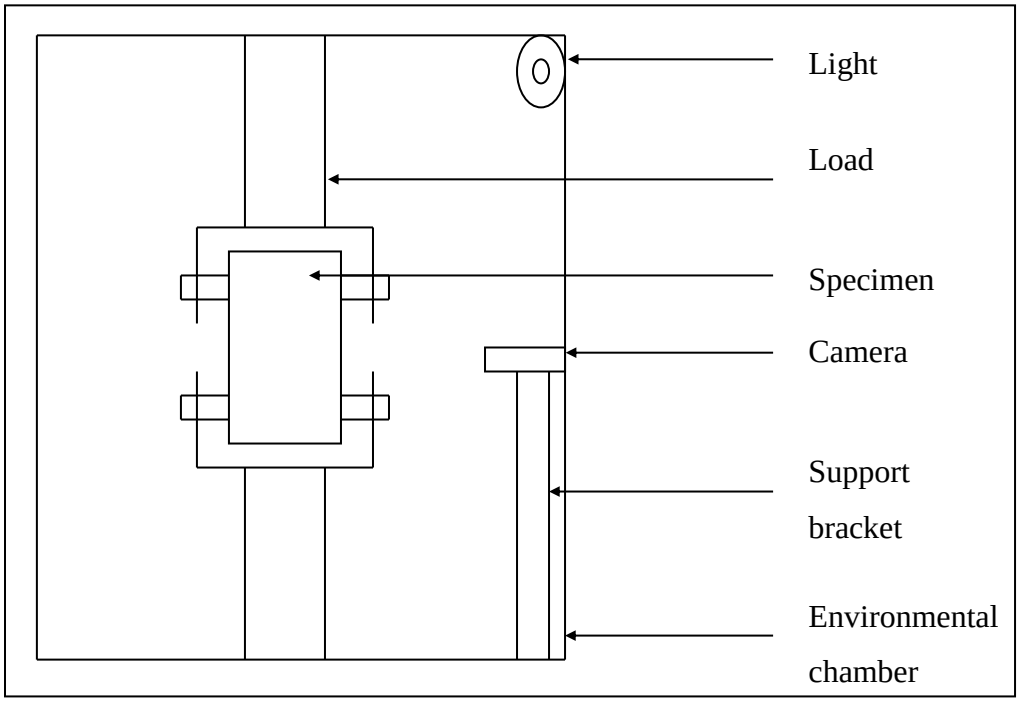

Figure 23: Compact Tension Set-up.

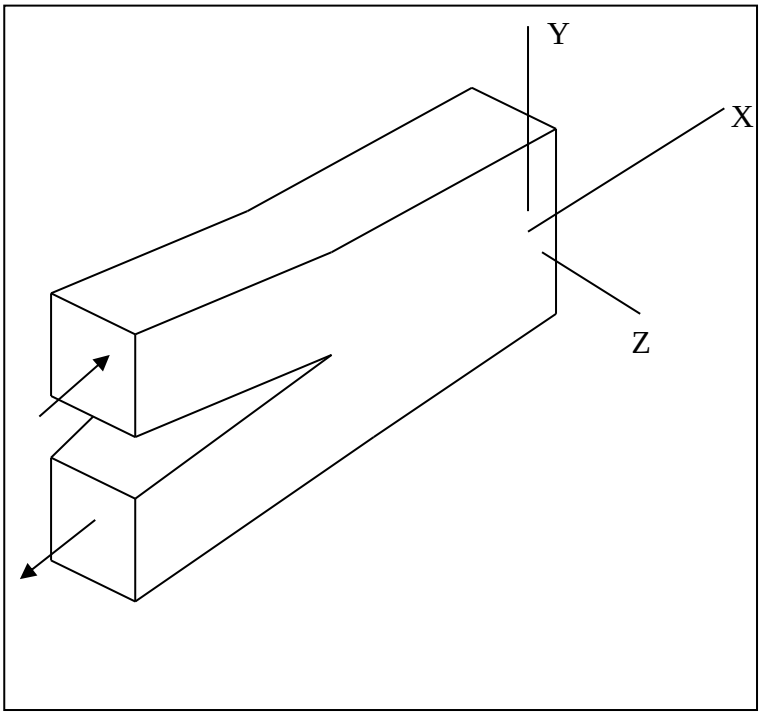

Figure 24: Mode II - Opening or Tensile Mode.

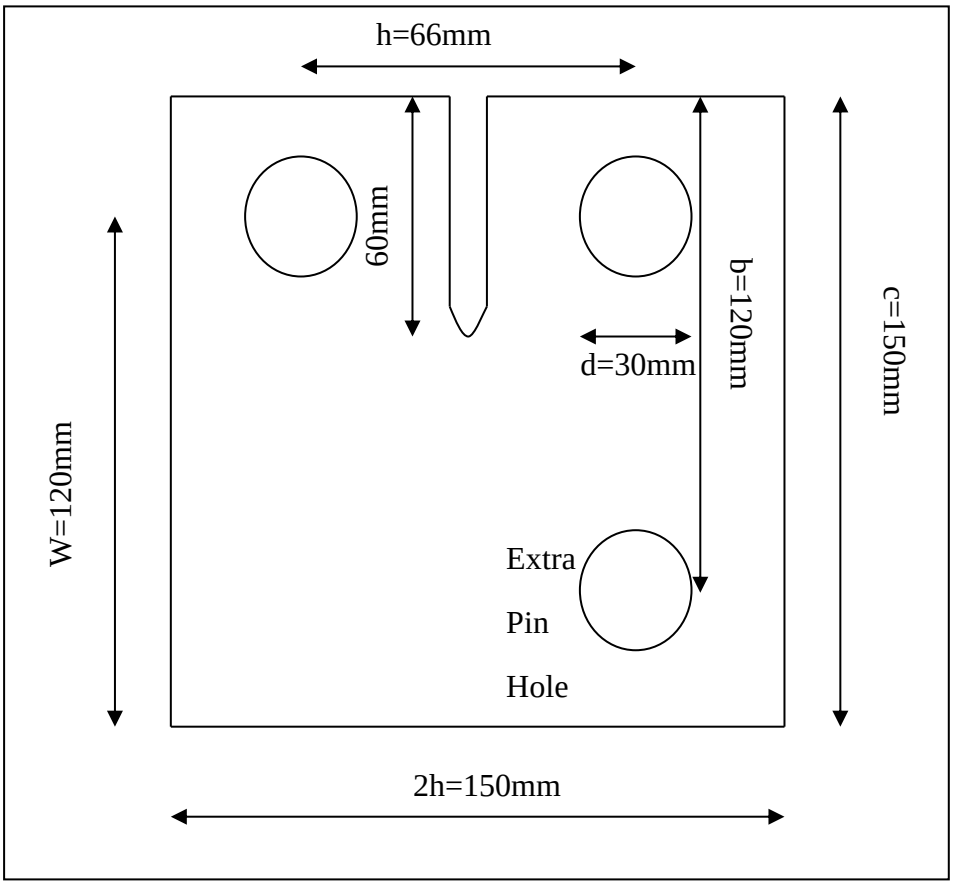

Figure 25: Position of the Extra Pin Hole in the CT Specimen.

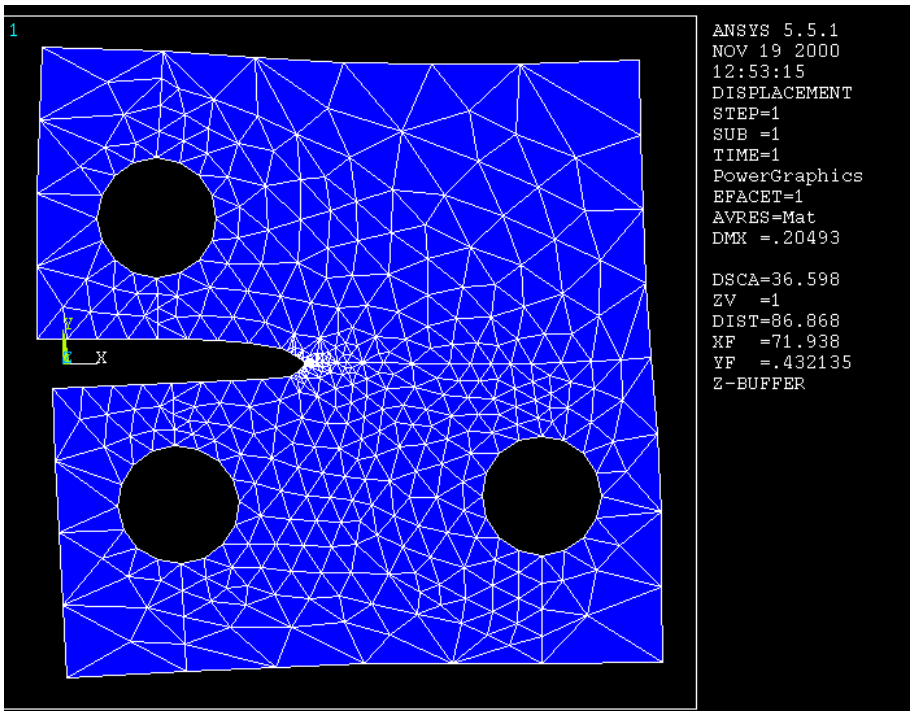

Figure 26: FE Analysis of CT specimen in Mode II test configuration.

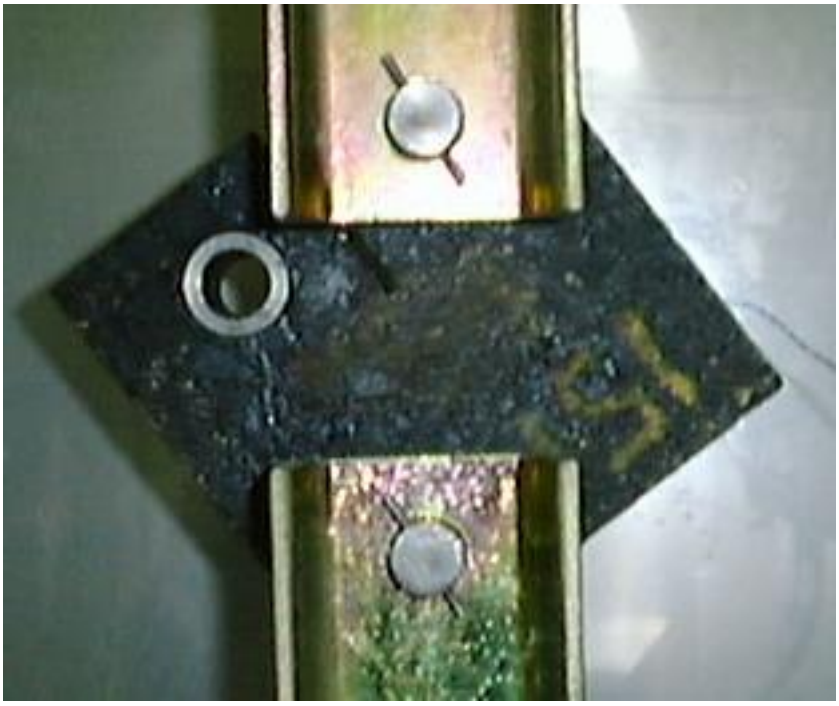

Figure 27: Mode II testing configuration.

Figure 28: Mode II sample after test.

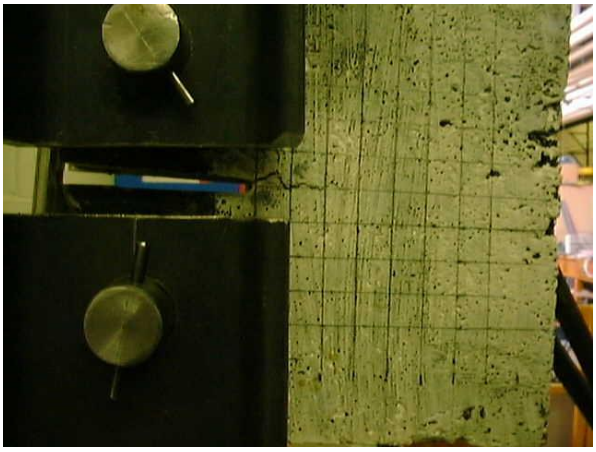

Figure 293: Measurement of Crack Length *a.*

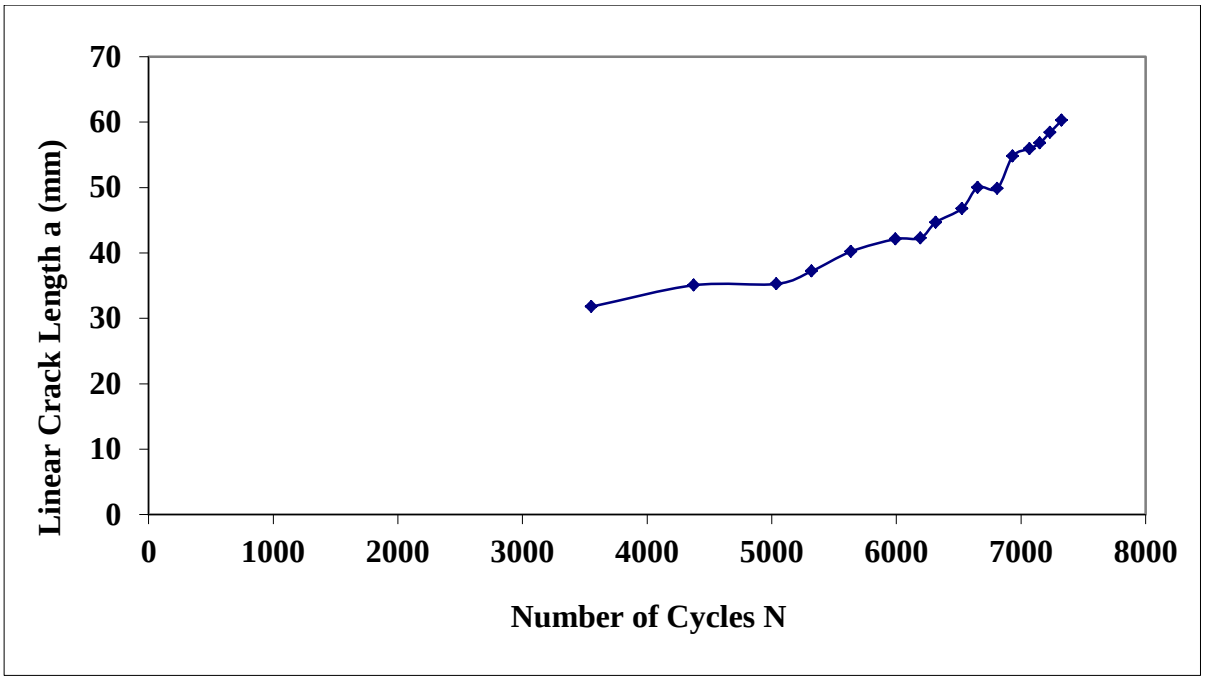

Figure 30: Crack Growth v Cycles for 50pen HMB mixture.

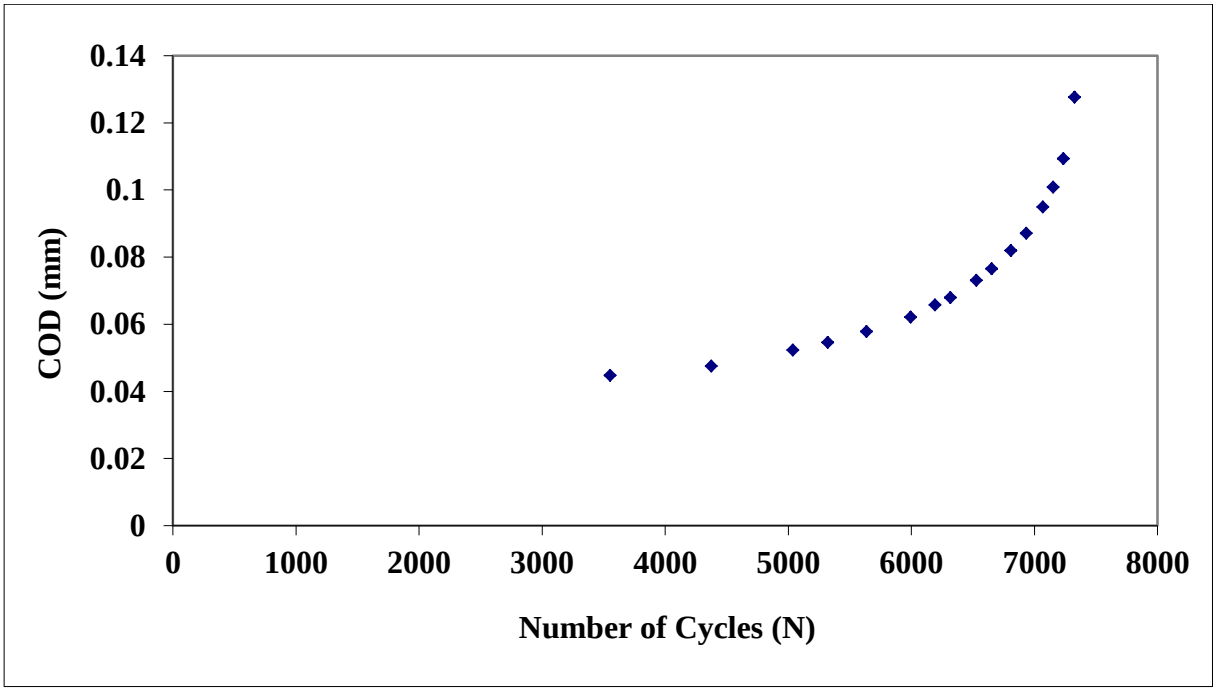

Figure 31: Plot of COD v Number of cycles for 50pen HMB mixture.

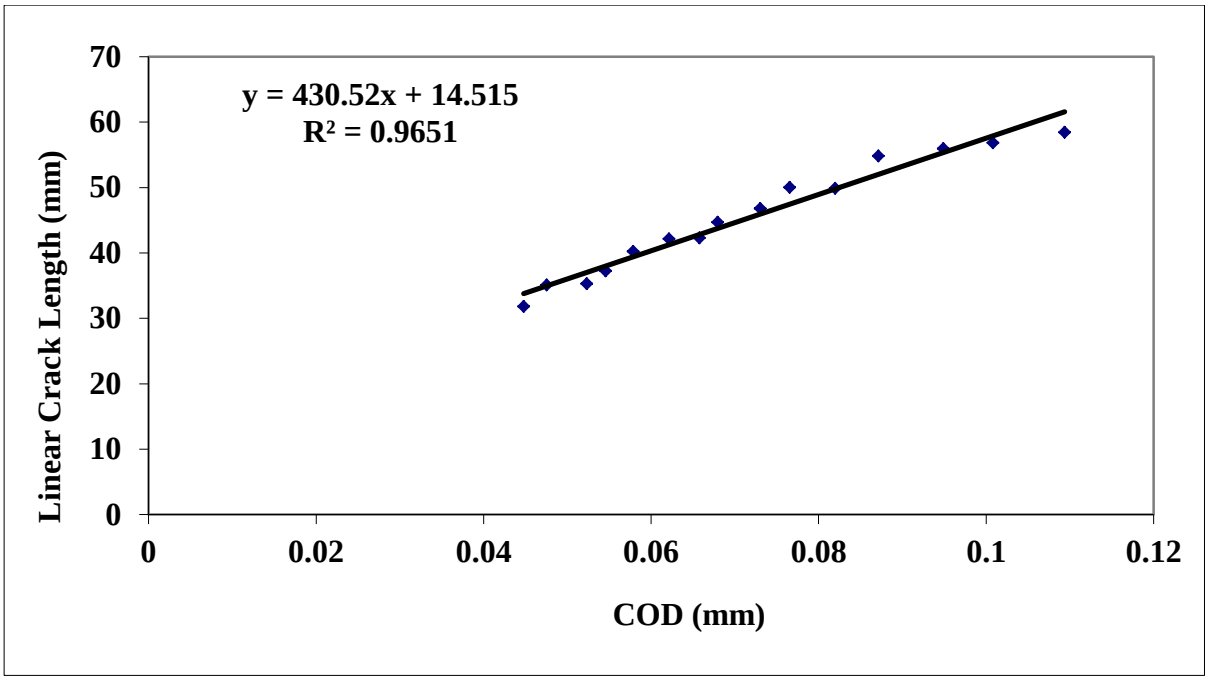

Figure 32: Relationship between measured crack length and COD.

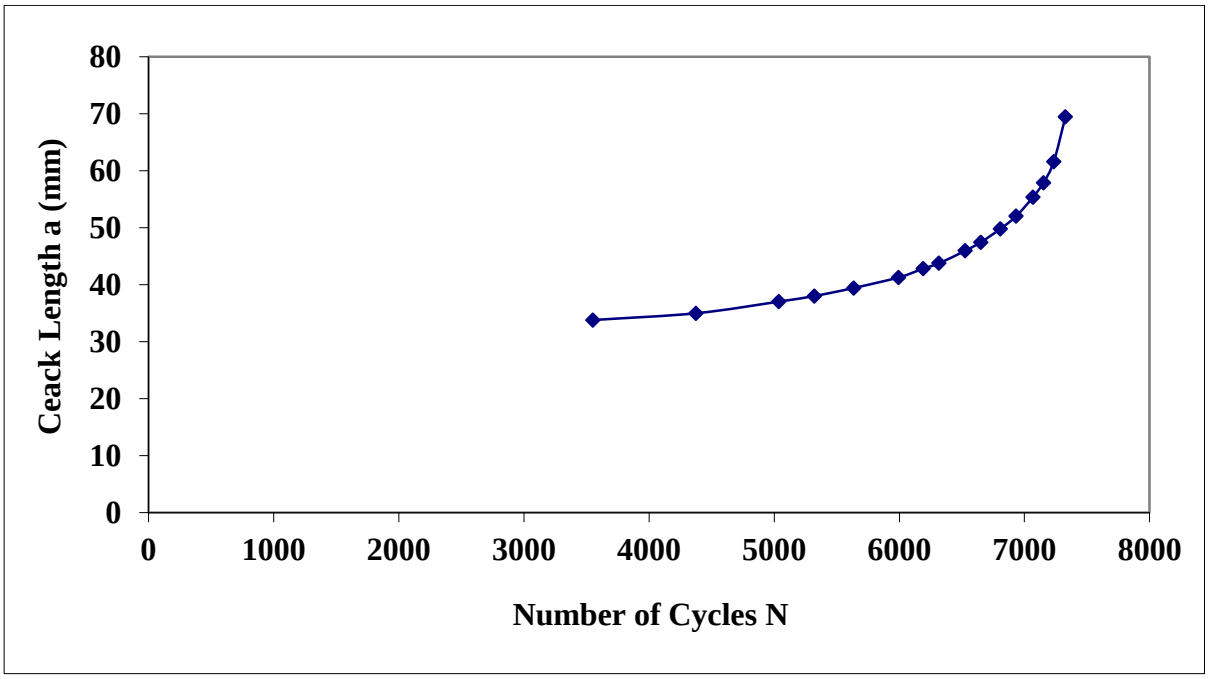

Figure 33: Effective crack length after applying COD relationship.

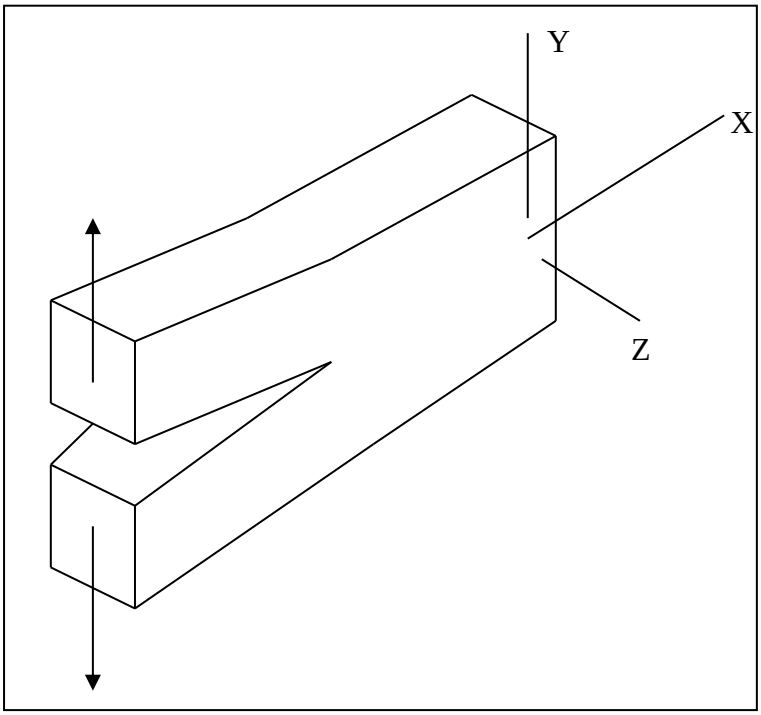

Figure 34: Mode I - Opening or Tensile Mode.

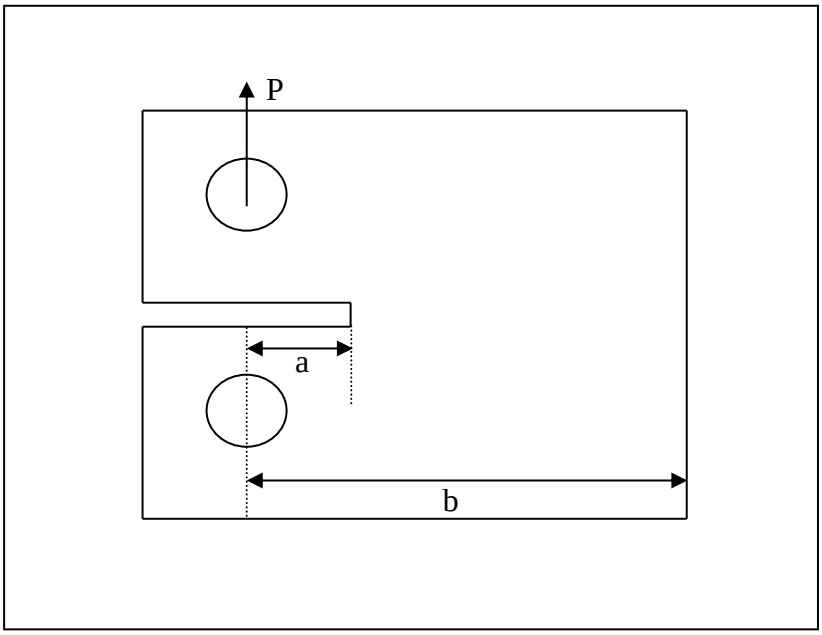

Figure 35: Compact Tension Geometry for Calculation of K_I.

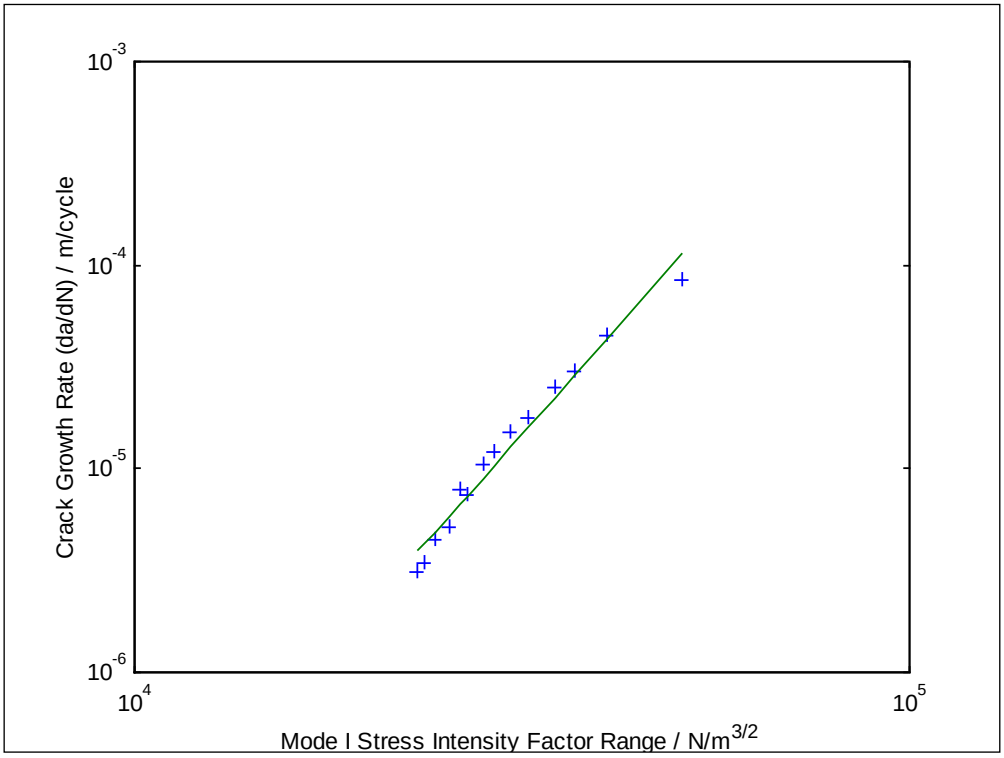

Figure 36: plot of crack growth in HMB sample.

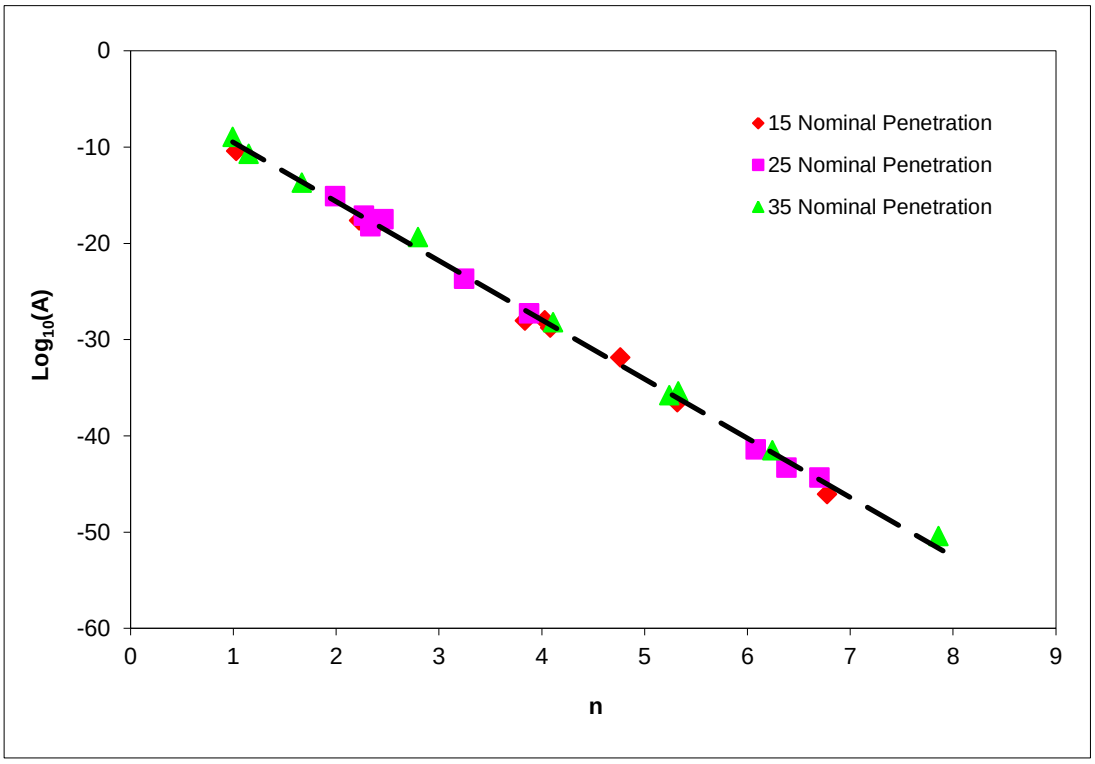

Figure 37: Plot of $Log_{10}(A)$ versus *n*.

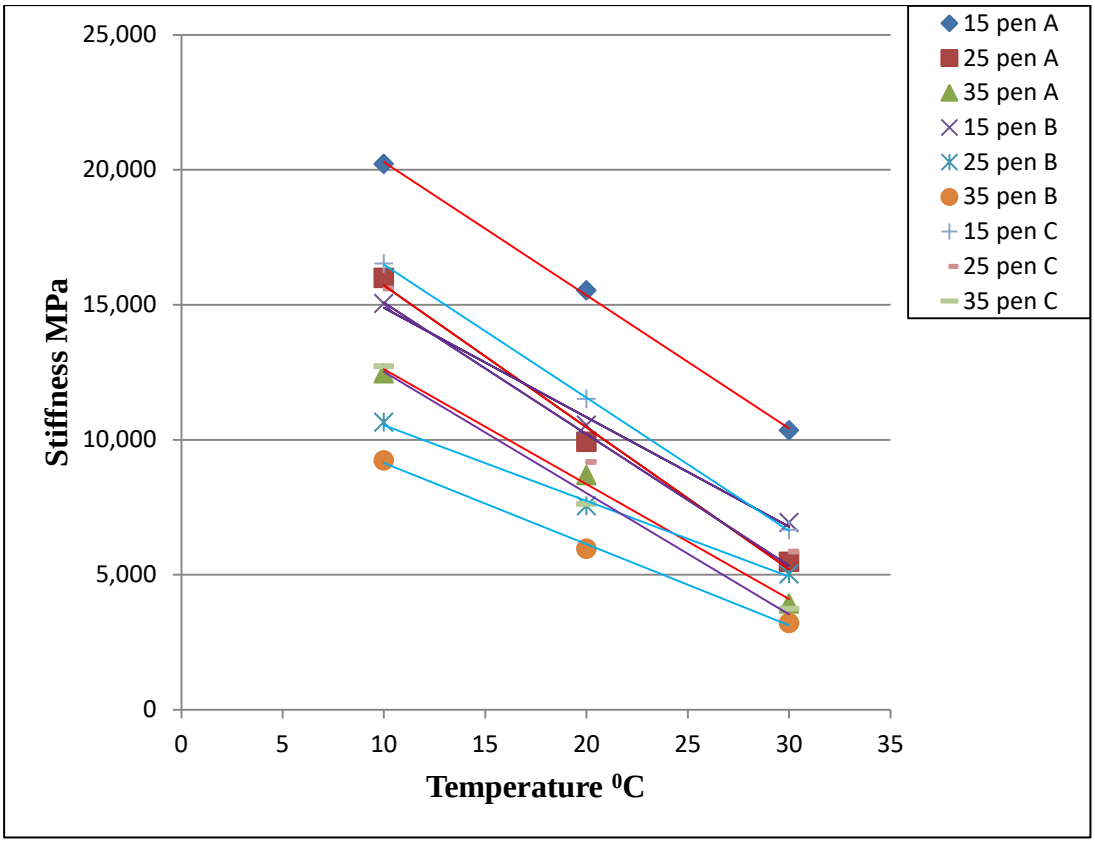

Figure 38: Stiffness against Temperature for Bitumen Source Types A, B & C.

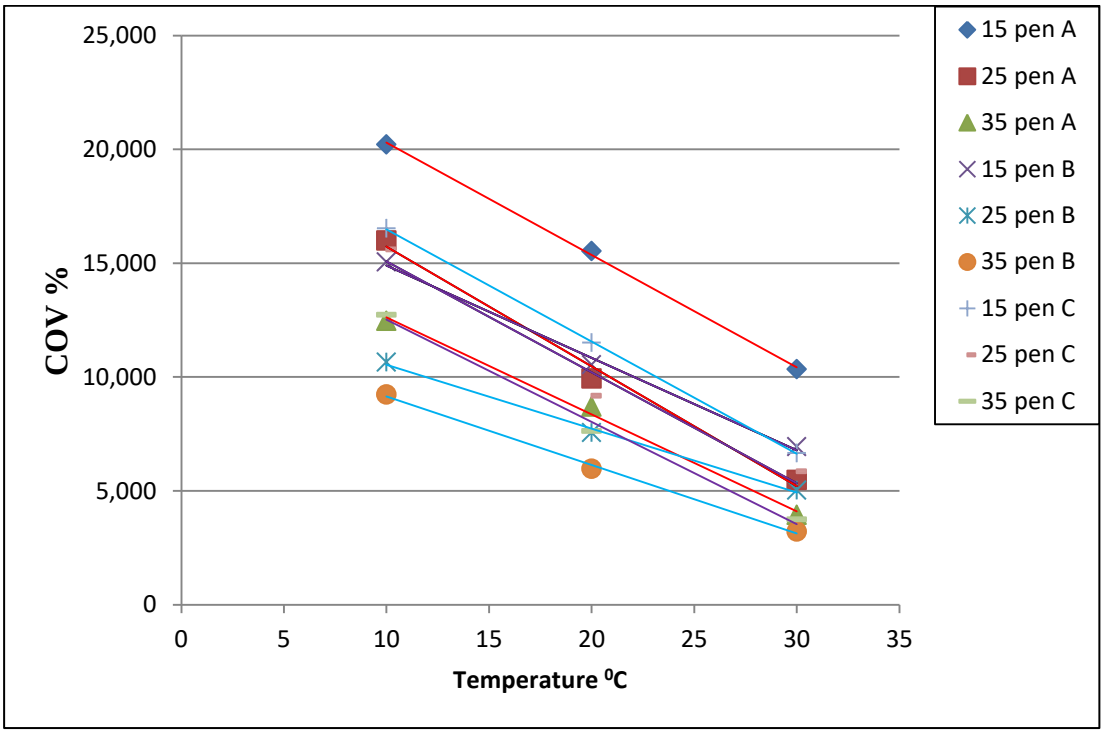

Figure 39: Plot of Stiffness COV against Temp for Bitumen Source Types A, B & C.

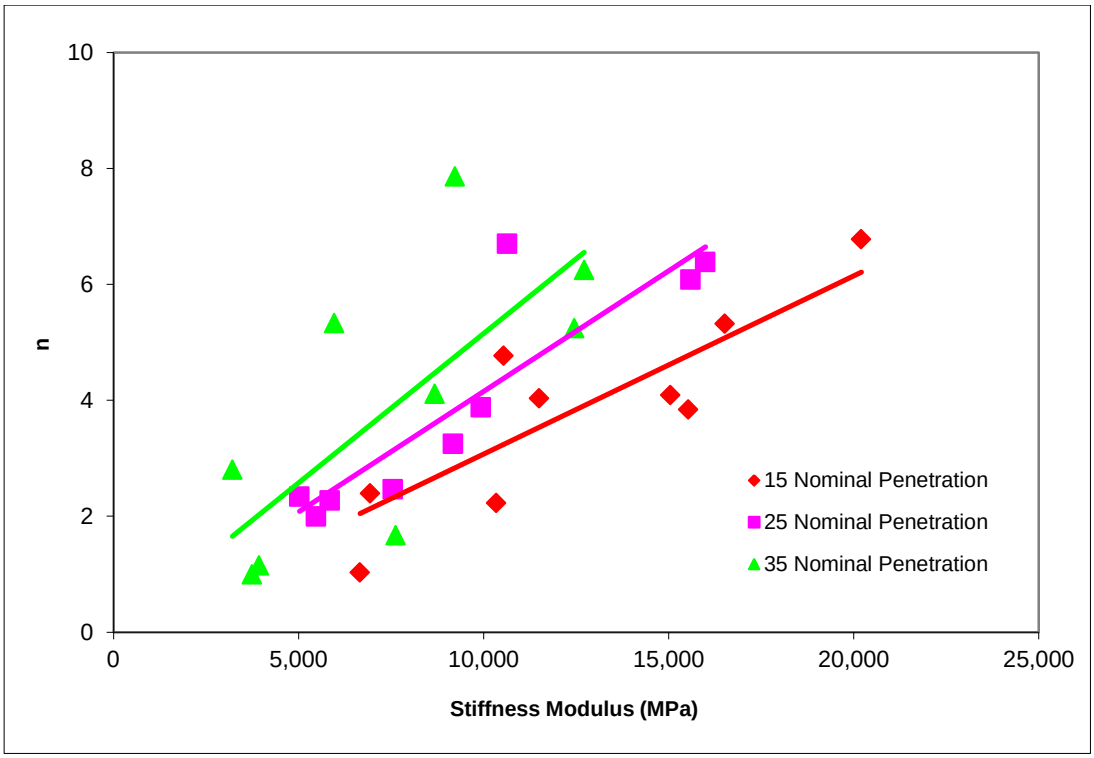

Figure 40: Plot of *n* versus stiffness modulus.

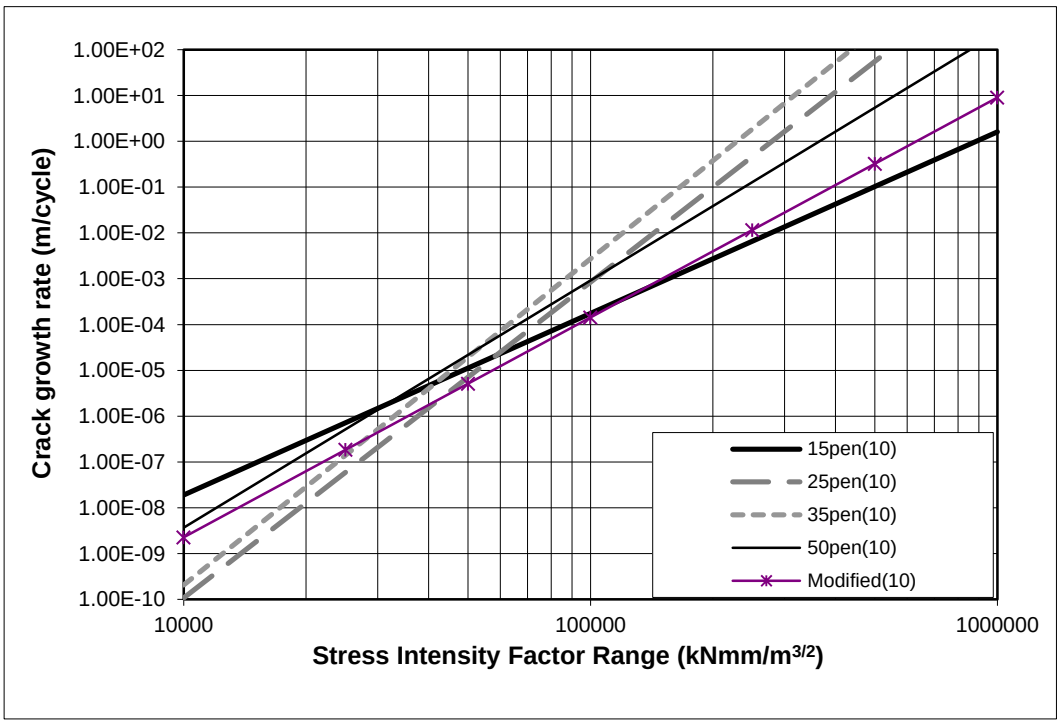

Figure 41: Averaged crack growth rate plots (10°C tests).

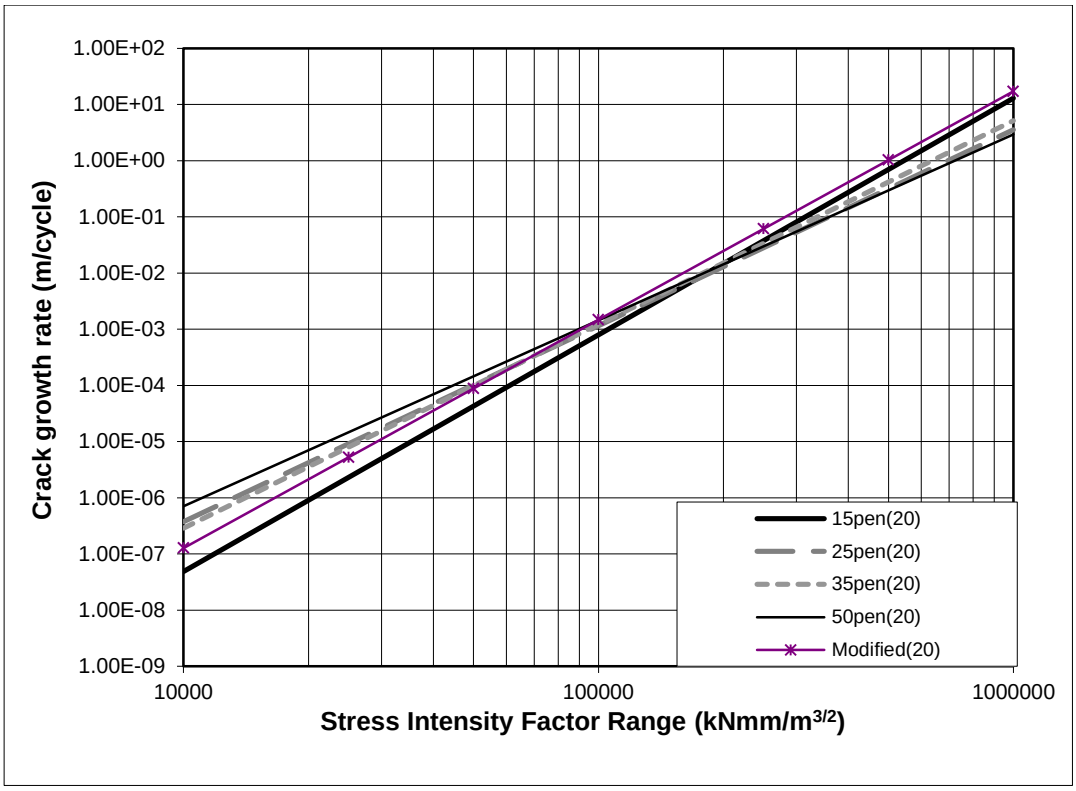

Figure 42: Averaged crack growth rate plots (20°C tests).

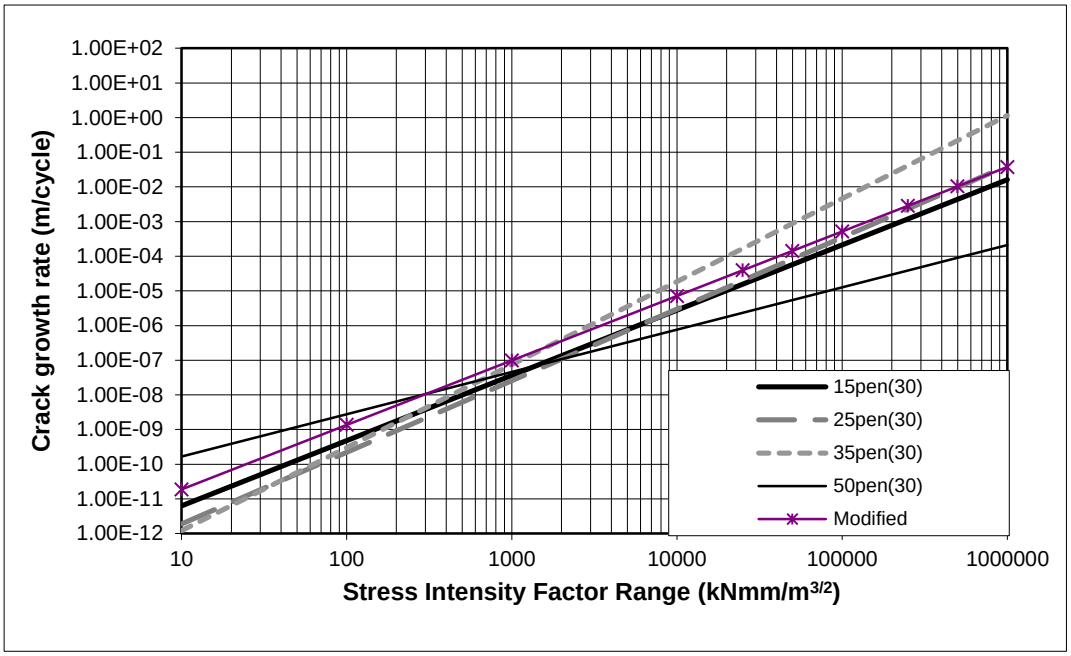

Figure 43: Averaged crack growth rate plots (30°C tests).

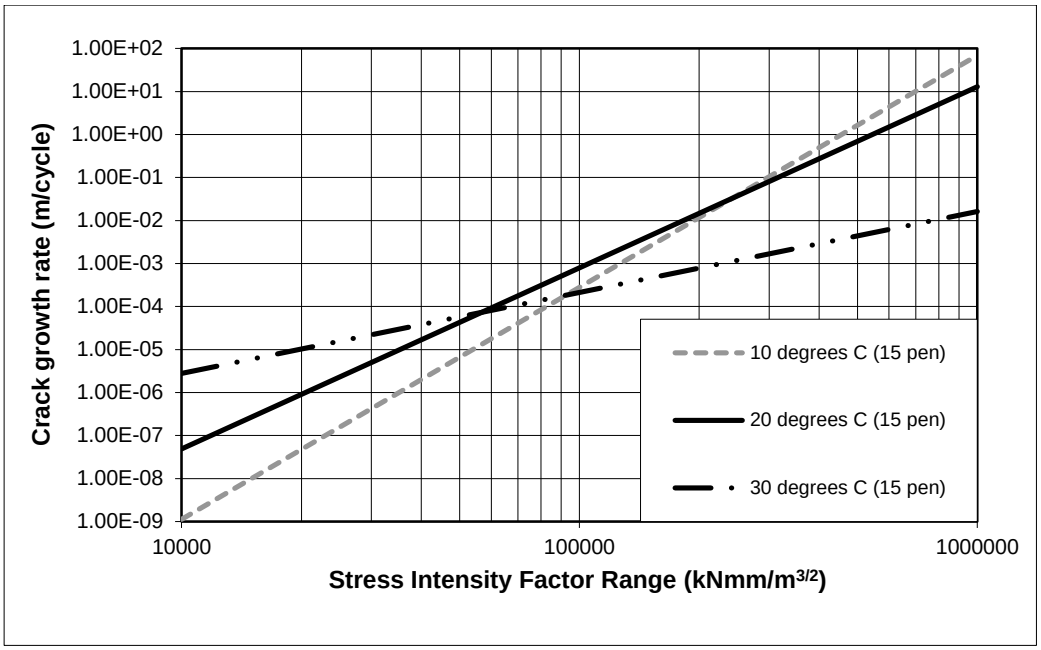

Figure 44: Averaged crack growth rate plots (15 Penetration Grade Binders).

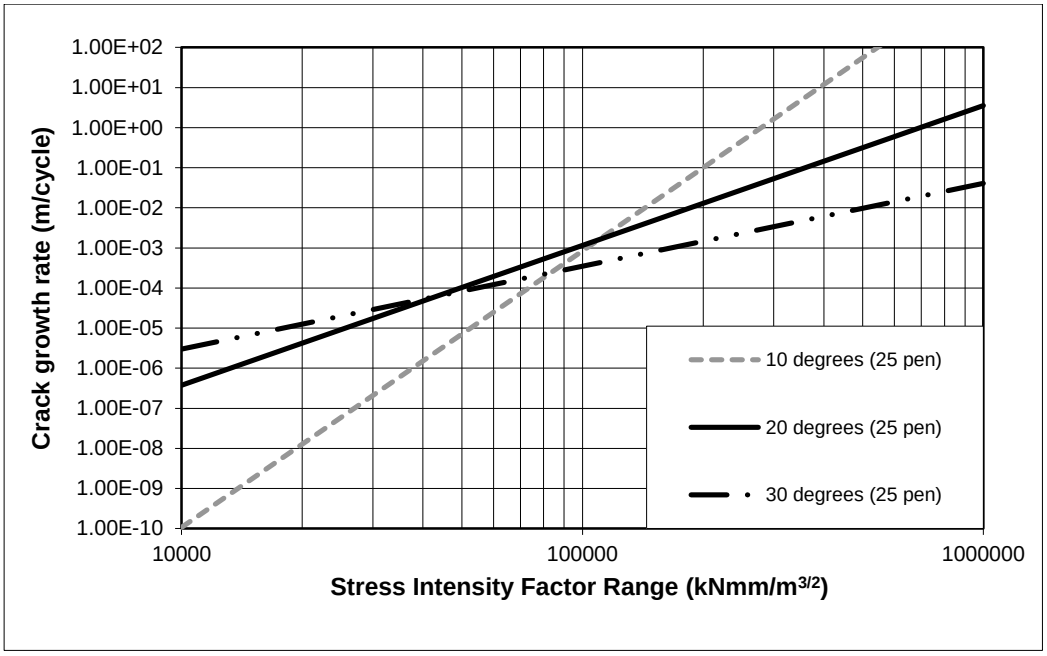

Figure 45: Averaged crack growth rate plots (25 Penetration Grade Binders).

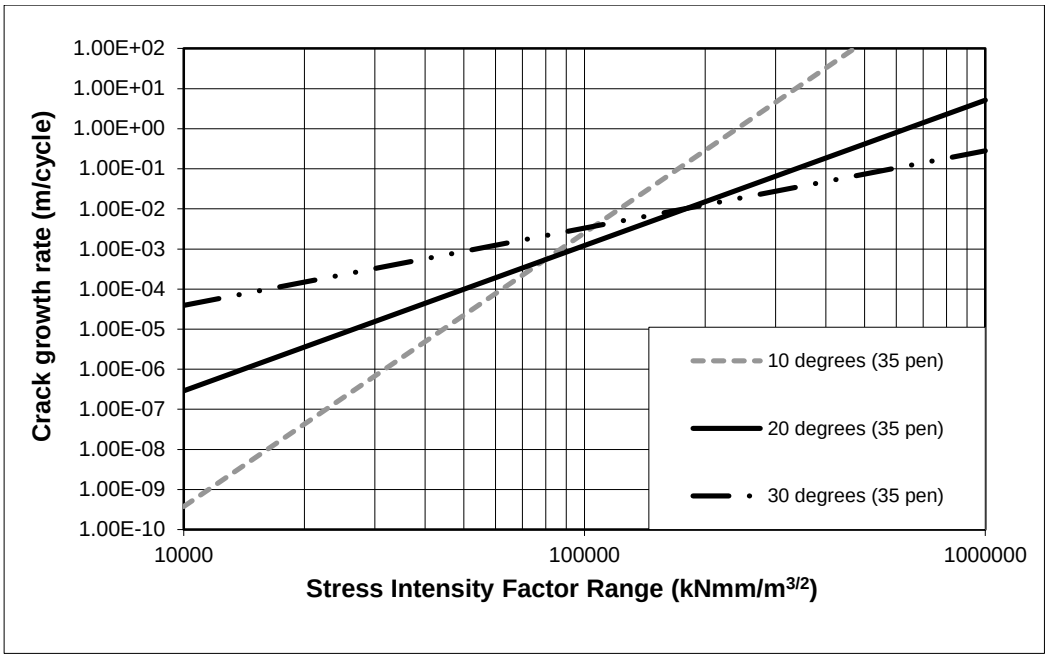

Figure 46: Averaged crack growth rate plots (35 Penetration Grade Binders).

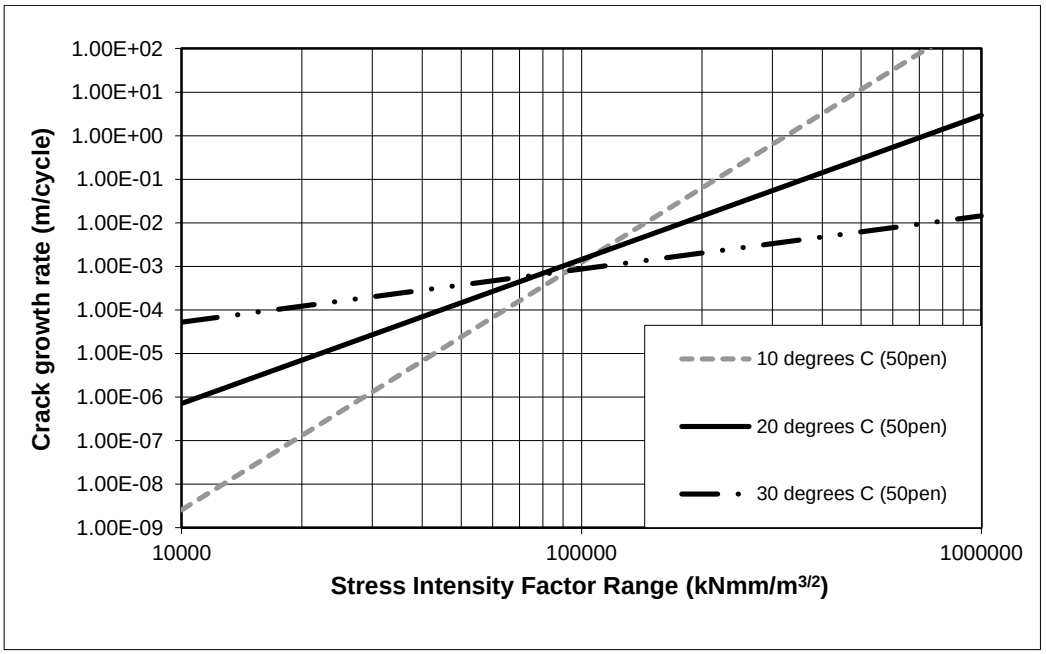

Figure 47: Averaged crack growth rate plots (50 Penetration Grade Binders).

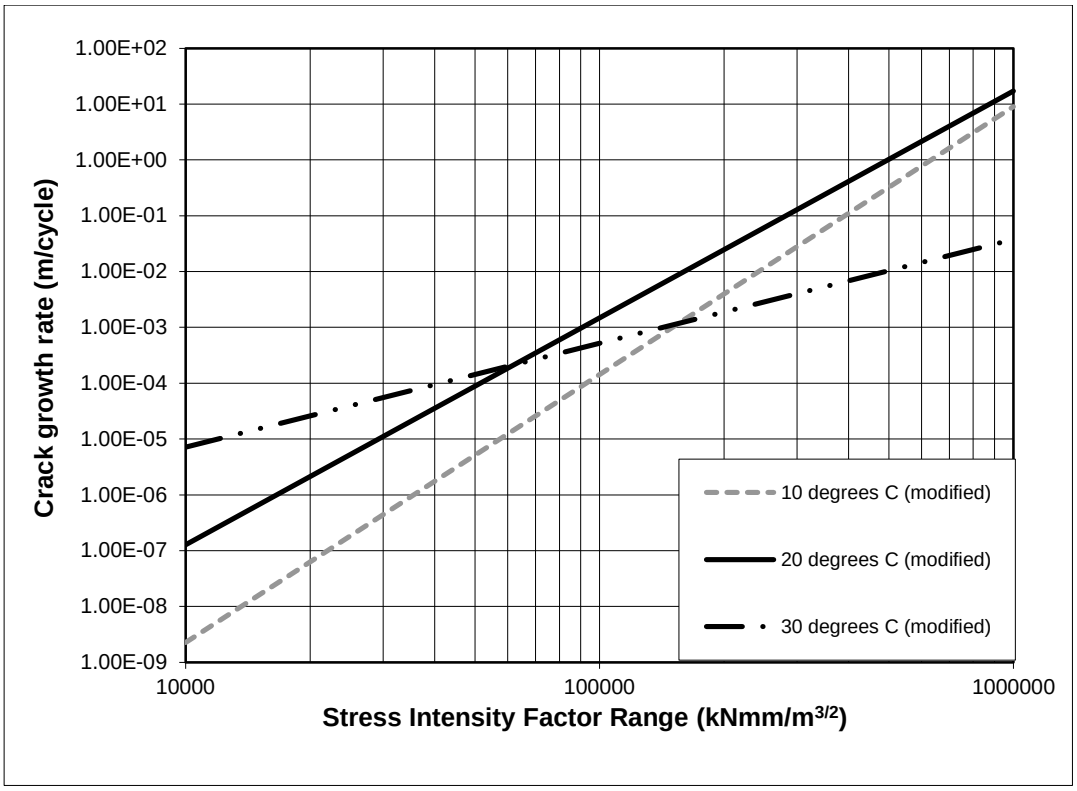

Figure 48: Averaged crack growth rate plots (Modified Binders).

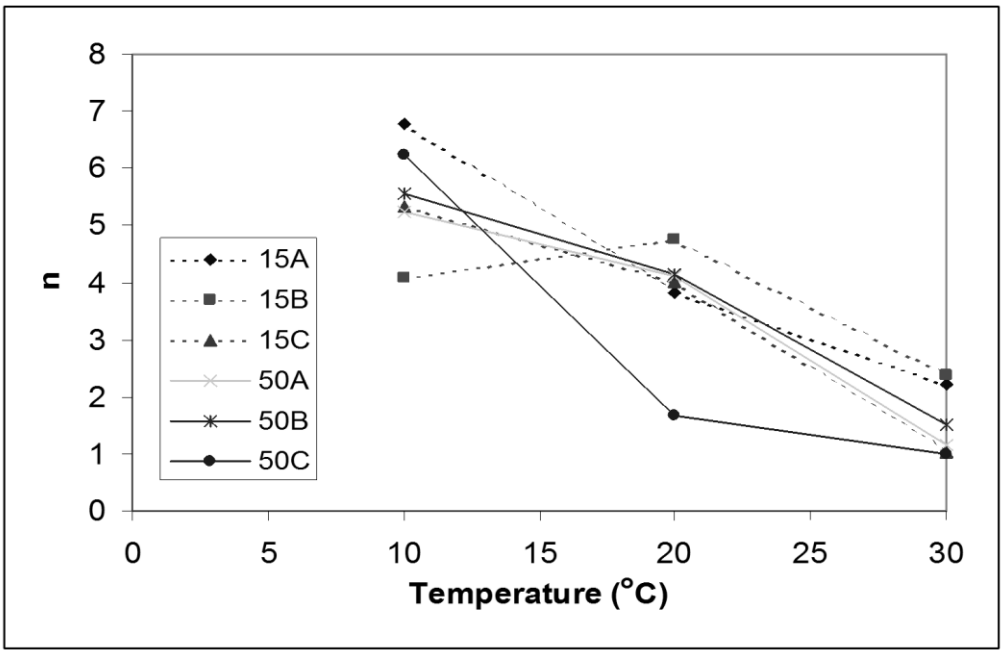

Figure 49: Variation of *n* with test temperature.

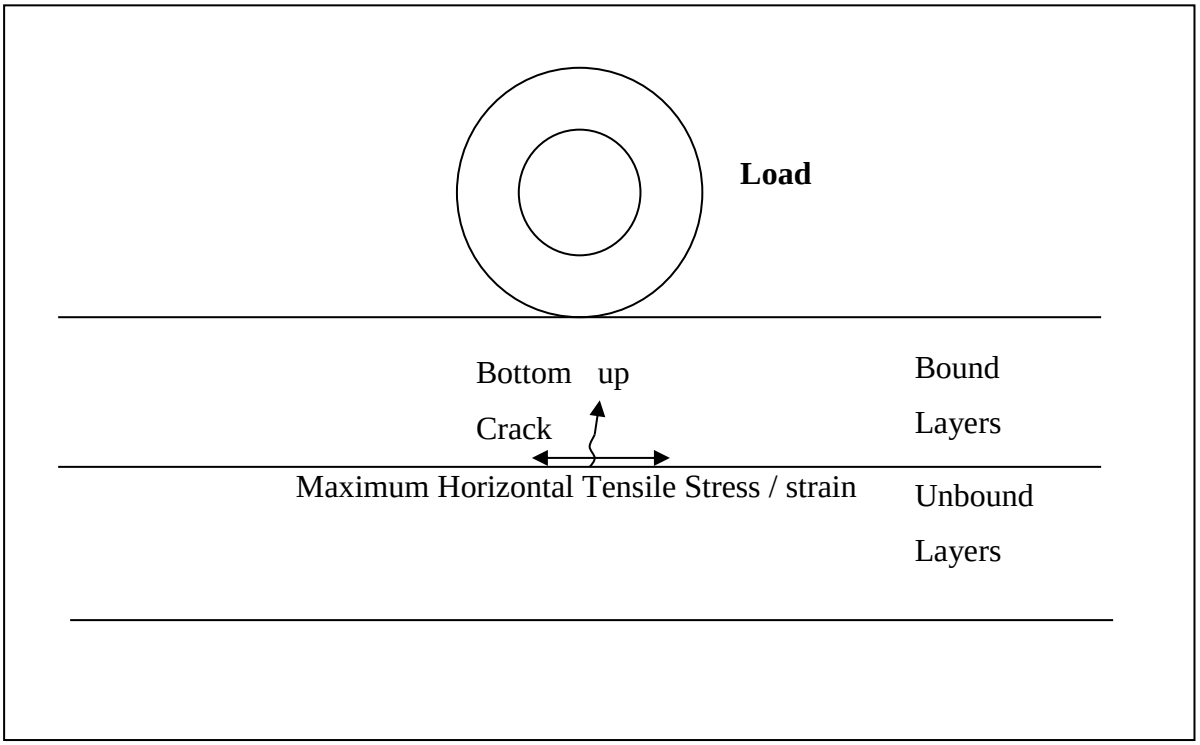

Figure 50: Tensile stress / strain generated within a Flexible Pavement.

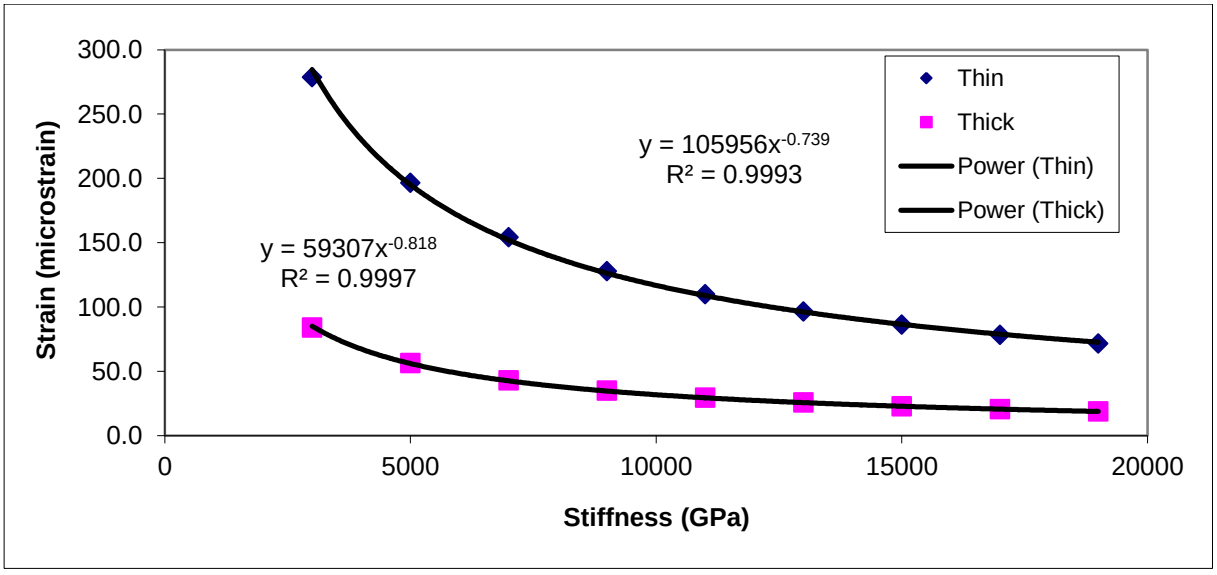

Figure 51: Plot of the Horizontal Strains in a Typical HMB Pavement Structure.

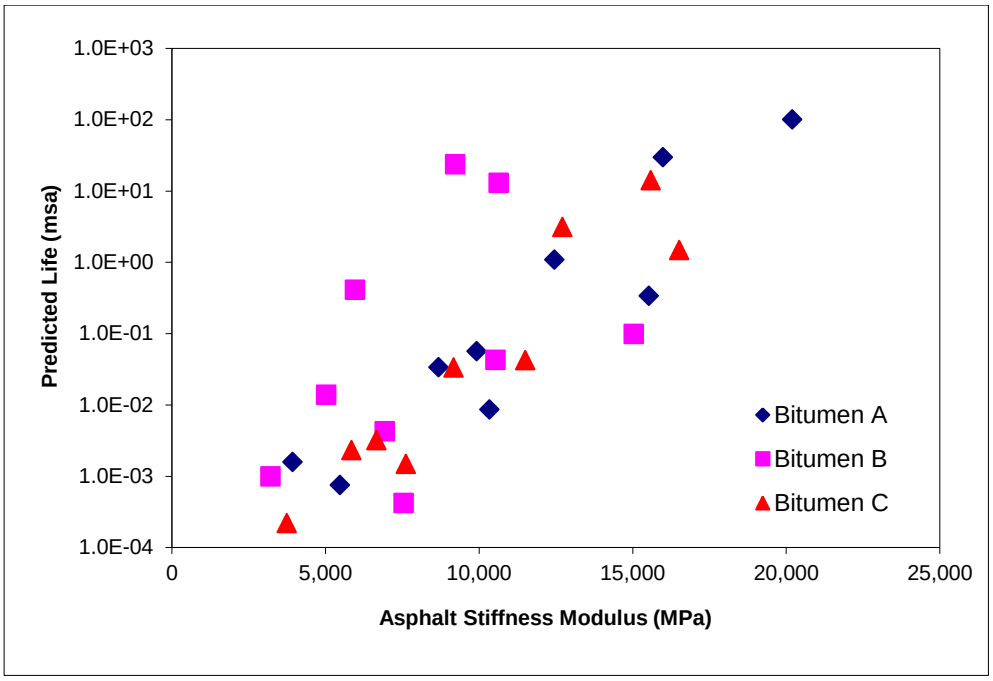

Figure 52: Predicted number of load applications to failure (minor structure).

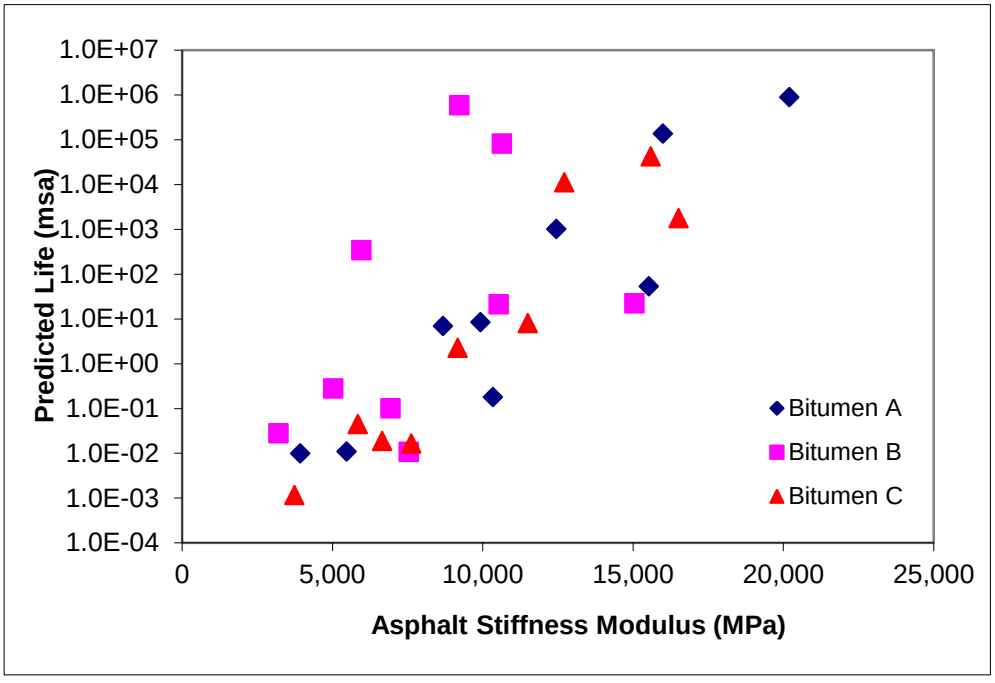

Figure 53: Predicted number of load applications to failure (major structure).

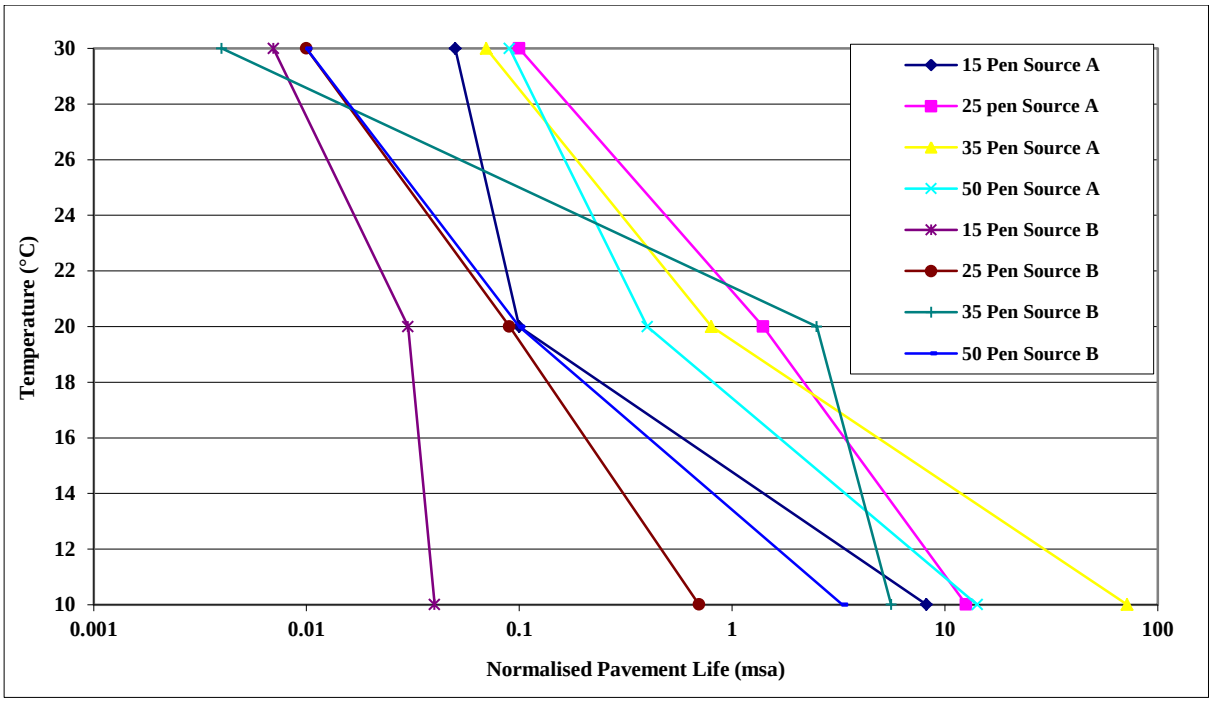

Figure 54: Normalised pavement lives from Source A and Source B.

8 Tables

Standard Dimension Limits laid down	Dimensions
B is the thickness	60mm
W is the effective width	120mm
W = 2B	
Total width, C = 1.25W min	150mm
Half Height H = 0.6W	72mm
Hole Diameter d = 0.25W	30mm
Half Distance between holes, h = 0.275W	33mm
Crack length, a = 0.45 to 0.55W	54-66mm

Table 1: Compact Tension Specimen Standard Dimensions.

CT-1 1 Minute Compaction Per side	Slice 1 Top	5.58
	Slice 2 Mid	3.72
	Slice 3 Bot	5.13
CT-2 1.5 Minute Compaction Per side	Slice 1 Top	2.75
	Slice 2 Mid	2.90
	Slice 3 Bot	2.40
CT-3 2 Minute Compaction Per side	Slice 1 Top	2.97
	Slice 2 Mid	2.79
	Slice 3 Bot	2.83

Table 2: Calibration of Air Voids Content for Compact Tension Specimens.

CT Sample Ref No	Density Kg/m^3	Air Voids %	Frequency Hz	Load kN		Cycles
				Min	Max	
1	2459	3.81	5	0.1	1.0	207113
2	2425	5.13	5	0.1	1.5	46814
3	2556	0	5	0.1	1.6	22448
4	2433	4.82	5	0.1	1.7	9400
5	2459	3.78	5	0.1	1.8	8400
6	2448	4.21	5	0.1	1.9	8961
7	2459	3.81	5	0.1	2.0	2800
8	2463	3.63	5	0.1	2.0	9489
9	2463	3.63	5	0.1	2.0	9613
10	2445	3.93	5	0.1	2.3	1890
11	2463	3.64	5	0.1	2.5	1598
12	2474	3.21	5	0.1	2.5	1296
13	2442	4.45	5	0.1	2.7	885

Table 3: Sample Details for Preliminary Testing

Nominal Binder Penetration Grade (dmm)	Temp. (^{o}C)	Bitumen A				Bitumen B				Bitumen C			
		A (m/cycle)/(N/m$^{3/2}$)^{n}		n		A (m/cycle)/(N/m$^{3/2}$)^{n}		n		A (m/cycle)/(N/m$^{3/2}$)^{n}		n	
		Mean	COV (%)	Mean	COV (%)	Mean	COV (%)	Mean	COV (%)	Mean	COV (%)	Mean	COV (%)
15	10	8.36E-47	12.33	6.78	13.47	1.72E-29	3.47	4.08	4.07	3.10E-37	32.99	5.32	39.27
	20	9.22E-29	9.53	3.84	13.03	1.40E-32	5.82	4.77	8.43	9.64E-29	7.09	4.03	9.60
	30	2.29E-18	32.31	2.23	45.60	8.06E-19	11.63	2.39	16.64	3.81E-11	15.40	1.03	31.37
25	10	4.86E-44	35.92	6.38	41.38	4.58E-45	3.81	6.70	5.23	3.83E-42	14.36	6.08	16.15
	20	5.10E-28	24.10	3.88	31.54	3.22E-18	2.07	2.46	11.32	2.02E-24	12.85	3.25	16.72
	30	7.87E-16	31.29	1.99	48.70	5.71E-19	14.19	2.34	15.38	7.35E-18	14.66	2.27	19.32
35	10	1.57E-36	2.08	5.24	2.87	3.73E-51	17.29	7.86	19.40	3.04E-42	28.25	6.25	34.37
	20	6.05E-29	11.97	4.11	13.52	3.92E-36	10.15	5.33	12.06	1.94E-14	39.60	1.67	60.82
	30	1.92E-11	25.43	1.15	44.38	4.27E-20	14.09	2.80	17.07	1.12E-09	28.24	0.99	50.62

Table 4: Fitted values of *A* and *n*

Nominal Binder Penetration Grade (dmm)	D_3	R^2
15	3.07E-04	0.75
25	4.15E-04	0.79
35	5.15E-04	0.48

Table 5: Fitted constants.

Distress/Defect Type	Distress/Defect Symptoms	Type of Repair
Low Bearing Capacity	• Combination of transverse and longitudinal cracking • Alligator cracking (fine) • Structural Rutting	Full re-construction
Surface Cracking	• Transverse cracking • Longitudinal cracking • Alligator cracking (coarse)	Sealing (surface dressing) Eventually resurfacing
Disintegration (ravelling, peeling and potholing)	• Fretting & ravelling • Interconnected cracking	Thin resurfacing
Longitudinal Unevenness	• Settlement of the sub-base • Undulation	Re-profile by regulating and resurfacing
Transverse Unevenness	• Non Structural Rutting	Resurfacing
Low Skid Resistance	• Polished surface • Bleeding	Retexturing / resurfacing
Drainage Failures	• Superelevation	Reshaping

Table 6: Summary of Pavement Distress Type

Nominal Binder Penetration Grade (dmm)	Temp. (^{o}C)	Bitumen A		Bitumen B		Bitumen C	
		σ_{xx} (MPa)	N (msa)	σ_{xx} (MPa)	N (msa)	σ_{xx} (MPa)	N (msa)
15	10	2.11	1.01E+02	1.98	9.82E-02	2.02	1.48E+00
	20	1.99	3.37E-01	1.81	4.26E-02	1.85	4.24E-02
	30	1.81	8.62E-03	1.62	4.25E-03	1.61	3.19E-03
25	10	2.00	2.97E+01	1.82	1.29E+01	1.99	1.41E+01
	20	1.79	5.63E-02	1.66	4.19E-04	1.75	3.33E-02
	30	1.52	7.46E-04	1.48	1.38E-02	1.55	2.31E-03
35	10	1.89	1.09E+00	1.75	2.36E+01	1.90	3.11E+00
	20	1.73	3.37E-02	1.56	4.12E-01	1.67	1.48E-03
	30	1.37	1.58E-03	1.27	9.88E-04	1.34	2.20E-04

Table 7: Predicted maximum tensile stress and number of standard wheel loads to failure (minor pavement).

Nominal Binder Penetration Grade (dmm)	Temp. (^{o}C)	Bitumen A		Bitumen B		Bitumen C	
		σ_{xx} (MPa)	N (msa)	σ_{xx} (MPa)	N (msa)	σ_{xx} (MPa)	N (msa)
15	10	0.55	8.74E+05	0.52	2.22E+01	0.53	1.75E+03
	20	0.53	5.27E+01	0.49	2.08E+01	0.50	8.00E+00
	30	0.49	1.79E-01	0.45	9.94E-02	0.45	1.86E-02
25	10	0.53	1.36E+05	0.49	8.12E+04	0.53	4.21E+04
	20	0.49	8.35E+00	0.46	1.07E-02	0.48	2.23E+00
	30	0.43	1.09E-02	0.43	2.75E-01	0.44	4.49E-02
35	10	0.51	9.99E+02	0.48	5.85E+05	0.51	1.10E+04
	20	0.47	6.91E+00	0.44	3.36E+02	0.46	1.63E-02
	30	0.40	9.79E-03	0.39	2.79E-02	0.40	1.16E-03

Table 8: Predicted maximum tensile stress and number of standard wheel load to failure (major pavement).

9 References

1. **Aglan, H. and Figueroa, J.,** 'Damage-evolution approach to fatigue cracking in pavements.' Journal of engineering mechanics, 119(6): p. 1243-1259, 1993.
2. **Ahmed, T.M. and Al-Khalid, H.,** A Simple Fracture Model for Hot Mix Asphalt Based on Fundamental Fatigue Parameters. 8th RILEM International Conference on Mechanisms of Cracking and De-bonding in Pavements, 2016.
3. **Airey, G.D.**, 'Rheological characteristics of polymer modified and aged bitumens.' PhD thesis, University of Nottingham, 1997.
4. **Anon.**, 'The AASHO Road Test: Report 5 – Pavement research.' American Association of State Highway and Transport Officials, HRB Special report 61E and 61G, 1962.
5. **Anon.,** 'Performance Graded Asphalt Binder Specification and Testing.' Superpave Series No 1, Asphalt Institute, 1995.
6. **Anon.,** 'Bituminous pavements: materials, design and evaluation.' University of Nottingham residential course, 1996.
7. **Anon.,** 'Specification for Highway Works.' Highways Agency, HMSO, 1998.
8. **Artamendi, I. and Al-Khalid, H.,** 'A comparison between beam and semi-circular bending fracture tests for asphalt.' Road Materials and Pavement Design, 2006.
9. **Artamendi, I. and Al-Khalid, H.,** 'Effect of specimen geometry and loading rate on the fracture properties of bituminous materials'. Advanced Characterisation of pavement and soil engineering materials conference. Edited by Loizos, Scarpas & Al-Qadi. 2007.
10. **Backlund, J., and Mackerle, J.,** 'Stress Intensity and Crack Opening of Compact Tension Specimens.' Engineering Fracture Mechanics, Vol 12, 1979.
11. **Bahgat, A.G., and Herrin, M.,** 'Brittle Fracture of Asphalt Mixtures.' Proceedings of the Association of Asphalt Paving Technologists, p32-55, 1968.
12. **Bazin, P., and Saunier, J.B.,** 'Deformability, Fatigue and Healing Properties of Asphalt Mixes.' Second International Conference on the Structural Design of Asphalt Pavements, Ann Arbor, University of Michigan, p553-569, 1967.
13. **Bolzan, P.E., and Huber, G.A.,** 'Direct tension test experiments.' Strategic Highway Research Program, National Research Council. 1993.

14. **British Standards Institution,** 'Bitumens for building and civil engineering.' B.S. 3690 : Part 1, 1989.
15. **British Standards Institution, '**Coated macadam for roads and other paved areas.' BS 4987: Part 1 Specification for constituent materials and for mixtures, 1988.
16. **British Standards Institution,** 'Fracture Mechanics Toughness Testing.' Part 1, Method of Determination of KI_c, Critical CTOD and Critical J values of Metallic Materials, 1991.
17. **BS EN,** 'Penetration of bituminous materials.' BS EN 1426, 2015.
18. **BS EN,** 'Softening point of bitumen (ring and ball).' BS EN 1427, 2015.
19. **British Standards Institution,** 'Sampling and Testing of mineral aggregates, sands and fillers: Determination of particle size distribution.' BS 812 part 3, 1985.
20. BS EN, 'Bituminous mixtures – Test methods for hot mix asphalt – Part 26: Stiffness', BS EN 12697-26:2004, BSI, London, UK.
21. BS EN, 'Bituminous mixtures – Test methods for hot mix asphalt – Part 25: Cyclic compression test', BS EN 12697-25:2005, BSI, London, UK.
22. **Brown, S.F.,** 'Practical Mechanical Tests for the Design and Control of Asphaltic Materials.' RILEM Symposium, Belgrade, 1983.
23. **Brown, S.F.,** 'A Simplified, Fundamental Design Procedure for Bituminous Pavements.' University of Nottingham, 1974.
24. **Brown SF, Stock AF and Pell PS.,** 'The structural design of asphalt pavements by computer.' *J. Inst. Highway Eng.,* p2-10, 1980.
25. **Brown, S.F., and Cooper, K.E.,** 'Improved Asphalt Mixes for Heavily Trafficked Roads.' CAPSA, Capetown, South Africa, p154-158, 1984.
26. **Bueckner, H.F.,** 'Some stress singularities and their computation by means of integral equations in Boundary Problems in Differential Equations.' Madison: University of Winsconsin, Press, 1960.
27. **Burgess, R.A., Kopvillem, O., and Young, F.D.,** 'St Anne Test road – Flexible Pavement Design to Resist Low Temperature Cracking.' Third International Conference on the Structural Design of Asphalt Pavements, London, p148-193. 1972.
28. **Chaddock, B., and Pledge, K.,** 'Accelerated and Field Curing of Asphalt Roadbase.' Transport Research Laboratory, 1994.

29. **Chan, S.K., Tuba, I.S., and Wilson, W.K.,** 'On the Finite Element Method in Linear Fracture Mechanics.' in Engineering Fracture Mechanics, Vol. 2, 1970 pp1-17.
30. **Collop, A.C., and Cebon, D.,** 'A theoretical analysis of fatigue cracking in flexible pavements.' IMechE Journal of Mechanical Engineering Science Vol. 209, pp 345-361, 1995.
31. **Cooper, K.E., and Brown, S.F.,** 'Simplified Methods for Determination of Fundamental Properties of Asphalt mixes.' Eurobitume Symposium, Madrid, 1989, pp494-498.
32. **Cooper, K.E. and Pell, P.S.,** 'The effect of mix variables on the fatigue strength of bituminous materials.' Transport and Road Research Laboratory, LR 663, 1974.
33. **Department of Transport,** 'The Structural Design of New Road Pavements.' Highway Design Standard, HD14/87, 1987.
34. **Dowling, N.E., and Wilson, W.K.,** 'Results of Elastic Analysis of Bluntly Notched Compact specimens,' Engineering Fracture Mechanics, Vol. 20, p569-572. 1984.
35. **Fordyce, D., Ferguson, A., and Khweir, K.,** 'The Design of High Modulus Base Mixtures.' 2nd European Symposium - Performance and Durability of Bituminous Materials, Leeds, p195-210. 1997.
36. **Gardner, R.R.,** 'The Fatigue Behaviour of Bitumen Sand Mixes.' The University of Nottingham, 1961.
37. **Goddard, R.T.N.,** 'The resistance of a bituminous road pavement design for very heavy traffic.' Transport and Road Research Laboratory, LR1050, 1982.
38. **Griffith, A.A.,** 'The Phenomena of Rupture and Flow in Solids.' Philosophical Transactions of the Royal Society, p163-198, 1920.
39. **Griffith, A.A., '**The Theory of Rupture.' Proceedings of the First International Congress of Applied Mechanics, Delft, Netherlands, p55-63, 1924.
40. **Hadipour, K., and Anderson, K.O.,** 'An Evaluation of Permanent Deformation and Low Temperature Characteristics of Some Recycled Asphalt Concrete Mixture.' Journal of the Association of Asphalt Paving Technologists, 57 p615-645, 1988.
41. **Hakim, B.A., Cheung, L.W., and Armitage, R.J.,** 'Use of FWD Data for Prediction of Bonding between Pavement Layers, International Journal Pavement Engineering,' p49-59, 2000.

42. **Harvey, J., and B.-W. Tsai.,** 'Effects of asphalt content and air void content on mix fatigue and stiffness.' Transportation Research Record: Journal of the Transportation Research Board, (1543): p38-45, 1996.
43. **Hertzberg, R.W.,** 'Deformation and Fracture Mechanics of Engineering Materials.' Fourth Edition, John Wiley & Sons, 1996.
44. **Hingley, C.E., Peattie, K.R., and Powell, W.D.,** 'French Experience with Grave-Bitume a Dense Bituminous Road Base.' Transport and Road Research Laboratory, TRRL Supplementary Report 242, 1976.
45. **Huang, C.W., et al.,** 'Nonlinearly viscoelastic analysis of asphalt mixes subjected to shear loading.' Mechanics of Time-Dependent Materials, 11(2): p91-110, 2007.
46. **Hunter, R.N.,** 'Asphalts in road construction.' Thomas Telford, 2000.
47. Hunter RN, Self A and Read JM, "The Shell Bitumen Handbook", 6th Ed., ICE Publishing, 2015, London, UK.
48. **Inglis, C.E.,** 'Stresses in Plate due to the Presence of Cracks and Sharp Corners.' Transactions - Institute of Naval Architects, London, 1913.
49. **Irwin, G.R.,** 'Analysis of Stresses and Strains Near the End of a Crack Traversing a Plate.' Journal of Applied Mechanics, Transactions - American Society of Mechanical Engineers, p361 – 364, 1957.
50. **Irwin, G.R.,** 'Fracture Dynamics.' Fracturing of Metals, Cleveland, p147-166, 1948.
51. **Jacobs, M.M.J.,** 'Crack Growth in Asphaltic Mixes.' Delft University of Technology 1995.
52. **Kachanov, L.M., '**On time to rupture in creep conditions.' Proceedings of the USSR Academy of Sciences, Department of Technical, 8: p26-31, 1958.
53. **Kim, K.W., and El Hussein, M.,** 'Variation of fracture toughness of asphalt concrete under low temperatures.' Construction and building Materials, 11(7): p403-411, 1997.
54. **Kuai, H., et al., '**Application of generalized J-integral to crack propagation modelling of asphalt concrete under repeated loading.' Transportation Research Record: Journal of the Transportation Research Board, (2127): p72-81, 2009.
55. **Lambert, Y., Saillard, P., and Bathias, C.,** 'Application of the J concept to fatigue crack growth in large-scale yielding.' Fracture Mechanics: Nineteenth Symposium.. ASTM International, 1988.

56. **Lee, H.J., J.S. Daniel, and Y.R. Kim.,** 'Continuum damage mechanics-based fatigue model of asphalt concrete. Journal of Materials in Civil Engineering,' 12: p105-112, 2000.
57. **Leech, D.,** 'A Dense Coated Roadbase Macadam of Improved Performance.' Transport and Road Research Laboratory, LR1060, 1982.
58. **Luo, X.,** 'characterization of fatigue cracking and healing of asphalt mixes.' PhD Dissertation, Texas A&M University, 2012.
59. **Luo, X., Luo, R., and Lytton, R.,** 'Modified Paris's Law to Predict Entire Crack Growth in Asphalt Mixtures.' Transportation Research Record: Journal of the Transportation Research Board, (2373): p54-62, 2013.
60. **Little, M.M., Krempl, E., and Shih, C.F.,** 'Viscoplastic Analyses of a Compact Tension Specimen in Mode I Loading.' Engineering Fracture Mechanics, Vol. 20, p307-325, 1984.
61. **Lytton, R.L., Shanmugham, U., and Garrett, B.D.,** 'Design of Asphalt Pavements for Thermal Fatigue Cracking.' Texas Transport Institute, Texas A&M University, 1983.
62. **Majidzadeh, K., Buranarom, C,. and Karakouzian, M.,** 'Application of Fracture Mechanics for Improved Design of Bituminous Concrete.' Federal Highway Administration: Report FHWA-RD-76-91 Washington DC, 1976.
63. **Majidzadeh, K., Kauffmann, E.M., Saraf, C.L.,** 'Analysis of fatigue of Paving mixtures from the Fracture Mechanics Viewpoint.' Fatigue of Compacted Bituminous Aggregate Mixtures, American Society for Testing and Materials, Atlantic City, 1971.
64. **Majidzadeh, K., Ramsammoj, D.V., and Kauffmann, E.M.,** 'The Analysis and Design of the Flexibility of Pavements.' Proceedings of the 3rd International Conference on the Structural Design of Asphalt Pavements, pp67-83, 1972.
65. **Majidzadeh, K., Ramsamooj, D.V. and Fletcher, T.A.,** 'Analysis of Fatigue of a Sand Asphalt Mixture.' Proceedings of the Association of Asphalt Paving Technologists, p495-518. 1969.
66. **Majidzadeth, K., et al,** 'Application of Fracture Mechanics in the Analysis of Pavement Fatigue.' Annual meeting of the Association of Asphalt Paving Technologists, 1971.

67. **Manjoine, M.J., ‘**Biaxial Brittle Fracture Tests.’ in Transactions of the ASME, Journal of Basic Engineering, 1965.
68. **Masad, E., and Somadevan, N.,** ‘Microstructural finite-element analysis of influence of localized strain distribution on asphalt mix properties.’ Journal of engineering mechanics, 128(10): p1105-1114, 2002.
69. **Moavenzadeh, F.,** ‘Asphalt Fracture.’ Proceedings of the Association of Asphalt Paving Technologists (AAPT), p51-79, 1967.
70. **Molenaar, A., et al.,** ‘Semi-circular bending test; simple but useful.’ Journal of the Association of Asphalt Paving Technologists, 71, 2002.
71. **Molenaar, J.,** ‘Dynamic Properties of Asphalt Concrete.’ Proceedings, European Flexible Pavement Study Group, 1990.
72. **Monismith, A.A.A.,** ‘Fatigue of Asphalt Paving Mixtures.’ Proceedings of the First Annual Street and Highway Conference’. University of Nevada, 1966.
73. **Mull, M., Stuart, K., and Yehia, A.,** ‘Fracture resistance characterization of chemically modified crumb rubber asphalt pavement.’ Journal of Materials Science, 37(3): p557-566, 2002.
74. **Mun, S. and Lee, H.,** ‘Modelling Viscoelastic Crack Growth in Hot-Mix Asphalt Concrete Mixtures Using a Disk-Shaped Compact Tension Test.’ Journal of Engineering Mechanics, 137(6): p431-438, 2010.
75. **Newman, J.C.,** ‘Stress analysis of the Compact Specimen Including the Effects of Pin Loading.’ Fracture Analysis, proceedings of the National Symposium on Fracture Mechanics, p105-121, 1973.
76. **Nishizawa, T., Shimeno, S., and Sekiguchi M.,** ‘Fatigue Analysis of Asphalt Pavements with Thick Asphalt Mixture Layer,’ Proceedings 7th International Conference on Asphalt Pavements, University of Washington, Seattle, p969-976 1997.
77. **Nunn, M.E.,** ‘Deterioration Mechanisms in Flexible Roads.’ 2nd European Symposium - Performance and Durability of Bituminous Materials University of Leeds, 1997.
78. **Nunn, M.E.,** ‘Theoretical evaluation of the effect of temperature on the fatigue behaviour of bituminous road-bases.’ Transport and Road Research Laboratory, LR594, 1973.
79. **Nunn, M.E., Brown, A., Weston, D., and Nicholls, J.C.,** ‘Design of Long-Life Flexible Pavements for Heavy Traffic.’ Transport Research Laboratory, TRL250, 1998.

80. **Nunn, M.E., Rant, C.J., and Schoepe, B.,** 'Improved Roadbase Macadams: Road Trials and Design Considerations.' Transport and Road Research Laboratory, 1987.
81. **Nunn, M.E. and Smith, T.,** 'Evaluation of enrobé a module elevé (EME): A French high modulus roadbase material.' Project Report 66 E111A/HM, Transport Research Laboratory, 1994.
82. **Nunn, M.E. and Smith, T.,** 'Road trials of high modulus base for heavily trafficked roads.' Transport Research Laboratory, Project Report 231, 1997.
83. **Nunn, N.,** Theoretical Evaluation of the Effect of Temperature on the Fatigue Behaviour of Bituminous Road-bases. 1973.
84. **Orowan, E.,** 'Fracture and Strength of Solids.' Report of Progress in Physics, 1949.
85. **Paris, P.C., Erdogan, F.J.,** 'A Critical Analysis of Crack Propagation Laws.' Journal of Basic Engineering, Series D, 85, No 3, of the Transactions of the ASME, 1963, pp528-534.
86. **Paris, P.C., Gomez, R.E., and Anderson, W.E.,** 'A Rational Analytic Theory of Fracture.' The Trend in Engineering, University of Washington, Seattle, Washington, 1961.
87. **Pell, P.S.,** 'Fatigue characteristics of bitumen-sand mixes.' University of Nottingham, 1959.
88. **Pell, P.S.,** 'Fatigue of Asphalt Pavement Mixes,' 2nd International Conference on Asphalt Design, Michegan, 1967.
89. **Powell, W.D., Potter, J.F., Mayhew, H.C., and Nunn, M.E.,** "The Structural Design of Bituminous Roads.' LR1132, Transport and road Research Laboratory, 1984.
90. **prEN 12597.,** 'Petroleum products - Bitumen and bituminous binders.'
91. **Qian, G.-p., et al.,** 'Experiment of Tension-compression Fatigue and Damage for Asphalt Mixtures.' Journal of Highway and Transportation Research and Development (English Edition), **7**(2): p15-21. 2013.
92. **Raithby, K.D., and Ramshaw, J.T.,** 'Effects of secondary compaction on the fatigue performance of a hot rolled asphalt.' Transport and Road Research Laboratory, 1972.
93. **Raithby, K.D., and Sterling, A.B.,** 'Some effects of loading history on the fatigue performance of rolled asphalt.' Transport and Road Research Laboratory, LR496, 1972.
94. **Ramsamooj, D.V.,** 'Fatigue Cracking of Asphalt Pavements.' Transportation Research Record, No 756, pp43-48, 1980.

95. **Read, J.M.,** 'A simple guide to viscosity and rheology' Institute of Asphalt Technology Yearbook, p67-73, 1999.
96. **Read, J.M.,** 'New Method for Measuring Crack Propagation in Asphalts.' International Journal of Pavement Engineering Volume 1, pp 15-34, 1999.
97. **Read, J.M.,** 'Fatigue Cracking of Bituminous Mixtures.' PhD Thesis, Department of Civil Engineering, University of Nottingham, 1996.
98. **Salam, Y.M., and Monismith, C.L.,** 'Fracture Characteristics of Asphalt Concrete.' Proceedings of the Association of Asphalt Paving Technologists, p215-256, 1972.
99. **Schapery, R.,** 'Correspondence principles and a generalized J integral for large deformation and fracture analysis of viscoelastic media.' International Journal of Fracture, 25(3): p195-223, 1984.
100. **Schapery, R.,** 'A method for predicting crack growth in nonhomogeneous viscoelastic media.' International Journal of Fracture, 14(3): p293-309, 1978.
101. **Schapery, R.A.,** 'A Theory of Crack Growth in Viscoelastic Media.' Report 2, MM 2764-73-1, Journal of the Franklin Institute, Volume 279, p268-289, 1965.
102. **Shell UK Oil Products Limited.,** 'Shell Design Manual'. I.P.C.L., 1978.
103. **Scholz, T.V.,** 'Durability of Bituminous Paving Mixtures.' Thesis, University of Nottingham, 1995.
104. **Si, Z, Little, D., and Lytton, R.,** 'Characterization of micro-damage and healing of asphalt concrete mixtures.' Journal of Materials in Civil Engineering, 14(6): p461-470. 2002.
105. **Slepetz, J.M., and Carlson, L,.** 'Fracture of Compact Tension Specimens.' Fracture Mechanics of Composites, ASTM, p146-162, 1975.
106. **Srawley, J.E.**, 'Wide Range Stress Intensity Factor Expressions for ASTM E 399 Standard Fracture Toughness Specimens.' International Journal of Fracture, Vol. 12, p 475–76, 1976.
107. Strickland D, "Design of flexible pavements", in The Shell Bitumen Handbook (ed. Hunter, Self and Read), 6th edition, ICE Publications, 2015, London, UK.
108. **Tada, H., Paris, P.C., and Irwin, G.R.,** 'The Stress Analysis of Cracks – Handbook.' Second edition, Paris Productions Incorporated, 1985.
109. **Taylor, I.F., Pell, P. S.,** 'Asphaltic Road Materials in Fatigue.' Proceedings of the Association of Asphalt Paving Technologists, Vol 38, 1969.

110. **Thom, N.,** Principles of Pavement Engineering. 2008: Thomas Telford Publishing Ltd 2008.

111. **Thrower, E.N.,** 'Calculations of stresses and displacements in a layered elastic structure.' Road Research Laboratory, LR160, 1968.

112. **Thrower, E.N.,** 'Calculations of stresses and displacements in a layered elastic structure, part II.' Road Research Laboratory, LR373, 1971.

113. **Thrower, E.N.,** *'Permanent deformation in a linear viscoelastic model of a road pavement.'* TRRL, Supplementary Report SR184UC, 1975.

114. **Tobbler, R.L., and Carpenter, W.C.,** 'A numerical and Experimental Verification of Compliance Functions for Compact Specimens.' Engineering Fracture Mechanics, Vol 21, 1985.

115. **TRL,** Road Note 29 – 'A Guide to the Structural Design of Pavements for New roads.' HMSO 1960, 1965, 1970.

116. **Ullidtz, P.,** 'Pavement Analysis.' Elsevier, Amsterdam, The Netherlands, 1987.

117. **Van der Poel, C.,** 'A General System Describing the Visco-Elastic Properties of Bitumens and Its Relation To Routine Test Data.' Journal of Applied Chemistry, volume 4, part 5, p221-236, 1954.

118. **Walubita, L.F., et al.,** 'Computation of pseudo strain energy and Paris law fracture coefficients from surface energy and uniaxial strain-controlled tension test data.' International Journal of Pavement Engineering, **7**(3): p. 167-178, 2006.

119. **Wessel, E.T.,** 'State of the Art of the WOL Specimen for K_IC Fracture Toughness Testing.' Engineering Fracture Mechanics, Vol. 1, p77-103, 1968.

120. **Whiteley, D.N.,** 'Observations and Results of Materials Assessment and Testing.' Contract Report, M.6. Junctions 36-37 Northbound Major Maintenance, Cumbria County Council, 1996.

121. **Whiteoak, D.,** 'The Shell Bitumen Handbook.' Shell Bitumen U.K. Ltd, 1990.

122. **Wnuk, M.P.,** 'Subcritical Growth of Fracture (Inelastic Fatigue).' International Journal of Fracture Mechanics, pp 383-407, 1971

123. **Xiao, F., Amirkhanian, S., and Juang, C.H.,** 'Rutting resistance of rubberized asphalt concrete pavements containing reclaimed asphalt pavement mixtures.' Journal of Materials in Civil Engineering, 19(6): p475-483, 2007.

124. **You, Z. and Buttlar, W.,** 'Discrete element modeling to predict the modulus of asphalt concrete mixtures.' Journal of Materials in Civil Engineering, 16(2): p140-146, 2004.
125. **Zhang, Y., Luo, R., and Lytton, R.L.,** Mechanistic modelling of fracture in asphalt mixtures under compressive loading. Journal of materials in civil engineering, 25(9): p1189-1197, 2012.
126. **Zhang, Y., Luo, R., and Lytton, R.L.,** Anisotropic characterization of crack growth in the tertiary flow of asphalt mixtures in compression. Journal of Engineering Mechanics, 140(6): p. 04014032. 2013.
127. **Zhang, Y., et al.,** 'Crack Evolution of Asphalt Mixtures Under Compressive Monotonic and Repeated Loads.' in 8th RILEM International Conference on Mechanisms of Cracking and Debonding in Pavements, Springer, 2016.

10 Appendix 1

10.4.4 Aggregates

The majority of pavement construction in the U.K. makes use of crushed rock, which is found in abundance throughout the country. A network of quarries extracts the natural rock by surface mining and generally supplies local markets (within 30 miles). The aggregates used in HMB materials are those which meet the criteria laid down in BS 4987 [11].

For the purposes of this project, the most common two aggregates have been considered, namely limestone and granite. Limestone has been considered to be the primary aggregate, as this accounts for over 50% of all U.K. crushed rock consumption [38].

Limestone is primarily composed of calcium carbonate, but also contains varying amounts of magnesium carbonate and siliceous matter. It is widely spread across the U.K. and extensively used for the production of macadams. Tarmac Products from Crich quarry close to Matlock supplied the limestone used for sample preparation within this project. This material is from the carboniferous era and is typical of many of the deposits worked in the U.K.

The standard mixture was a combination of the designed grading and HMB bitumen. The mixture requires placing into the mould in such a way that when it cools it exhibits similar properties to those that the same material would possess if it were laid on a site.

10.4.4.1 Particle Size Distribution (PSD)

Particle size distribution (PSD) separates the aggregate sample into percentages by mass of the various size fractions occurring within that sample. These quantities are determined by separating the aggregates into portions, which are retained on a number of sieves or screens having the specified openings, which are suitably graded from coarse to fine. B.S.4987 [11] states the specification limits using the ‘total percentage passing’ method, which is the method used for this project. The total percentage passing method is very convenient for the graphical representation of a PSD analysis and is widely used for specification testing. The PSD of an aggregate is important due to its direct influence upon the quality and cost of the pavement. The PSD of aggregates used in the production of 20 mm size dense basecourse

macadams is shown in B.S.4987 [11]. This specification has been chosen as the reference grading for the duration of this project (See Table 3).

The size fractions of limestone aggregate were tested for PSD and the mixture proportions of each adjusted to best fit the specification. The mixture proportions are displayed in Table 4.

Figure 17 displays a PSD plot of the mixture used for this project. For the PSD shown in

Figure 17 the material's compactibility can be assessed by using the coefficient of uniformity:

$$C_u = \frac{d_{60}}{d_{10}} \qquad \textbf{Equation 10-1}$$

where

C_u = Coefficient of uniformity

d_{60} = sieve size through which 60% of material passes

d_{10} = sieve size through which 10% of material passes

Using Equation 3-1 a coefficient of uniformity value of 60 is achieved, which categorises the material as being 'well graded' and hence suitable to achieve the degree of compaction that is required from a macadam grading.

10.4.4.2 Aggregate Density

The density of an aggregate is required to determine the theoretical amount of compaction that can be achieved when it is used in a bituminous mixture. Such tests were performed on the limestone aggregate. From BS 812 [14] it is necessary to obtain the relative density (RD) of the material using:

$$RD = \frac{M}{A - (B - C)} \qquad \textbf{Equation 10-2}$$

where

A = mass in air of the saturated surface dry aggregate

B = mass in air of the container + water + plus the sample

C = mass in air of the container + water

M = mass in air of the oven dried aggregate

And the apparent relative density (ARD) is given by:

$$ARD = \frac{M}{M - (B - C)}$$ **Equation 10-3**

Using Equation 3-2 and 3-3 a RD of 2.67gm/cm^3 was measured for the coarse limestone aggregate and an ARD of 2.70gm/cm^3. The RD is the ratio of the mass in air of the total aggregate volume (including voids which are permeable and impermeable to water intrusion) to the mass in air of an equal volume of distilled water (this value is used in most normal aggregate tests). The ARD is the ratio of the mass in air of the solid aggregate volume (including the impermeable voids but excluding the permeable voids) to the mass in air of an equal volume of distilled water. The ARD is therefore used in bituminous mixture calculations as a porous aggregate could give an erroneous result. Similar tests were performed on the fine aggregate fraction and the filler giving values of ARD of 2.75gm/cm^3 and 2.65gm/cm^3 respectively.

The density of the mixed aggregate can now be calculated from:

$$D_a = \frac{100}{\frac{X}{D_X} + \frac{Y}{D_Y} + \frac{Z}{D_Z}}$$ **Equation 10-4**

where:

X, Y and Z are the proportions of coarse, fine and filler aggregate content.

The actual mixed aggregate density value for the limestone aggregate calculated from Equation 3-4 was found to be 2.755 gm/cm^2.

10.4.4.3 Discussion of Aggregate Test Results

The aggregate that is to be used as the reference material throughout this project has been tested and suitable proportions determined which satisfy the specification. The mixture density of the aggregate, which is required to calculate the density of the theoretical bituminous mixture density, was then determined.

10.5 Figures

Figure 17: PSD of Limestone Aggregate used for HMB samples.

Tables

Aggregate grading for 20mm size dense basecourse			
Test sieve aperture size	Percentage by mass passing of aggregate	Mid point	Actual found
28mm	100	100	100
20mm	95 to 100	97.5	100
14mm	65 to 85	75	78
10mm	52 to 72	62	62

Table 3: Specification for 20mm size dense basecourse.

Aggregate Size	20	14	10	6	Dust	Filler
Proportion in mixture	2	1	1	1	2.85	0.15

Table 4: Proportions of aggregates used in standard mixture.

11 Appendix 2

11.1Bitumen

Bitumen is defined in prEN 12597 [73], as "virtually in-volatile, adhesive and waterproofing material derived from crude petroleum, or present in natural asphalt, which is completely or nearly completely soluble in toluene, and very viscous or nearly solid at ambient temperatures". This definition is the most suitable to use for this project. Other substances such as natural bitumens and tar are almost obsolete in the U.K. and will not be discussed further.

Bitumen is produced during the fractional distillation of crude oil [66]. The lighter fractions are removed from the distillation column until a residue is left which is known as the "long residue". This long residue is a complex mixture of high molecular weight hydrocarbons, which requires further processing before it can be used as a feedstock for bitumen production. It is again distilled, under vacuum, until a short residue is produced which is then processed to produce the penetration grade bitumens used in modern highway construction. This further processing involves oxidising the bitumen, which hardens it. The hardened bitumen can then be blended to produce bitumen that fulfils criteria which specifications such as British Standards (BS) set out.

In the U.K., bitumen is produced to BS 3690, part 1 [10]. The bitumens used in the production of HMB materials are characterised by the use of the penetration and softening point tests. They are, however, designated by their penetration grade only (e.g. 50 pen bitumen). The range of penetration grades produced is from 15 pen to 450 pen but, for the purposes of this project, only the range 15 pen to 50 pen will be discussed. The specification requirements of these grades of bitumen have been reproduced in Table 5.

11.2Consistency Tests for Bitumens

The penetration test [12] measures the consistency of bitumen at a fixed temperature of 25ºC, allowing a needle of specified dimensions, loaded by a mass of 100g, for a known time of 5 seconds, to penetrate into the surface of the material. The penetration value is obtained in units of dmm (0.1 mm), being the distance the needle penetrates into the bitumen. Three tests are undertaken on each specimen and the average is taken as the penetration value. This value is used to classify the bitumen into penetration ranges. The test suffers from some

disadvantages due to its empirical nature but has been approximately related to a measure of stiffness at a loading time of 0.4 seconds [66]. The results from penetration tests taken on bitumens used in the HMB project are displayed in Table 6.

The softening point test [13] is also a measure of bitumen consistency. In this test a steel ball (3.5g) is placed on a sample of bitumen contained in a brass ring suspended in a water bath. The bath temperature is raised at 5ºC per minute; the bitumen softens and eventually deforms slowly with the ball falling through the ring. At the moment the bitumen and steel ball touch a base plate 25mm below the ring, the temperature of the water is recorded. The test is performed in duplicate and the mean of the two measured temperatures is reported to the nearest 0.2ºC for a penetration grade and 0.5ºC for an oxidised grade. The reported temperature is designated the softening point of the bitumen and, for unmodified bitumens, represents an equi-viscous temperature at a viscosity of approximately 1200Pa.s. Van der Poel [74] has shown that the softening point is approximately the temperature at which the penetration is 800. The results of softening point tests carried out on HMB bitumens are displayed in Table 7.

11.3Tables

Property	Grade of Bitumen			
	15 pen	25 pen	35 pen	50 pen
Pen @ 25ºC	15±5	25±5	35±7	50±10
SP ºC	63-76	57-69	52-64	47-58
Loss on heating for 5h @ 163ºC				
(a) loss in mass, %	0.1	0.2	0.2	0.2
(b) drop in pen, %	20	20	20	20
Solubility in trichloroethylene, %	99.5	99.5	99.5	99.5

Table 5 - BS 3690: Part 1 Specification for penetration grade bitumens.

Source	15 pen	25 pen	35 pen	50 pen
A	13	20	27	38
B	16	24	40 (35/50)	
C	16	25	36	50
Specification	15±5	25±5	35±7	50±10

Table 6: Results of penetration testing.

Source	15 pen	25 pen	35 pen	50 pen
A	74	65	61	57
B	73	63	55 (35/50)	
C	75	68	61	52
Specification	63-76	57-69	52-64	47-58

Table 7: Results of softening point testing.

12 Appendix 3 Typical Crack Growth Measurements

Image	Crack Length (mm)	Picture No	No of cycles	Trigger value
1	0	1	234	1.02
2	0	2	720	0.94
3	1.78	3	3552	0.88
4	5.06	4	4374	0.82
5	5.26	5	5039	0.78
6	7.22	6	5321	0.74
7	10.23	7	5637	0.7
8	12.12	8	5994	0.66
9	12.28	9	6193	0.63
10	14.69	1	6318	0.6
11	16.8	11	6527	0.57
12	20.03	12	6652	0.54
13	19.86	13	6809	0.51
14	24.79	14	6934	0.48
15	25.94	15	7068	0.45
16	26.82	16	7152	0.42
17	28.45	17	7234	0.4
18	30.27	18	7327	0.38
19	fracture	19	7410	0.36

Table 10: Results of Typical Crack Growth Measurements and Image Records.

13 Appendix 4 Paris Law Coefficients and Volumetric Data for all Samples Tested

Sample No	Density	Air Voids	Load kN	*A*	*Log10(A)*	*n*
1	2463	3.65	3.2	1.86×10^{-47}	-46.7304	6.8544
2	2448	4.21	3.0	7.97×10^{-41}	-40.0983	5.8291
3	2466	3.52	3.3	3.93×10^{-52}	-51.4052	7.6508
Average				8.36×10^{-47}		6.7781

Table 11: Source A 15 Pen @ 10°C.

Sample No	Density	Air Voids	Load kN	*A*	*Log10(A)*	*n*
1	2446	3.81	2.0	5.21×10^{-30}	-29.2834	4.1420
2	2459	3.63	2.2	1.08×10^{-25}	-24.9683	3.2607
3	2463	3.64	2.5	1.40×10^{-30}	-29.8535	4.1104
Average				9.22×10^{-29}		3.8377

Table 12: Source A 15 Pen @ 20°C.

Sample No	Density	Air Voids	Load kN	*A*	*Log10(A)*	*n*
1	2454	4.01	1.4	1.94×10^{-13}	-12.7118	1.4224
2	2460	3.77	1.0	4.73×10^{-17}	-16.3253	1.8886
3	2456	3.92	1.2	1.31×10^{-24}	-23.8825	3.3663
Average				2.29×10^{-18}		2.2258

Table 13: Source A 15 Pen @ 30°C.

Sample No	Density	Air Voids	Load kN	*A*	*Log10(A)*	*n*
1	2464	3.61	2.6	6.90×10^{-62}	-61.1611	9.4315
2	2453	4.03	2.1	4.27×10^{-52}	-51.3693	7.7950
3	2449	4.19	2.4	1.08×10^{-44}	-43.9656	6.4765
Average				6.83×10^{-53}		7.901

Table 14: Source A 25 Pen @ 10°C.

Sample No	Density	Air Voids	Load kN	*A*	*Log10(A)*	*n*
1	2470	3.37	1.8	1.78×10^{-31}	-30.7487	4.3656
2	2451	4.12	1.5	5.59×10^{-38}	-37.2528	5.5483
3	2460	3.74	1.6	6.99×10^{-31}	-30.1554	4.3443
Average				1.91×10^{-33}		4.7527

Table 15: Source A 25 Pen @ 20°C.

Sample No	Density	Air Voids	Load kN	*A*	*Log10(A)*	*n*
1	2465	3.57	0.4	5.07×10^{-14}	-13.295	1.5983
2	2474	3.19	0.6	5.36×10^{-13}	-12.2706	1.3038
3	2442	4.46	0.5	7.12×10^{-16}	-15.1477	1.8779
Average				$2.69\ 10x^{-14}$		1.5933

Table 16: Source A 25 Pen @ 30°C.

Sample No	Density	Air Voids	Load kN	*A*	*Log10(A)*	*n*
1	2479	3.00	2.3	1.93×10^{-60}	-59.7154	9.1587
2	2482	2.90	2.0	3.47×10^{-42}	-41.4598	6.0861
3	2483	2.84	2.4	1.72×10^{-29}	-28.7645	3.9020
Average				4.86×10^{-44}		6.3823

Table 17: Source A 35 Pen @ 10°C.

Sample No	Density	Air Voids	Load kN	*A*	*Log10(A)*	*n*
1	2486	2.76	1.1	3.40×10^{-29}	-28.4689	4.0420
2	2478	3.06	1.0	6.23×10^{-21}	-20.2054	2.5805
3	2482	2.88	0.9	6.28×10^{-34}	-33.202	5.0093
Average				5.10×10^{-28}		3.8773

Table 18: Source A 35 Pen @ 20°C.

Sample No	Density	Air Voids	Load kN	*A*	*Log10(A)*	*n*
1	2475	3.16	0.3	3.76×10^{-11}	-10.425	0.9792
2	2473	3.23	0.5	1.33×10^{-20}	-19.8771	2.9129
3	2475	3.17	0.4	9.77×10^{-16}	-15.0099	2.0836
Average				7.87×10^{-16}		1.9919

Table 19: Source A 35 Pen @ 30°C.

Sample No	Density	Air Voids	Load kN	*A*	*Log10(A)*	*n*
1	2467	3.47	1.7	2.19×10^{-37}	-36.6588	5.4141
2	2481	2.92	1.5	3.62×10^{-36}	-35.4407	5.1758
3	2461	3.70	1.8	4.90×10^{-36}	-35.3097	5.1357
Average				1.57×10^{-36}		5.2419

Table 20: Source A 50 Pen @ 10°C.

Sample No	Density	Air Voids	Load kN	*A*	*Log10(A)*	*n*
1	2454	4.01	1.0	9.87×10^{-27}	-26.0056	3.7822
2	2471	3.33	1.2	7.80×10^{-33}	-32.1078	4.7521
3	2450	4.16	1.3	2.87×10^{-27}	-26.5421	3.7970
Average				6.05×10^{-29}		4.1104

Table 21: Source A 50 Pen @ 20°C.

Sample No	Density	Air Voids	Load kN	*A*	*Log10(A)*	*n*
1	2476	3.11	0.5	4.08×10^{-14}	-13.3892	1.6434
2	2477	3.10	0.4	1.14×10^{-08}	-7.9424	0.6236
3	2471	3.32	0.3	1.53×10^{-11}	-10.8161	1.1859
Average				1.92×10^{-11}		1.1510

Table 22: Source A 50 Pen @ 30°C.

Sample No	Density	Air Voids	Load kN	*A*	*Log10(A)*	*n*
1	2417	5.44	2.3	2.42×10^{-28}	-27.6169	3.8981
2	2434	4.78	2.8	3.61×10^{-30}	-29.4424	4.2169
3	2439	4.56	2.5	5.82×10^{-30}	-29.2352	4.1388
Average				1.72×10^{-29}		4.0846

Table 23: Source B 15 Pen @ 10°C.

Sample No	Density	Air Voids	Load kN	*A*	*Log10(A)*	*n*
1	2463	3.62	1.4	4.23×10^{-32}	-31.3742	4.6088
2	2464	3.60	1.5	5.18×10^{-31}	-30.286	4.4660
3	2470	3.38	1.3	1.26×10^{-34}	-33.901	5.2221
Average				1.40×10^{-32}		4.7656

Table 24: Source B 15 Pen @ 20°C.

Sample No	Density	Air Voids	Load kN	*A*	*Log10(A)*	*n*
1	2472	3.30	1.0	1.98×10^{-17}	-16.7029	2.1521
2	2479	3.00	0.9	3.07×10^{-21}	-20.5134	2.8518
3	2471	3.31	0.8	8.63×10^{-18}	-17.0639	2.1732
Average				8.06×10^{-19}		2.3924

Table 25: Source B 15 Pen @ 30°C.

Sample No	Density	Air Voids	Load kN	*A*	*Log10(A)*	*n*
1	2464	3.58	2.5	1.54×10^{-45}	-44.8136	6.8116
2	2476	3.12	2.6	1.83×10^{-46}	-45.7383	6.9827
3	2474	3.23	2.3	3.43×10^{-43}	-42.4641	6.3090
Average				4.59×10^{-45}		6.7011

Table 26: Source B 25 Pen @ 10°C.

Sample No	Density	Air Voids	Load kN	*A*	*Log10(A)*	*n*
1	2464	3.60	1.6	2.61×10^{-18}	-17.5836	2.7752
2	2463	3.64	1.3	1.58×10^{-18}	-17.8009	2.3741
3	2463	3.63	1.1	8.06×10^{-18}	-17.0934	2.2394
Average				3.22×10^{-18}		2.4629

Table 27: Source B 25 Pen @ 20°C.

Sample No	Density	Air Voids	Load kN	*A*	*Log10(A)*	*n*
1	2471	3.32	0.6	4.85×10^{-16}	-15.3143	1.9216
2	2471	3.32	0.7	6.00×10^{-21}	-20.2219	2.5168
3	2476	3.11	0.4	6.40×10^{-20}	-19.194	2.5675
Average				5.71×10^{-19}		2.3353

Table 28: Source B 25 Pen @ 30°C.

Sample No	Density	Air Voids	Load kN	*A*	*Log10(A)*	*n*
1	2457	3.88	1.9	2.29×10^{-41}	-40.6393	6.1359
2	2451	4.11	2.1	5.19×10^{-54}	-53.2847	8.4103
3	2456	3.90	2.4	4.37×10^{-58}	-57.3598	9.0322
Average				3.73×10^{-51}		7.8595

Table 29: Source B 35 Pen @ 10°C.

Sample No	Density	Air Voids	Load kN	*A*	*Log10(A)*	*n*
1	2450	4.15	1.3	5.14×10^{-32}	-31.2894	4.5883
2	2434	4.77	1.7	1.21×10^{-38}	-37.9184	5.7147
3	2484	2.80	1.2	9.73×10^{-38}	-37.0117	5.6875
Average				3.92×10^{-36}		5.3302

Table 30: Source B 35 Pen @ 20°C.

Sample No	Density	Air Voids	Load kN	*A*	*Log10(A)*	*n*
1	2471	3.33	0.4	5.46×10^{-17}	-16.2627	2.2683
2	2474	3.19	0.7	3.40×10^{-21}	-20.4684	2.9301
3	2474	3.21	0.6	4.18×10^{-22}	-21.3783	3.1960
Average				4.27×10^{-20}		2.7981

Table 31: Source B 35 Pen @ 30°C.

Sample No	Density	Air Voids	Load kN	*A*	*Log10(A)*	*n*
1	2471	3.32	1.9	1.22×10^{-33}	-32.9127	4.8012
2	2480	2.98	2.0	4.07×10^{-36}	-35.3903	5.1895
3	2481	2.92	1.8	9.71×10^{-45}	-44.0128	6.6691
Average				3.64×10^{-38}		5.5533

Table 32: Source B 50 Pen @ 10°C.

Sample No	Density	Air Voids	Load kN	*A*	*Log10(A)*	*n*
1	2435	4.75	1.0	4.52×10^{-28}	-27.3447	4.0108
2	2451	4.11	1.3	4.48×10^{-32}	-31.3487	4.6660
3	2473	3.24	1.1	4.63×10^{-27}	-26.3341	3.7596
Average				4.55×10^{-29}		4.1455

Table 33: Source B 50 Pen @ 20°C.

Sample No	Density	Air Voids	Load kN	*A*	*Log10(A)*	*n*
1	2481	2.94	0.2	2.19×10^{-12}	-11.6605	1.4961
2	2476	3.14	0.5	1.48×10^{-10}	-9.82965	1.0695
3	2481	2.93	0.4	3.95×10^{-16}	-15.4034	1.9831
Average				5.04×10^{-13}		1.5162

Table 34: Source B 50 Pen @ 30°C.

Sample No	Density	Air Voids	Load kN	*A*	*Log10(A)*	*n*
1	2478	3.03	2.6	4.35×10^{-51}	-50.3617	7.7243
2	2485	2.79	2.4	2.16×10^{-31}	-30.6654	4.3064
3	2478	3.04	2.5	3.16×10^{-29}	-28.5002	3.9321
Average				3.10×10^{-37}		5.3209

Table 35: Source C 15 Pen @ 10°C.

Sample No	Density	Air Voids	Load kN	*A*	*Log10(A)*	*n*
1	2467	3.49	1.5	1.03×10^{-30}	-29.9887	4.3982
2	2451	4.09	1.6	9.59×10^{-27}	-26.018	3.6271
3	2458	3.84	1.4	9.09×10^{-29}	-28.0414	4.0664
Average				9.64×10^{-29}		4.0306

Table 36: Source C 15 Pen @ 20°C.

Sample No	Density	Air Voids	Load kN	*A*	*Log10(A)*	*n*
1	2463	3.65	1.1	4.43×10^{-10}	-9.35401	0.9266
2	2468	3.43	1.0	5.43×10^{-13}	-12.265	1.3907
3	2464	3.59	0.9	2.29×10^{-10}	-9.63979	0.7700
Average				3.81×10^{-11}		1.0291

Table 37: Source C 15 Pen @ 30°C.

Sample No	Density	Air Voids	Load kN	*A*	*Log10(A)*	*n*
1	2468	3.44	2.7	1.25×10^{-47}	-46.9023	6.9894
2	2457	3.86	2.5	8.04×10^{-36}	-35.0947	5.0393
3	2463	3.63	2.4	5.57×10^{-43}	-42.2543	6.2187
Average				3.83×10^{-42}		6.0825

Table 38: Source C 25 Pen @ 10°C.

Sample No	Density	Air Voids	Load kN	*A*	*Log10(A)*	*n*
1	2462	3.68	1.0	6.32×10^{-28}	-27.1996	3.8709
2	2469	3.40	1.4	6.46×10^{-23}	-22.1899	2.9863
3	2453	4.01	1.1	2.01×10^{-22}	-21.6961	2.8830
Average				2.02×10^{-24}		3.2467

Table 39: Source C 25 Pen @ 20°C.

Sample No	Density	Air Voids	Load kN	*A*	*Log10(A)*	*n*
1	2487	2.70	0.5	4.04×10^{-20}	-19.3939	2.7303
2	2488	2.67	0.8	2.64×10^{-18}	-17.5786	2.2303
3	2482	2.91	0.9	3.73×10^{-15}	-14.4282	1.8554
Average				7.35×10^{-18}		2.2720

Table 40: Source C 25 Pen @ 30°C.

Sample No	Density	Air Voids	Load kN	*A*	*Log10(A)*	*n*
1	2476	3.14	1.6	7.27×10^{-53}	-52.1387	8.1720
2	2470	3.37	1.8	3.30×10^{-44}	-43.4819	6.6325
3	2475	3.16	1.7	1.18×10^{-29}	-28.9297	3.9315
Average				3.04×10^{-42}		6.2453

Table 41: Source C 35/50 Pen @ 10°C.

Sample No	Density	Air Voids	Load kN	*A*	*Log10(A)*	*n*
1	2486	2.75	0.8	1.22×10^{-11}	-10.9138	1.2205
2	2487	2.71	0.9	1.07×10^{-20}	-19.9688	2.8304
3	2484	2.81	0.8	5.61×10^{-11}	-10.251	0.9551
Average				1.95×10^{-14}		1.6687

Table 42: Source C 35/50 Pen @ 20°C.

Sample No	Density	Air Voids	Load kN	*A*	*Log10(A)*	*n*
1	2473	3.25	0.2	3.86×10^{-12}	-11.4136	1.4792
2	2481	2.92	0.3	8.30×10^{-10}	-9.08107	1.0289
3	2473	3.27	0.4	4.35×10^{-07}	-6.36149	0.4745
Average				1.12×10^{-09}		0.9942

Table 43: Source C 35/50 Pen @ 30°C.

Sample No	Density	Air Voids	Load kN	*A*	*Log10(A)*	*n*
1	2480	2.97	2.5	3.39×10^{-36}	-35.4698	5.0506
2	2474	3.21	2.3	1.65×10^{-32}	-31.7815	4.5282
3	2475	3.25	2.6	1.30×10^{-34}	-33.8854	4.8221
Average				1.94×10^{-34}		6.2453

Table 44: Source D Modified @ 10°C.

Sample No	Density	Air Voids	Load kN	*A*	*Log10(A)*	*n*
1	2452	4.08	1.5	5.86×10^{-26}	-25.2317	3.5639
2	2435	4.74	1.5	1.69×10^{-31}	-30.7721	4.5113
3	2434	4.78	1.5	4.47×10^{-29}	-28.3497	4.1177
Average				7.62×10^{-29}		1.6687

Table 45: Source D Modified @ 20°C.

Sample No	Density	Air Voids	Load kN	*A*	*Log10(A)*	*n*
1	2445	4.34	0.6	2.58×10^{-18}	-17.589	2.3397
2	2464	3.60	0.5	8.82×10^{-14}	-13.0545	1.5124
3	2434	4.78	0.7	1.14×10^{-14}	-13.9432	1.7303
Average				1.37×10^{-15}		0.9942

Table 46: Source D Modified @ 30°C.